An exploration of neural heterogeneity and its consequences on network dynamics and neuromodulation

Daniel Trotter

Thesis submitted to the University of Ottawa in partial fulfillment of the requirements for the degree of Doctor of Philosophy, Physics

Department of Physics
Faculty of Science
University of Ottawa

Abstract

Heterogeneity is a pervasive and ubiquitous aspect of physical and biological systems. This is especially true in the brain, where heterogeneity exists across all scales, from genetics and ion channel distribution to cell types and patterns of neuron connectivity. This heterogeneity has been linked to stable, persistent behaviour, increased information transmission, and effective neural encoding. Importantly, although neural heterogeneity is often regarded as a static property and modelled as a fixed meta-parameter, this is not the case in the brain. Rather, heterogeneity is, in many instances, a dynamic property of the brain that alters in response to persistent activity and brain state which has been associated with increased stability and robustness. However, the importance of specific manifestations of heterogeneity, in static or dynamic forms, is less clear. That is, recent research has shown that, despite many decades of research exploring animal-to-animal and cell-to-cell heterogeneity, it may have no bearing on the net electrical output of the cells and that neurons possess considerable electrophysiological overlap despite their heterogeneous composition.

In this thesis, we explore heterogeneity in both its malleable and static forms. We first propose a model for a firing rate-based homeostatic adaptation of neural excitability (e.g. gain). Endowing a simple network model of excitatory neurons with this candidate mechanism and heterogeneous excitability. Measuring the net heterogeneity as a function of the average pairwise difference between neurons, we explore how this heterogeneity may be up- or down-regulated in response to external stimulation and network-related factors such as degree of connectivity, and presynaptic firing rate and weights. Maintaining heterogeneity in neural excitability has been experimentally and computationally demonstrated to be crucial to having persistently stable network dynamics. Notably, these observations have been made in very generalized frameworks, where the heterogeneity in neural excitability is assumed to arise from similar distributions for all cell types. However, highly detailed datasets of human cortical neurons have demonstrated this to be inaccurate. Rather, subtypes of cells have characteristic groupings of responsiveness and input sensitivity (e.g. excitability). Leveraging one such dataset made freely available by the Allen Institute for Brain Science, we investigate the effects of distinct excitabilities between the excitatory and inhibitory neurons on network dynamics.

Beyond excitability, we consider the effects of morphological (e.g. neuron architecture) heterogeneity on neurons' responses to external stimulation. Using biophysically accurate,

freely available models of mouse primary visual cortex neurons, we do a detailed characterization of their whole cell (e.g. length, volume, etc.) and compartmental (e.g. branch thickness and length, etc.) traits. Simulating the neuron models under a uniform electric field, we record the somatic membrane potential response and link it to the strength of the applied field to define the susceptibility of each neuron to simulation. Thereafter, correlation and partial correlation analyses are performed to explore the importance of morphological traits to neuron susceptibility. The null results of these efforts then suggest that the high degree of heterogeneity in neuron morphology may limit the selectivity with which they can be targeted, and support the notion that neurons demonstrate high electrophysiological overlap.

Acknowledgements

The completion of this thesis has been an incredible, if at times winding and tumultuous journey. It would not have been possible without a considerable amount of help and support along the way, not least of which from my wonderful supervisor Jeremie. Starting with a bang in what was admittedly a rather memorable icebreaker, I owe him heartfelt thanks for his many hours of guidance and throughout the completion of this work, and moreover for his unflinching support of my too many side quests. With him, I would also like to thank the rest of the Lefebvre lab, in all the iterations it has seen, especially to Aref, for many hours of commiseration and thoughtful discussions.

Thanks must assuredly also go to several dear friends. Adrian for our many hours of mutual support, struggle and the occasional triumph; Bronwyn, who has graciously listened to entirely more rambling explanations and frustrated rants than anyone had any business asking for, and broken up many an arduous day with her humour; Tanaya, for years of laughter and support, providing new perspective on the definition of chaos and our many walks; and the Adundo family for allowing me to join your adventure as surely as you've followed mine.

To Ania, who was, in many ways, the catalyst for this journey that she has watched from the start. Thank you for all your many years of unflinching support, friendship, and guidance - those which made me a physicist and let me grow into myself, both.

And finally, thanks to Pangur, menace that he is, for relentless oversight in the form only a judgmental cat can give.

Statement of Contributions

This thesis is an article-based work as opposed to a monograph. Following Chapter 2, which presents the essential materials necessary to understand the remainder of this thesis, it presents papers that are either published, submitted or in preparation for submission. The status of each paper or manuscript is clearly indicated in the following list, as well as the respective contributions of the co-authors. The work in all the papers was guided by my supervisor.

- **Chapter 3:** This chapter is a copy of the article:

  D. Trotter, T. Valiante and J. Lefebvre. Intrinsic plasticity underlies the malleability of neural network heterogeneity. *PRX Life*, 2025. [Accepted]

  In this article, we endow a network of neurons with heterogeneous excitability (i.e. neural gain) and a mechanism for homeostatic, activity-dependent adaptation of the excitability. Through external stimulation and network architecture we explore how this mechanism can regulate the level of excitability heterogeneity in the network. I performed all numerical simulations and analysis. I am the main author of the text and figures, while corrections and comments were added by T. Valiante and J. Lefebvre.

- **Chapter 4:** This chapter is a copy of the article:

  D. Trotter and J. Lefebvre. Exploring the influence of cell-type-specific human cortical excitability on network dynamics (2025) [In preparation]

  In this manuscript, we use open-source electrophysiology data for human neurons from the Allen Institute for Brain Science to influence a network model of excitatory and inhibitory neurons and explore the effects of between- and within-cell-type excitability heterogeneity on the dynamics. In particular, we investigate the influence of human excitability heterogeneity on firing rate, synchrony and sensitivity to synaptic weights. I performed all numerical simulations and analysis. I am the main author of the text and figures, while corrections and comments were added by J. Lefebvre.

- **Chapter 5:** This chapter is a copy of the article:

  D. Trotter, A. Pariz, A. Hutt and J. Lefebvre. Morphological variability may limit single-cell specificity to electric field stimulation. *Frontiers in Synaptic Neuroscience*, **17**:1621352, 2025. [Published]

  This article analyzes the relationship between the variability in the physical morphologies (i.e. architecture) of single neurons and their response to uniform electric field stimulation. In particular, leveraging detailed, biophysical single neuron models made available by the Allen Institute for Brain Science, we characterized the neuron morphologies and studied the relationship of these features to the neurons response to increasing strengths of uniform electric fields. I performed all numerical simulations and analysis. I am the main author of the text and figures, while corrections and comments were added by A. Pariz, A. Hutt and J. Lefebvre.

In addition to these works, though not a part of this thesis, some of the modelling choices made and questions of interest in the included articles were influenced by other projects I contributed to during my program, including:

- A. Pariz, D. Trotter, A. Hutt and J. Lefebvre. Selective control of synaptic plasticity in heterogeneous networks through transcranial alternating current stimulation (tACS). *PLoS Computational Biology*, **19**:e1010736, 2023.

  This article introduced variations in intrinsic neuronal timescales and showed how this heterogeneity enables selective and directional control of synaptic connectivity by tACS. A. Pariz performed all simulations and analysis. A. Pariz and J. Lefebvre were the main authors of the text and figures. A. Hutt and I added corrections and comments.

- A. Hutt, D. Trotter, A. Pariz and J. Lefebvre. Diversity-induced trivialization and resilience of neural dynamics. *Chaos*, **34**, 2024.

  In this article, a nonlinear neural network model is used to analyze the relationship between excitability heterogeneity and resilience. Specifically, heterogeneity was mathematically demonstrated to decrease (i.e. trivialize) the number of stationary states and increase network resilience. A. Hutt and J. Lefebvre performed all simulations and analysis. A. Hutt and J. Lefebvre were the main authors of the text and figures. A. Pariz and I added corrections and comments.

Contents

List of Figures

List of Tables

1

Introduction

Diversity, or heterogeneity, is found across scales throughout physical and biological systems. Specifically, in the context of complex systems, heterogeneity refers to the idea that individual instances of a specific type of system are not identical in composition. Importantly, this is a scale-dependent concept and can refer to characteristics as large as the number of stars within different galaxies to details as small as the expression of one different base pair on the same DNA strand between siblings. Having such widespread breadth,

it is perhaps unsurprising that heterogeneity is found in a multitude of systems in our world, ranging from the different species of animals and plants in food webs and ecosystems, differential gene expression between members of the same species, and the multitude of configurations of chemical elements that comprise the various molecules of our world [215, 168, 12, 178]. Despite its pervasiveness, heterogeneity was long treated as an insignificant confound or noise to be reduced or neglected while studying the underlying signal patterns [137]. Nevertheless, the question has remained: Given its ubiquity, what, if any, functional role(s) does heterogeneity have? The answer to this remains poorly understood.

Early intuition, based largely on qualitative observation in ecosystems, speculated that maximal levels of heterogeneity were the most stabilizing for any complex system [200, 178]. However, the mathematical interrogations of this relationship by numerical [110] and rigorous analytical [212, 213] approaches found network stability to decrease with increased diversity and complexity. These perplexing theoretical works were subsequently challenged as over-simplifications in comparison to real-world systems (e.g. ecosystems, the internet, etc.), which began the long-standing debate on the true relationship between complexity and stability [178]. In line with the initial qualitative observations, an increasing body of theoretical and numerical studies across many different complex systems [9, 168, 12, 312, 60, 23, 275, 218, 153, 152] have found that heterogeneity plays a role in determining their stability, resilience, and robustness. Understanding this relationship and what source(s) of heterogeneity contribute to it [243, 105] is of great interest for predicting the long-term dynamics and sustainability of a given system. Indeed, studies of this exact relationship have canvased a variety of fields over the past century, from ecosystems [200, 110, 212,

213], to immune response [25, 244, 89, 294] and disease [289, 137], and more recently the brain [248, 335, 324, 275, 153, 149, 152, 112].

The same principles that were applied to ecosystems can, and have been, extended to other complex systems such as communication networks [9, 116], social interaction [190, 218], and neural networks [343, 154, 153, 152]. Within this thesis, we consider heterogeneity in the context of the brain at the cell-to-cell level. In recent years, the accumulation of datasets with unparalleled resolution [182, 44] has made it increasingly evident that the brain is rife with diversity. Across scales from genomics [314, 295, 298, 161] and electrophysiological properties of individual cells [205, 204, 226, 182] to the cellular architecture (e.g. morphology) [259, 42, 129], types [122, 58] and connectivity [159, 93]. Moreover, cell-to-cell heterogeneity has been linked to the functional specialization of neurons in different regions of the brain [98, 167], and differs across species [26, 210]. Cumulatively, this marks heterogeneity as an unavoidable feature of neural circuits, whose functional role(s) are poorly understood.

Importantly, though often described and considered as a static meta-parameter [137] that results solely from genetic disposition, recent work [205, 204, 226, 275, 227] has shown that heterogeneity is a highly dynamic property of neural circuits. This is, in part, due to the neurons' own ability to change through time via *adaptation*. In the brain, adaptation refers to a variety of activity-dependent mechanisms that give neurons the flexibility needed to respond to the range of input they receive while maintaining stable neuronal dynamics. Like heterogeneity, these mechanisms occur on different scales, from ionic currents and synaptic connection strengths to the overall sensitivity of a neuron (i.e. excitability) [332,

364, 77, 78, 94, 31]. The ability of neurons to adapt is crucial for neural encoding [347, 346], information transmission [117], development and learning [332, 333]. However, at odds with this continual change is the brain's need for stability. An ever-growing body of literature [332, 83, 77, 333, 205, 78, 204, 246, 97, 31, 14, 208] supports that the brain's dynamical stability is maintained through engaging several types of homeostatic adaptation (i.e. adaptation returning a neuron, or network of neurons, to an equilibrium state following a perturbation). Moreover, in line with ecological research, neural heterogeneity has been linked to stability, robustness, and increased computational potential [248, 153, 112, 152]. Conversely, loss of heterogeneity between neurons was found to be conducive to the onset of pathologies, including tinnitus [192, 138], neuropathic pain [69], and epilepsy [275, 153, 227], suggesting an important functional role.

In this thesis, we are interested in exploring the heterogeneity of neurons at a cell-to-cell level within a few different contexts. First, we investigate the malleability of electrophysiological heterogeneity in terms of neural excitability. Second, the role(s) of the diversity found in the neural excitability of human cortical neurons are interrogated for their contributions to circuit-level dynamics. Finally, at the level of single cells, we explore the role of heterogeneity in neuron morphology (e.g. cell structure) in the response variability observed under stimulation conditions.

Neural excitability is a measure of the gain of a given neuron as an input-output (IO) function, often experimentally recorded in terms of the response frequency to different strengths of fixed current input (e.g. a frequency-current, or fI, curve) [155, 305, 193, 97]. These relationships define the type of excitability a neuron has, as established by

Hodgkin in early work on squid axons [143], whether it is continuous and able to respond to arbitrarily low frequencies of input (Type I), or discontinuous and requires a certain strength of input to evoke response (Type II) [155, 305]. From a physical standpoint, these different classifications are of great importance to the dynamical behaviour of a network as they capture the spiking response and bifurcations that occur for a given neuron [281, 307]. Beyond such considerations, the heterogeneity observed in neural excitability neuron-to-neuron even within a single class [226] is of particular interest, as excitability is known to be dynamically modulated by network activity [331, 77, 193], and its heterogeneity has been found important in maintaining healthy, stable brain activity and information optimization [165, 275, 153, 152, 112].

Despite its commonality as a measure in classifying the electrophysiological properties of neurons, much remains unknown about neural excitability in the brain. Specifically, though homeostatic adaptation of neural excitability is known to occur [331, 77, 193, 97, 31], the exact mechanism by which it occurs is less clear, although phenomenological models and experimental works have supported intracellular calcium as a key regulator [188, 2, 239, 246, 245]. Despite this, many questions remain around the heterogeneity observed in neural excitability, how it is maintained, and what effects it has on network dynamics. This is especially true as the curation of evermore precise electrophysiological datasets [237, 58, 182, 67, 210] has made clear that subclasses of cortical neurons (e.g. pyramidal excitatory neurons, parvalbumin interneurons, somatostatin interneurons, etc.) have distinct groupings of excitability profiles. The importance of these groupings to maintaining stable network dynamics is further unknown.

Beyond neural excitability, widespread heterogeneity is also observed within and between the morphologies of neurons of various subtypes and layers [362, 122, 123, 226, 58, 182, 67]. Indeed, many neurons have been classified into subtypes based in part on stereotypical architectures [56, 173, 362, 42, 122], and morphology has been known to contribute to neuron response due to its influence on synapse location and density, and hence dendritic integration [140, 286, 325]. Moreover, recent research has associated specific morphological arbours with functional role in object-related memory formation [167]. Such stereotypical architectures and functions have been of increasing interest in the last three decades as targets for selective activation for therapeutic purposes [263, 359, 194, 4]. However, the tractability of such an approach remains unclear. Moreover, recent results have demonstrated morphological heterogeneity alone to be insufficient [17] or unnecessary [243] in replicating the electrical responses of neurons.

To this end, in the context of neural heterogeneity, we ask three fundamental questions: 1) Which feature(s) of neural activity contribute to the homeostatic adaptation of neural excitability, and is there an impact on heterogeneity? 2) What are the dynamical consequences of physiological, heterogeneous excitability profiles? and 3) To what extent does morphological heterogeneity help or hinder the specificity with which neurons can be activated? Each of these questions is answered in a different chapter of this thesis.

Previous studies have made their own forays into investigating the questions of this thesis. In terms of neural excitability, many studies have noted the wide variety of ion channels that endow neurons, controlling their excitability and contributing to their activity [78, 246, 63, 119], the most well known of which are sodium (Na+) and potassium (K+)

that were described in the seminal work of Hodgkin and Huxley [143, 144]. The exact distribution of these ion channels, and hence neural excitability, varies between brain regions, across cell types, and throughout the parts of individual neurons [119, 208]. Importantly, as has been of increasing interest in the last thirty years, the expression of these channels is flexible and, as has been observed under a variety of experimental conditions, can modulate neural excitability by up and down regulating expression [188, 2, 331, 83, 332, 205, 204, 193, 354, 10, 247]. Specifically, separate from the dynamical questions of interest in this thesis, it has been shown that the expression of the genes that regulate ion channels, and hence their distribution, can change through time and in response to altered activity [78, 119, 208]. An example of this comes from a study in which rat cortical neurons were cultured with tetrodotoxin (TTX), a voltage-gated Na + channel blocker, for 2 days before being washed out [83]. Although the kinetics of the Na+ channels were unaffected, the current densities of both the inward Na+ and outward K+ had changed in compensatory fashion. That is, it was not the Na+ conductance itself that mattered, but the dynamic ratio of all the involved conductances. A similar work, [309], furthered this result by studying the effect of acute (TTX, similar to [83]) and long-term changes (genetic knockout of Na+ channels) in mouse Purkinje neurons. Recording the relative contributions of other conductances, it was found in both conditions that, despite variability between cells, the spiking behaviour was made resilient to changes in Na+ via compensatory feedback mechanisms by altering the availability for action and expression levels of other ion channels. The feedback control of these ion channel expressions has been phenomenologically linked to calcium expression as a monitor of cellular excitability [188, 2, 78]. More recent models

[239, 246, 245] have built on this to better reflect the biophysics of different ion channel types (e.g. turnover rate, channel correlations, multiple solutions, etc) and improve understanding of the homeostatic mechanisms underlying excitability adaptation. Despite this increasingly improved understanding of the biological mechanisms involved in excitability homeostasis, the heterogeneity involved between neurons makes it challenging to resolve and much remains unknown about it.

Importantly, the cell-to-cell heterogeneity of excitability has also been modelled and shown both numerically and analytically to increase the stability of network-level activity [153, 152, 112] and improve information encoding of sensory information when subpopulations have different excitabilities in low noise regimes [165]. From a dynamics perspective, the increased heterogeneity of the excitability has a linearizing effect on the mean excitability of the population [187, 275, 153]. That is, broadening the distribution of excitabilities leads to lower variance and reduced correlation in the population dynamics. This has additionally been shown theoretically to reduce the number of stationary states [152] and hence increase the resilience of the network.

What has remained unaddressed is the assemblage of these ideas. That is, an exploration into the relationship of homeostatic adaptation in excitability to the heterogeneity observed between cells and the increased stability it provides. Here, we aim to shed light on this by introducing a candidate mechanism for the homeostatic adaptation of excitability and exploring how it may drive heterogeneity up and down. Thereafter, we endow a network model of excitatory and inhibitory neurons with physiological excitabilities and explore the effects of their subpopulation differences and heterogeneity on the asynchronous

state of the network.

Finally, we interrogate the importance of morphological heterogeneity. Leveraging biophysically detailed models with accurate morphologies of real cells, we characterize, in detail, the physical traits of each model. The models are then subjected to various strengths of electrical field stimulation, and their response is recorded. The relative response to each stimulation strength is then related to the various morphological features, and correlation analyses are performed to interrogate the influence of each feature on the neuron response.

The thesis is organized as follows. In Chapter 2, we present the essential notions and concepts from both physics and neuroscience necessary to understand the rest of the thesis. We review neural heterogeneity starting at the macroscopic scale of the brain and leading to increasingly smaller scales before concluding with a more in-depth description of the electrophyisological and morphological scales of cell-to-cell heterogeneity that are the focus of this work. Thereafter, we review descriptions of neurons themselves including examples of how they have been modelled in both single-neuron and circuit-level networks. Special attention is paid to neural excitability which is the heterogeneity source of interest in Chapters 3 and 4. Several mechanisms of neural adaptation are subsequently overviewed in both their neurological and modelling frameworks, including descriptions of how adaptation has been implemented in different model frameworks. Within this, we pay particular attention to homeostatic gain modulation as a mechanism of adaption for neural excitability, a major theme of Chapter 3. In this we additionally introduce maladaptive versions of this modulation and subsequently describe non-invasive brain stimulation techniques, which have been used as neuromodulatory interventions in such circumstances. In

this, focus is placed on transcranial electric stimulation, which is utilized in Chapter 5. The chapter closes by revising key concepts from dynamical systems and describing the numerical methods used for the simulations throughout this thesis.

Chapter 3 presents a model of a simple network of excitatory neurons endowed with heterogeneous excitability that is modulated by an activity-dependent homeostatic mechanism. We define the model and homeostatic mechanism of neural excitability in detail, deriving the underlying factors that modulate the amount of heterogeneity in the neuron-to-neuron excitability. The response of the network heterogeneity level to perturbations of in-network (e.g. connectivity) and external (e.g. stimulation) factors is computed. Finally, the persistence of induced heterogeneity within the model network is assessed.

Chapter 4 leverages a recent dataset of human cortical neuron excitabilities [58, 182] for both excitatory (E) and inhibitory (I) cells. These excitabilities are randomly assigned to neurons within a simple EI network model to perform an exploratory study into how their between- and within-cell-type heterogeneity influences the network dynamics. We begin by characterizing the excitabilities and parameterizing the baseline state of the network, in one which shows largely asynchronous irregular spiking [49]. Beginning with the mean excitabilities of the two populations, we explore the role of between-cell-type heterogeneity on the firing rate and synchrony of the networks. Thereafter, expanding into the within-cell-type heterogeneity, we continue our investigation into the effects on the firing rates and synchrony, as well as considering sensitivity to presynaptic weight changes and additive noise correlations. From this, we find that the between- and within-cell-type heterogeneity of the excitabilities both contribute to network firing rates and synchrony, and that the

more homogeneous, hyperexcitable inhibitory excitabilities may contribute to insensitivity to changes in presynaptic inhibitory, but not excitatory, weights.

Finally, in Chapter 5, we interrogate the relationship between heterogeneous neuron morphology and response variability to transcranial direct current stimulation. Using open-source, biophysically detailed models of real mouse neurons, we characterize the morphological properties of pyramidal neurons and parvalbumin interneurons from layers 2/3, 4 and 5 at both the whole-cell level (e.g. neuron length, volume, etc.) and microscopic level (e.g. number of branch, branch width, etc.). The models are simulated under conditions of variable uniform electric field strengths, with the somatic membrane potential recorded and their relationship quantified by a metric of susceptibility, which relates relative responsiveness to stimulus strength. Thereafter, the susceptibility of each model is interrogated with respect to its morphological properties to identify any correlations between neuron morphology and response. The chapter closes with correlation and partial correlation analyses, as well as dimensionality reduction, which find no significant correlation between any singular morphological feature and neuron responsiveness.

2

Background

In this thesis, we are interested in exploring the neural heterogeneity at the cell-to-cell level in a few different contexts. In this chapter, to understand the language and properties of the models herein, we will outline the most relevant aspects of neuroscience and the fundamental properties of dynamical processes for modelling and analyzing such systems.

To this end, while this review is by no means exhaustive, we begin in Section (2.1) where

we describe the neuron and review some classical models of single neurons and networks. We then introduce neural heterogeneity first in its broad presence across multiple scales and review in detail the cell-to-cell scale differences, and their inclusion in model frameworks, as the area of interest to this thesis (Sections (2.1.3) and (2.1.3)). Thereafter, in Section (2.2), we introduce mechanisms and models of neural adaptation, followed by a brief review of neuromodulation via stimulation in the lens of the non-invasive variety relevant to this work. Section (2.4) overviews neural networks and the analysis in the context of dynamical systems. Finally, Section (2.5) briefly reviews the numerical methods used in this work. Explicit references will follow in the text.

2.1 The Neuron

The cells that mediate all neural interactions are called *neurons*, and are themselves responsible for the transmission of electrical pulses in the form of propagating chemical gradients of electrically charged molecules known as *action potentials* [232, 183]. Neurons are comprised of three major, functionally distinct, sections: the dendrites, soma and axons [115]. In broad terms, the dendrites can be thought of functionally as the input device, collecting and integrating all of the transmissions received by the neuron; the soma is the central processing unit, performing important nonlinear steps whereby an output is created after sufficiently large input is received; and the axons are the output device, transmitting the electrical signal on to other neurons (Fig (2.1)). This oversimplified representation of the complex biophysical processes involved in neuron activity can be traced back to

the McCulloch-Pitts model [216], which reduced action potential transmission to a simple logic operation. Such simplified approaches have been widely utilized in neural network models, such as the Hopfield model of associative memory [145], and made significant contributions to scientific advancement in the artificial intelligence and statistical mechanics communities.

In their less simplified form, the exact shape, size and arrangement of neuron architectures vary immensely throughout the brain [42, 226, 182, 64], as described in Section (2.1.3). Despite this widespread heterogeneity, some populations of neurons have been found to be remarkably electronically compact [243] and, more generally, neurons demonstrate a startling amount of electrophysiological overlap [226]. Moreover, irrespective of their shape, size, location, or functional role, neurons relay their electrical signals via the sequential polarization and depolarization of their membranes via sudden discharges of electrically charged particles from the starting region of the axon (e.g. axon hillock - where the axon attaches to the soma) [232]. For modelling purposes, where biophysical detail is simplified, this discharge event is often attributed to the soma.

When neurons are at rest, the various charged particles are separated into their respective groups on either side of the membrane, creating a chemical gradient that yields a baseline or resting membrane potential of, on average, between -70 and $-80mV$ at equilibrium [71]. When this equilibriated state is perturbed by impinging chemical or electrical signals, the transmembrane voltage increases. In the event that this increased voltage surpasses a threshold level, usually around -50 to $-40mV$ [232, 183, 305, 115], a characteristic depolarization and repolarization event occurs. While various cations and anions

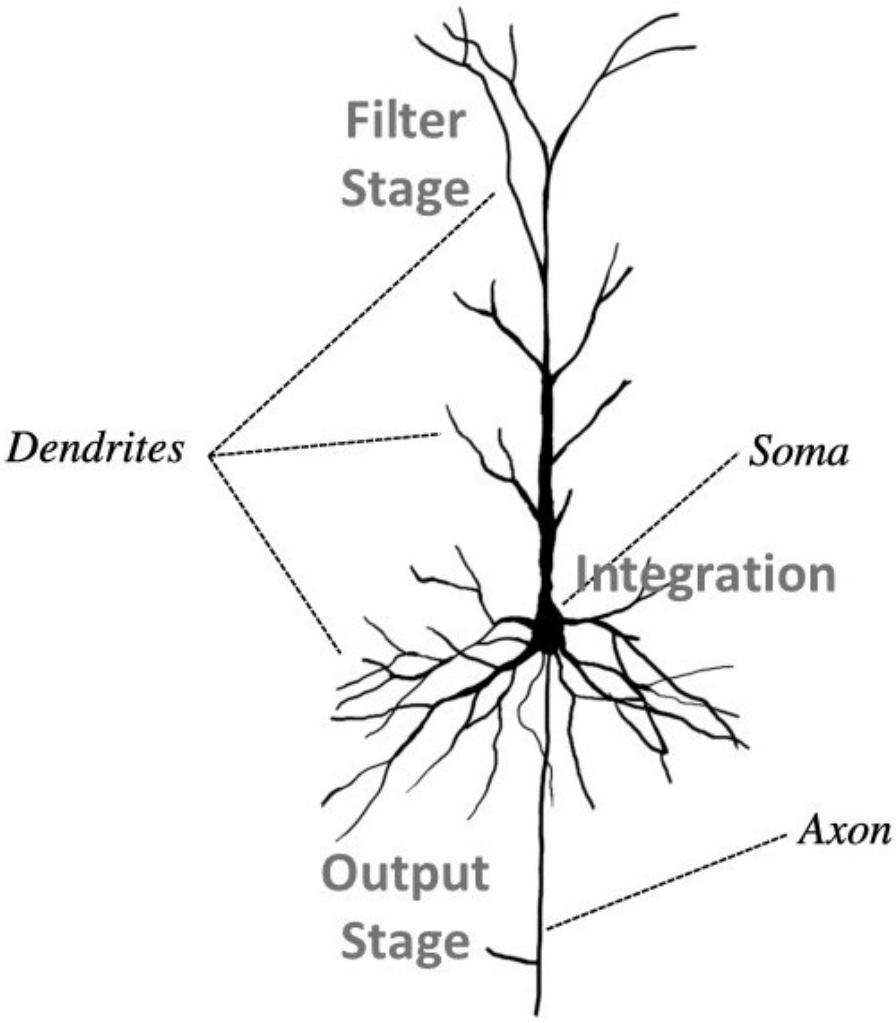

Figure 2.1: An example neuron (image from [344]) labelled to indicate the stages of processing in relation to McCulloch-Pitts like neuron models [216, 145].

(Ca2+, Na+, K+, Cl-, etc.) are involved in the overall process, the canonical conductances underlying the action potential are Na+ and K+ [231]. Specifically, when the local potential increases to the threshold level, the voltage-gated Na+ channels open, allowing an influx of Na+ ions (depolarization). This sharp, stereotyped jump in voltage is often called a *spike*. At the peak depolarization, the voltage-gated Na+ channels close, and the voltage-gated K+ channels open, allowing K+ ions to flow out (repolarization). The whole of this interaction forms an action potential, whose electrical pulse is propagated down to the axon terminals (connecting junction(s) with recipient neurons) where the post-synaptic cell(s) receive the activity as new input.

Neural excitability

Neurons receive a vast array of electrical and chemical inputs via their synapses over time. The strength with which an individual neuron responds to such incoming signals, its propensity to fire action potentials [363], is referred to as the *excitability* of the neuron. The excitability depends on an ensemble of intrinsic properties, including resting potential, input resistance, membrane capacitance, membrane pumps, and time- and voltage-dependent membrane conductances [229]. How excitable a given neuron is comes from the expression, localization and kinetics of the voltage- and calcium-gated ion channels that populate the neuron's surface [102], as well as those transmitting potassium, sodium and chloride [99]. In addition to active control by the ion channels, neural excitability is also passively regulated by the architecture or morphology of the neurons. This then contributes to type-specific excitabilities throughout the brain [237, 58], including differences for neurons across layers

for neurons of the same type [226].

Experimentally, the excitability is characterized by a form of input-output relationship of a neuron, usually obtained by application of fixed-time current pulses and measuring the frequency of action potentials evoked [229, 226]. The excitability then reflects the amount of action potentials evoked and what amplitude of current is required to generate them (e.g. the neuron's rheobase, or threshold of activation) (see Fig (2.2)). Specifically, neurons that receive low levels of average activity tend to be more excitable, such that they can respond strongly when a stimulus arrives. This manifests as producing high numbers of action potentials from lower stimulus strengths than less excitable neurons. Conversely, neurons that receive high levels of input on average need to be less responsive (e.g. only respond to strong input) and so tend to be less excitable and have a higher rheobase. This relationship can then be modelled by a number of different mathematical functions (see Section (2.1.1)).

The excitability of a neuron reflects its sensitivity to any incoming input. From a physical standpoint, it can be described as a reflection of the proximity a given neuron is to a bifurcation point [155]. That is, where a slight increase (or decrease) in input will move the neuron from quiescent to spiking behaviour (or from spiking to quiescent). The excitability, itself, can additionally be subdivided into two major classes: Type I, in which the excitability curve is continuous and has a non-zero response to even low amplitude input, and Type II, where below some critical current value there is no response, and above which an abruptly strong response is evoked [143, 155, 305].

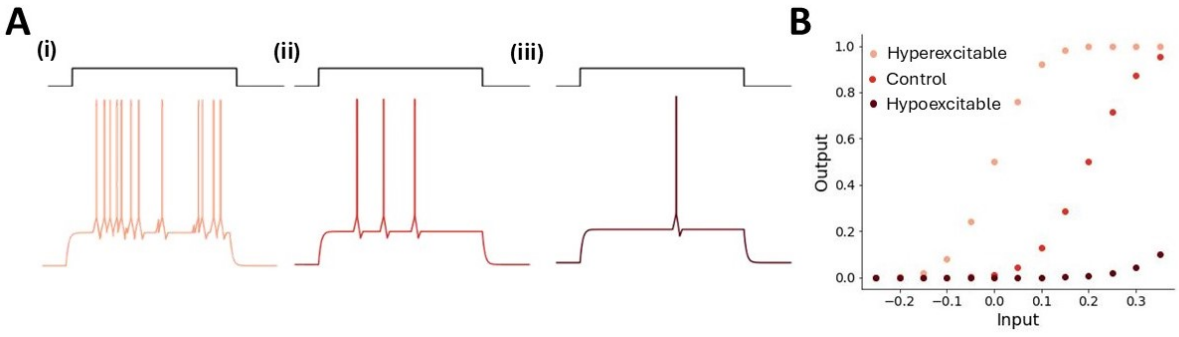

Figure 2.2: The excitability of a neuron describes the sensitivity, or responsiveness, of a neuron to a given incoming current. This is demonstrated here in three example cases of (i) hyperexcitability, (ii) mid-range (or control) excitability and (iii) hypoexcitability. When the three cases are simulated with a step current of fixed amplitude, we see that **A)** the firing rate of the hyperexcitable neuron is much higher than either the control of hypoexcitable cases. When measured experimentally, excitability describes the curve of a neuron's output (e.g. firing rate) as a function of the strength of input it receives (e.g. current amplitude). For the three cases here, **B)** examples of the excitability curve expected of the excitability levels in cases (i), (ii) and (iii) of (A) are shown. In a rate-based homeostatic framework (see Chapter 3), the hyperexcitable neuron results from adaptation to receiving low-strength input, and the hypoexcitable neuron results from receiving high-strength input.

2.1.1 Single neuron models

The long-studied [143, 144, 163, 231] sequence of events involved in depolarization and action potential generation are highly complex, with underlying molecular details that far exceed the scope of this thesis. However, since Lapique's efforts in the early 20th century ([50] and references therein), many efforts have been made to represent these complex actions of neurons in more simplistic ways by leveraging mathematical and computational tools [216, 144, 145, 114, 155, 115]. Herein, we will briefly describe a few such models, focusing on those salient to the work in this thesis.

Leaky-integrate and fire neuron model

Theorized in the early 20th century, the leaky-integrate and fire (LIF) model is the oldest and simplest neuron model. It captures the change in membrane voltage during the initial depolarization stage up to the threshold value where, biologically, the sharp voltage change of the spike occurs [305]. In simple terms, this model can be thought of as an RC circuit model, wherein a small patch of passive membrane is modelled up to the threshold and, upon reaching that threshold, a spike generation and reset mechanism is implemented.

The standard equation for an LIF below the threshold, although many variations have seen been developed [155, 305, 115], is given by:

$$C\frac{dV}{dt} = -g_{leak}V + I \tag{2.1}$$

where V is the membrane potential, C is the membrane capacitance, g_{leak} is the conductance, and I is the total current flowing through the cell. Whenever the artificial threshold membrane potential value, V_{th}, is reached (e.g. $V = V_{th}$), the neuron fires a spike and V is reset to some chosen resting membrane potential value, V_r (see Fig (2.3A)). The LIF model is an early example of a conductance-based model where, representing passive phase of somatic activity, the incoming currents, I, determine the neuron's subthreshold dynamics.

This simple model represents a case of a single compartment model, neglecting dendritic and axonal considerations. Nevertheless, LIF models have persisted in use due to their ability to simplistically mimic membrane potential dynamics sub-threshold. This is of great computational benefit, as it allows for modelling of populations in a simplified manner without losing all the relevant dynamics. Moreover, when somewhat more accuracy has been desired, LIF models have been modified in a number of ways to incorporate noise, specific ion-currents, adaptation currents, and synaptic currents due to recurrent connections [114, 115].

Hodgkin-Huxley neuron model

In their seminal research in 1952, Andrew Hodgkin and Alan Huxley created the first detailed mathematical and computational model of the ionic currents involved in action potential formation [144]. In contrast to the LIF, this model (hereafter referred to as the HH model), was created based on their recordings from squid giant axons, where they subsequently modelled the activity of three major ion types: K+, Na+, and a leak current

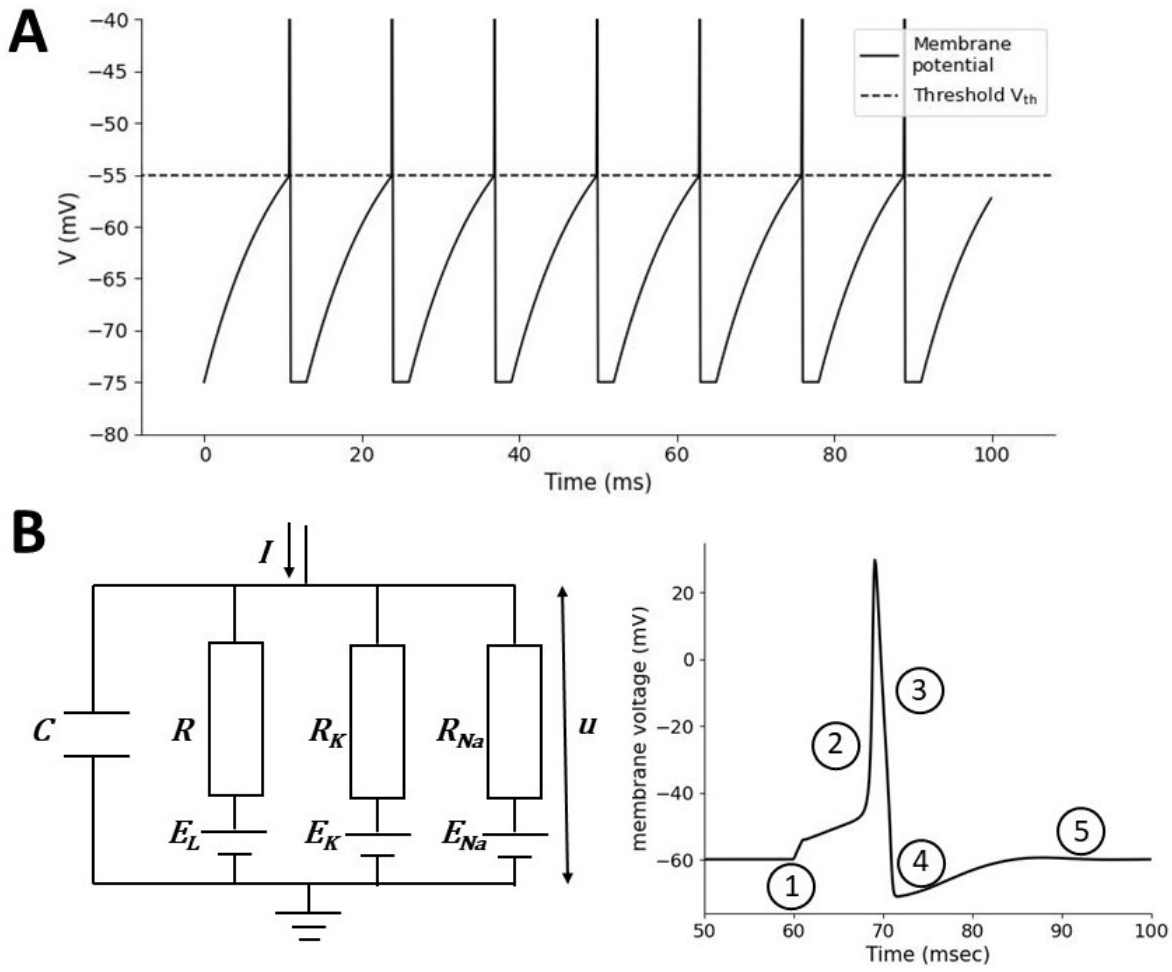

Figure 2.3: **A)** An example trace of the membrane potential from the simulation of a LIF neuron model. Threshold $V_{th} = -55mV$ and reset potential, $V_r = -75mV$. **B)** A schematic of the circuit for a Hodgkin-Huxley model (left) and an example action potential generated by the model (right). The action potential has five stages indicated by the numbers: 1) stimulation, 2) depolarization (e.g. Na+ ions in), 3) repolarization (e.g. K+ ions out), 4) hyperpolarization, and 5) return to the resting state voltage.

that consisted primarily of Cl- ions (Fig (2.3B)). Specifically, they were able to relate the membrane potential dynamics to the interplay in timing of multiple voltage-gated ion channels, with their activation and deactivation acting based on membrane current dynamics (Fig (2.3B)). This led to quite a realistic description of action potentials, for which Hodgkin and Huxley later won the Nobel Prize.

The concentration of inside and outside the soma of a given ion species, i, responsible for their equilibrium potentials, E_i (also called Nernst potentials) is related by:

$$E_i = \frac{RT}{zF} ln \frac{C_{i,out}}{C_{i,in}}$$

where $C_{i,out}, C_{i,in}$ are the respective outside and inside ion concentrations, z is the valence of the ion, R is the ideal gas constant, T is the temperature, and F is the Faraday constant. The Nernst potentials indicate the equilibrium voltage for a given neuron. When electrical perturbations are induced, the ion-species dependent currents that result are a function of the instantaneous voltage, V, the conductance of ion-type i, g_i, and the Nernst potential of that ion type. The relationship for this interaction is given by:

$$I_i = g_i(V - E_i).$$

According to Kirchoff's laws, the sum of the currents across a given patch of membrane must equal to zero. Hence, we can write,

$$0 = \sum_i I_i + C\frac{dV}{dt} - I$$

where I is the presynaptic input to the neuron, C is the capacitance equal to the inverse resistance (R^{-1}), and $C\frac{dV}{dt}$ is the capacitive current of the membrane potential and i are the sum over the various ionic currents. If we substitute in Eq 2.1.1 and expand the summation, this can be rewritten such that the dynamics of the membrane potential arises,

$$C\frac{dV}{dt} = -g_{Ca}(V - E_{Ca}) - g_K(V - E_K) - g_{Na}(V - E_{Na}) - g_{Cl}(V - E_{Cl}) + I \qquad (2.2)$$

where g_i and E_i are the conductance and Nernst potential, respectively for ion $i = \{Ca2+, Na+, K+, Cl-\}$. The exact structure of a given conductance function, $g_i(V)$, has been omitted here. However, it can be found in any of [232, 305, 115]. Although the original HH model described a three-current system, later iterations expanded this initial trio to include other ion channel dynamics [163, 114, 1, 115]. In addition to its expansion to include other ion species, the HH model remains foundational to computational neuroscience and is still frequently used, particularly for detailed, multi-compartment models of neurons [140, 141, 316, 317], used in Chapter 5.

Other conductance-based models

The HH model and LIF model, represents only two of the more famous types of single

neuron models. However, between them, a variety of neuron models at similar or intermediate levels of detail exist. Generally, these conductance-based models follow a standard formulation written as,

$$C\frac{dV}{dt} = -\sum_j g_j(V - E_j) + I_{ext}$$

where $g_j = \bar{g_j} a_j^x b_j^y$, such that a_j and b_j are activation and inactivation gating variables for ion channel, j, raised to integer powers x, y and described by equations with first-order kinetics [300, 155]. $\bar{g_j}$ is the maximal conductance for ion channel j. That is, conductance-based models consist of sets of ordinary differential equations (ODEs), as derived from current flow in a circuit representation following Kirchoff's law. Indeed, generally, any conductance-based model is based on four assumptions: i) different ion channels in the cell membrane are independent from each other, ii) gating variables for the (in)activation of these voltage-dependent channels are independent of each other for a given ion channel type, iii) every gating variable follows first-order kinetics and iv) the model cell compartment is isopotential [300].

Many examples of such models exist, such as the Morris-Lecar model [228], where a calcium current with instantaneous activation is paired with a slower activation potassium current and a leak current; and the FitzHugh-Nagumo model [100], a two-dimensional equivalent to the HH model with the detailed conductance dynamics replaced with an artificial recovery variable. These models, in particular, leverage their comparative mathematical simplicity to the HH model, and have been studied in detail using dynamical

system and bifurcation analyses. Further details on these models can be found in [155, 305, 115].

Compared to simplified cases like the LIF or McCulloch-Pitts models, when biophysical detail is required, many dendritic and axonal compartments must be modelled to represent the neurons' features [316, 317, 359, 3, 4]. With this increase in compartment number comes an increase in degrees of freedom and mathematical complexity. For computational efficiency, such models are often solved using the NEURON simulation environment [140, 141], which leverages a number of simplifications and assumptions to allow reasonably timed simulations (see Section (2.5)). As a result, computational representation of hundreds of physiological and chemical variables can be allowed to evolve in real time while complying with the constraints of the neuron's design.

Rate based models

The conductance based models described thus far have great utility in understanding the dynamics of individual neurons through time with respect to their more biophysical underpinings, if somewhat coarsely. However, from the perspective of theoretical and computational neuroscience, such detail is not always necessary and can, indeed, be further simplified even beyond what is done for single-compartment LIF neurons. That is, while for some cases, such as information encoding in the fly visual system [279, 202] and the phase of low-frequency oscillations when rat place cells fire to encode position [156], the specific timing of a given action potential is crucial, this is not always the case. In fact, early experiments in the cutaneous receptors of frogs [6, 305] found that the firing frequency was

proportional to the input intensity. If we ignore the different phases of the action potential (Fig (2.3B)), one can represent the spiking activity of a neuron as a spike train, $S(t)$. This is used in rate based models, with a cell's spiking activity given by,

$$S(t) = \sum_k \delta(t - t_k) \tag{2.3}$$

where t_k are the moments at which the cell fired and δ is a Dirac delta function. This description is very well suited to the statistical and probabilistic way neurons are often modelled for theoretical frameworks.

The firing rate of such a neuron can then be calculated by analyzing the time course of the spike train over a sliding window of time, τ. That is, the firing rate, $r(t)$, is given by,

$$r(t) = \frac{1}{T} \int_t^{t+T} S(\tau) d\tau \tag{2.4}$$

where T is an averaging period. This may subsequently be further averaged over some number of neurons, N, to obtain a population average firing rate, $\langle r(t) \rangle_N$. The most straightforward way to arrive at the firing rate a neuron is to use the output of a conductance-based model like Eq 2.1 or 2.2, and find the rate of the resulting spike train from Eq. 2.4.

Model excitability functions

Biophysically, neuron excitability represents the instantaneous sensitivity of a given

neuron to any input it receives by mapping the frequency of the output firing rate to the continuous input injection over a range of increasing amplitudes (see Section (2.1) and Fig (2.2)). The excitability itself can be thought of as an input-output function, whereby the input collected and integrated throughout the dendritic arbor is filtered and transformed to the resultant firing rate [350]. In computational and theoretical works, this transformation is modelled as a nonlinear input-output function (i.e. neural gain), [72, 66, 299] hereafter referred to as the *excitability curve*. Experimentally, the excitability curve is measurable as the output firing rate of a neuron in response to injections of continuous input current. However, many cortical neurons do not receive continuous input *in vivo*.

The excitability curve, f, although experimentally shaped by the temporal fluctuations of the input currents to a given neuron, is commonly formulated as a sigmoid [183, 185, 276, 275, 311] as a shape close to that seen from experiments [226]. However, other nonlinear functions (e.g. Heaviside functions [216, 305] and error functions [153, 152]) have also been used. The parameterization of these functions typically involves a threshold, h, around which firing rate increases significantly, and its slope, β, at the inflection point. The parameters used, and hence shape, of the excitability curve determines the dynamics of each neuron [183, 90]. An example of this was shown in network simulations [90], where instances of more linear excitability are less selective and allow both weak and strong inputs to propagate to the output. Conversely, very nonlinear excitabilities respond only to strong streams of input. Moreover, endowing network models with heterogeneous excitability curves has been shown to reduce the probability of the network entering hypersynchronous regimes, stabilizing the dynamics [275, 153].

When the net input to a neuron, u, is sufficiently high, the excitability curve will yield sustained firing activity, and eventually saturate to the refractory period. However, for cases where the input is time dependent (e.g. $u \to u(t)$), the firing rate, r, can be thought of as a linear activity around the steady-state solution such that,

$$\frac{dr}{dt} = -r + f(u(t)) \tag{2.5}$$

This approximation of the firing rate works only under specific conditions. Notably, it assumes that each neuron is integrating a large number of inputs and its ability to predict the spiking behaviour accurately is heavily dependent on the averaging time, T, over which the rate is computed. Further details can be found in [305, 115].

Beyond the rate, provided the timescale of action potential duration is small relative to the synaptic time scale, it may also be shown [45, 183] that these smooth excitability curves characterize the spike train (Eq (2.3)). That is,

$$S(t) = \sum_k \delta(t - t_k) \approx f(u) \tag{2.6}$$

These excitability curves are particularly important as they enable neurons to integrate information from different sources nonlinearly [293], crucial for its applications in encoding, attention, perception and cognition [72, 293, 66, 299, 97].

Importantly, although excitability is frequently included in models as a form of static heterogeneity [220, 275, 112] (see Section (2.1.4)), the exact features made heterogeneous

are not ubiquitous across models. That is, the excitability may be modelled as a threshold, a slope, a maximum amplitude of response, or a combination of these features [229, 299, 220, 97, 153]. Often, models tend to use thresholds as the most easily accessible value. However, leveraging only one aspect of the excitability does represent a limitation - one that is often shared with experimental analyses, which, similarly, often consider only the threshold [220, 275, 153, 152] - as it neglects to explore the full parameter space [229]. It may be, if more fully explored, that the excitabilities across neurons or within a certain subpopulation are more ubiquitous than they initially appear. However, the stimuli used to experimentally generate excitabilities are often somewhat arbitrary. This can support the use of less detailed models of excitability as the excitability itself can be directly influenced by the duration of stimuli [229].

2.1.2 Network models

Beyond single neurons, it is a natural progression to model the interaction of groups, or networks, of neurons. For computational efficiency, these models are commonly designed so each neuron in the network is represented by a simplistic model along the lines of LIF or rate-based units rather than a more detailed HH model. Network scale models represent an important contribution to the study of neural systems as, in the brain, neurons do not act in isolation. Rather, each neuron has along its dendrites (Fig (2.1)) a series of connection points, called *synapses*, that allow electrical impulses and chemical signals to propagate in from the axons of other cells. It is, thus, incredibly rare for neurons to act without at

least some input from other connected cells in the same ensemble. Indeed, far from the complexities of ion channel activity described in the neuron models discussed above, at the network level, the dynamics are a function of the connectivity scheme of the network and the strength or *weight* of those connections [115].

The connections between any two neurons can be *excitatory*, wherein the input from the pre-synaptic cell promotes more activity in the recipient post-synaptic cell, or *inhibitory*, where the input pushes the post-synaptic cell toward quiescence. Physiologically, these interactions are determined by the type of neurotransmitters (e.g. molecules) released from the presynaptic cell and taken up by the postsynaptic cell [163]. The timing, strength and frequency of these interactions lead to a whole host of dynamics within a given ensemble of neurons [92, 115]. As will be elaborated on in Section (2.2), these interactions are, themselves, adaptable in time. Physiologically, this occurs through biological pressures and shapes the function and dynamics of different circuit ensembles.

Collectively, the study of connected ensembles of neurons in networks represents a cornerstone in understanding the brain. However, as was the case with single neuron models, there have been and continue to be a variety of models and approaches taken to such a study [92]. Broadly, network models are often classified as those that are spiking and those that are rate-based. In both cases, the dynamics observed in the network will be affected by the scale, connectivity, synaptic weights, and delays (if present) in the network [92, 155, 115]. The inclusion of realistic network synaptic connectivities, for example, has been shown to have nontrivial effects on phase transitions of neural networks [154]. Moreover, increased variability in the in-degree (e.g. pre-synaptic connections) has been computa-

tionally shown in a rate-model to drive transitions between asynchronous and oscillatory regimes [287]. Meanwhile, the same study showed that increasing the variability of the out-degree (e.g. post-synaptic projections) increased the amplitude of cross-correlations between neurons by elevating the number of common inputs between neurons. The choices for such parameterization depend on multiple factors, including the scale of interaction of interest (e.g. a localized region versus whole brain dynamics), computational efficiency, the dynamics of interest, and what level of detail is necessary for the question(s) being asked.

Although a wide range of classes of network models exist, the network-level modelling done in this thesis primarily leverages a generic network of spiking neurons [151]. In this network, the membrane potential, $u_i(t)$, of the neurons $i = 1, ..., N$, evolves according to a set of nonlinear equations given by

$$\tau \frac{du_i}{dt} = -u_i + \frac{1}{N} \sum_{j=1}^{N} w_{ij} S_j(t) + I_i(t) \tag{2.7}$$

where τ is the membrane time constant, w_{ij} are the synaptic weights between neurons i and j, $I_i(t)$ is a baseline current and $S_j(t)$ is the spike train of neuron j (see Eq (2.3)). In line with Section (2.1.1), this spike train can be characterized by the excitabilities of the neurons (Eq (2.6)), thus allowing the excitability of the neurons to be included in the model.

The dynamics of this network are similar to a modified version [151, 275, 153] of the Wilson-Cowan model, which we will briefly review below. For an expansive review of different types of network models, see [92, 155, 115].

Wilson-Cowan network models

For studies in which it is of interest to understand the interplay between excitatory (E) and inhibitory (I) cell populations, the phenomenological model developed in the 1970s by Hugh Wilson and Jack Cowan [353, 352] is widely used, having been cited over 1000 times [84, 276, 275]. Their model focuses not on the microscopic properties of neurons, but was instead formulated to capture the large-scale dynamics of populations of neurons, modelling them as very simple cells. Their approach leverages mean-field theory from statistical mechanics to describe the mean activity level in a population of neurons over time through a set of ordinary differential equations and uses a nonlinear readout function (most commonly a sigmoid) to represent the interaction between populations [352]. Owing to its widespread use, many formalisms of the Wilson-Cowan model exist; we briefly describe one such formalism (see [87]).

For two populations of neurons, one excitatory (E) and the other inhibitory (I), the model can be expressed as,

$$\frac{dr^E}{dt} = -\alpha^E r^E + (1 - r^E)p^E f(s^E) \tag{2.8}$$

and

$$\frac{dr^I}{dt} = -\alpha^I r^I + (1 - r^I)p^I f(s^I) \tag{2.9}$$

where $r^{E,I}$ are the firing rates of the E and I neurons, $p^{E,I}$ is the probability of an

excitatory or inhibitory neuron going from quiescent to active in a given time step, $\alpha^{E,I}$ are the time constants, f is a sigmoidal excitability curve (see Section (2.1.1)), and $s^{E,I}$ are the activity of the two neuron types given by,

$$s^E = (w^{EE}m)/K^E - (w^{IE}n/K^I + I^E) \tag{2.10}$$

and

$$s^I = (w^{EI}m)/K^E - (w^{II}n)/K^I + I^I \tag{2.11}$$

where the w's are the synaptic weights, $I^{E,I}$ are applied stimulus to each population, $K^{E,I}$ are the number of excitatory and inhibitory neurons total, and m and n are, respectively, the number of active excitatory and inhibitory neurons in a given time step.

Owing to its relative mathematical simplicity, these types of Wilson-Cowan models have been extensively studied in their dynamical properties, including the ability to generate limit cycle (e.g. neural oscillation) dynamics, hysteresis and stable states [84]. Moreover, the Wilson-Cowan model has since been adapted to model a number of different frameworks and served as a starting point for many extensions. A non-exhaustive listing of examples of its usage includes explorations into *balanced* networks (where the excitatory and inhibitory inputs cancel on average) [271], response robustness of networks to stimulation [151, 276], and epilepsy [275, 153].

2.1.3 Neuronal Heterogeneity

As described in Chapter 1, heterogeneity is a widespread property of many biological and physical systems. This includes the brain, where heterogeneity is pervasive across scales [42, 62, 226, 227]. At the macroscopic level, the brain is comprised of functionally distinct regions (e.g. cerebral cortex, brain stem etc.) [163, 252]. While the presence of these high-level structures is ubiquitous within species, their size has been observed to be heterogeneous between individuals as a function of age, sex, and head size [328, 256, 355, 198, 16]. These heterogeneities have functional outcomes, such as sex-specific latencies in auditory brain stem response [157, 328] and correlations between cortical volume and memory [283, 158].

The focus of much research in the mammalian, and especially human brain, has been on the cortex. This structure is comprised of many sub-regions (e.g. visual cortex, motor cortex, etc.) [163, 252]. Importantly, despite these regions being populated by many of the same neuronal subtypes [58], each has its own functional role(s). Indeed, the identification of these regions was a crucial part of historical neuroscience, starting in the late 18th century, when observational descriptions of the brain were being regularly updated as new autopsies and experimentation elucidated evidence that moved science away from the original notion of the cortex as one uniform entity without substructure [118]. As time went on and experimentation improved, mappings of the different cortical areas began to arise, including famous examples such as Broca's 1861 classification of the speech-language center in the left hemisphere [47], and Penfield's homunculus description of the motor

cortex [254]. Importantly, similar to the macroscopic scale, though the subregions are present across individuals in a given species, their volume and density are heterogeneous across individuals and may change with age and development [126, 125, 16, 113]. The exact extent of inter-individual heterogeneity of these regions remains unknown, and has made their identification a complex task despite advancements in imaging techniques such as magnetic resonance imaging (MRI) [113]. Nevertheless, their identification represents many important applications to the study of aging [355], pathologies [132, 280, 158] and linking structure and cognition [113]. Moreover, recent research in macaque monkeys has found the neurons in different cortical regions have different biophysical properties that support the functional outcomes of the region [98].

Many of the functional differences at the microscopic level of the brain are attributed to the respective patterns and strengths of connectivity within the microcircuits that comprise them [159, 58]. Within the cortex, different layers and cell types have stereotypical motifs of connectivity [159, 93, 58]. However, the exact connectivity of any given cortical circuit is heterogeneous with respect to other circuits, and between individual brains [125, 113, 58]. These heterogeneous connectivities are of interest for how they influence the computational properties and dynamics of local microcircuits [273, 40, 179, 207, 93]. The inter-individual heterogeneities in connectivity have further contributed to large response variability in neuromodulatory interventions [198, 16, 126]. Abnormal connectivities have been linked to a variety of pathologies, including major depression, schizophrenia and autism [233, 237, 322].

Beyond these more macroscopic heterogeneities, the heterogeneity of interest for this

thesis is that of the neurons themselves. The observed heterogeneity at the neuron level can, broadly, be broken down into two major contributing groups, which will be discussed more thoroughly below: the morphology (e.g. architecture) of the neurons and their electrophysiological (e.g. biophysical) properties. These intercellular heterogeneities have been shown to be important to neural coding [324, 220], dynamical stability [153, 152], decorrelation [149] and maximizing information optimization [335]. That is, the underlying heterogeneity of the neurons contributes to the observed network dynamics, which can, in itself, be heterogeneous (e.g. asynchronous) or not (e.g. synchronous). Importantly, the heterogeneities observed intercellularly also exist between cells of the same type [42, 226], and we are thus interested in exploring the consequences of underlying heterogeneity both between and within cell types.

Neuron morphology

The arrangement of cellular projections (e.g. dendrites and axons) about the somatic body of a neuron is called the cellular architecture or *morphology*. Among the vast number of neuron types [295, 182], many morphologies exist both between and within neuron types. Classifying neuron morphologies has long been of interest [173], and attempts to define distinct groups based on these properties continue to be of interest [56, 42, 122]. In more recent works, morphological features including dendritic and axonal shapes, and branching patterns have been found to be particularly informative in creating appropriate classifications [362]; however, more detailed features such as soma size, spine density, cell size, and dendtric and axonal length have also been considered [359, 182, 67, 327].

From early explorations, one of the primary interests in studying the architectures of neurons, beyond classification, was to understand their potential contribution to dendritic integration [222]. Specifically, neuron morphologies are directly related to the number and position of the synapses along any given dendrite. This is related both to the connectivity available to a given neuron [58] and, based on the impinging pre-synaptic activity it receives, the net integration of input that reaches the soma [286].

As methodologies and our ability to fully visualize the morphologies of neurons improved, it became apparent that, while some groups of neurons share similar morphological features [362], there is considerable heterogeneity within cell types [226, 182, 67]. As a result, in addition to renewed efforts to define specific classes, interest grew in understanding the role of morphology in a larger context. Owing to the experimental difficulty of this task, computational approaches have been leveraged to build detailed models [316, 317], which have been used to explore the effect of morphology on neuron response [226], circuit-level dynamics [207], and stimulation [359, 327].

Recent work has demonstrated further potential for a functional role of morphology, with a class of excitatory hippocampal neurons being found morphologically distinct from their pyramidal counterparts and having specialized dendritic architecture associated with object memory [167].

Electrophysiology

As with morphology, the heterogeneity in the electrophysiological properties within and between cell types has become increasingly apparent as databases have reached new

heights of precision [226, 58, 182, 67, 227]. Examples of such traits include input resistance, rheobase, sag voltage, action potential width, resting potential, average firing rate, average interspike intervals, myelination patterns, and neural excitability [226, 58, 182, 67, 57, 227], the latter of which is the primary source of heterogeneity considered in much of the work in this thesis.

These properties have long been targeted as traits of interest for classification [182, 67, 44] in how they influence neuron response to input (e.g. stimulation, noise, etc.). Moreover, recent work has demonstrated the importance of such heterogeneity to maintaining stability in the dynamics of networks of neurons [152, 5] and avoiding pathological states [275, 153]. Additionally, electrophysiological heterogeneity has been implicated in improved information encoding [219, 112], signal decorrelation [248], and synchronization [121, 120, 349, 46]. Although there are many contributing factors to the net heterogeneity in the electrophysiological properties of neurons, for the purposes of this thesis, we will focus on the neural excitability.

2.1.4 Including heterogeneity in neuron models

As the pervasive nature of heterogeneity in neural systems has become increasingly clear, the question has arisen of how much and what kind(s) of heterogeneity should be included in model systems for the replication of experimental data [243, 17] and to appropriately investigate neural dynamics [248, 220, 275]. The answer to this question remains unknown.

Despite this relative uncertainty, over the last three decades, heterogeneity has been

increasingly of interest for study within computational and theoretical studies. Among the aspects heterogeneity has been found to affect are synchronization [121, 349, 120, 287, 219, 46], phase transition [11, 154, 22], encoding and decoding [219, 112], neuronal correlations [287, 360] and stability [275, 23, 153, 152]. The source of heterogeneity in these studies varies, although common choices include the connectivity and threshold (see Section (2.1.1)).

In many cases, when heterogeneity is incorporated in neural models, it is included as a static metaparameter, or assumed to be accounted for by additive noise [137]. However, it is well known that many of the heterogeneous properties of neurons are non-static [205, 204, 246, 245, 208]. In fact, many of the properties of neurons undergo forms of adaptation in response to past activity.

2.2 Mechanisms and models of neural adaptation

Neural activity exists in a state of constant fluctuation as it contends with an unending stream of sensory input and noise. These inputs span a wide range of time scales, frequency, and strength [92, 81, 305, 115]. The relationship between this incoming information and the neuron response is often referred to as the neural code, wherein the output firing activity of neurons is presumed to be directly reflective of the parsed input they received. Specifically, the neurons are presumed to selectively encode and propagate the pertinent information extracted from the net sensory input [90, 94, 347]. To contend with these vast sources of input, the neural input-output relationship must be history and context-dependent. Many

time- and activity-dependent mechanisms act to ensure this at the synaptic, neuronal and network levels. This is broadly classed as *adaptation* and is critical for continued brain function.

At its core, neural adaptation is a dynamic process. That is, it is the combination of the fast response of neurons to abrupt changes in the input they receive and the slow, inhibitory effect that gradually decreases the responsiveness of the neuron to persistent activity [347, 31] (see Fig (2.4)). The decrease in response to constant stimulus is seen in the majority of neurons, which demonstrate phasic-tonic responses [31], indicating inhibitory contribution. Indeed, an example mechanism for adaptation is seen in voltage-gated calcium channels, which open during action potentials to allow calcium influx into the neuron. The calcium-activated potassium currents subsequently act subtractively on the input current and inhibit the generation of action potentials [163]. Said otherwise, the inhibitory effects recruited during adaptation gradually shift the threshold of input required for high-frequency output to persist. This decay in response acts as a high-pass filter, suppressing the response of the neuron to low-frequency stimulus components [32, 31].

Biologically, this adaptation represents a response by *output*-driven mechanisms to self-inhibit neuron response. This is an important distinction from *input*-driven mechanisms, such as synaptic plasticity, where the changes occur to inhibit the pre-synaptic input before it is translated into neuron response. Examples of this inhibition include mechanisms such as short-term depression and synaptic pruning (see [163]), wherein the strength or number of pre-synaptic connections are modulated (Fig (2.5A)). This synaptic plasticity, being input-driven, is far more specific in its modulation. That is, unlike the adaptation

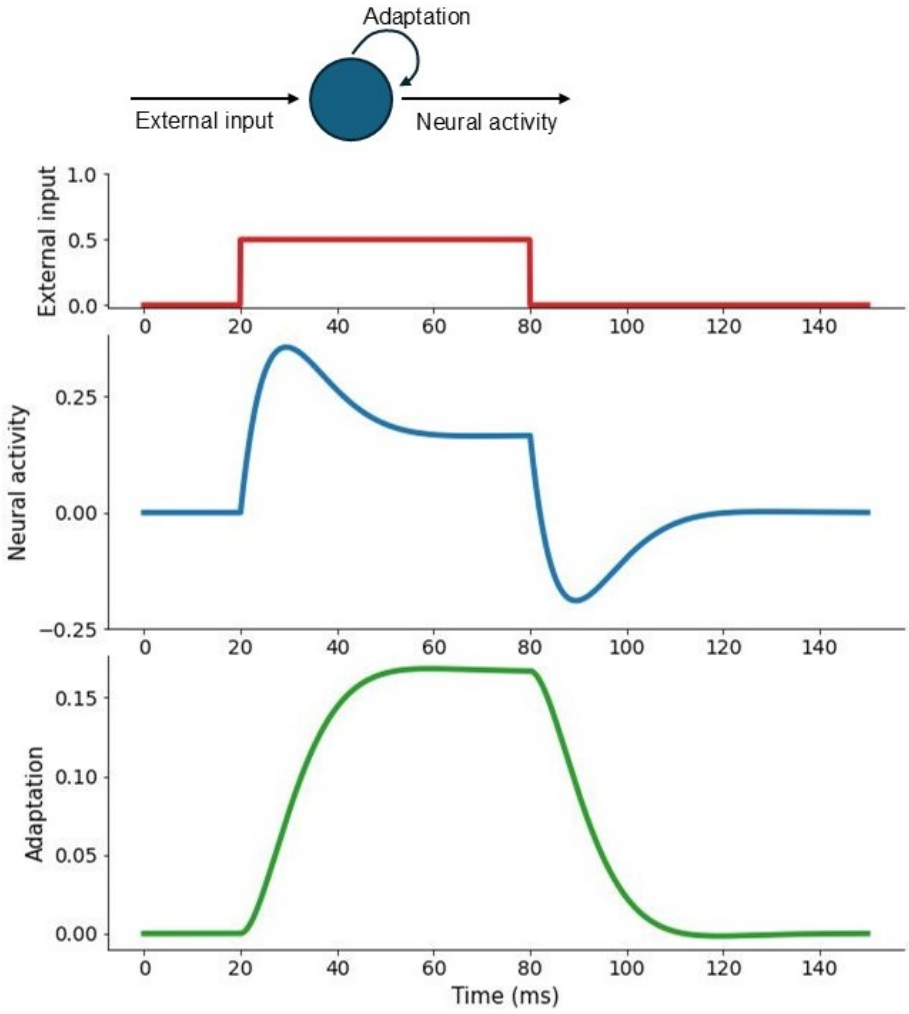

Figure 2.4: A schematic and simulation of neural adaptation. For a given neuron, the response to increased input via stimulation can be attenuated through adaptation mechanisms. The cessation of external input then results in a reversal of this adaptation. Here, this is simulated for a single neuron with activity, x, receiving an external input, I, with dynamics following $dx/dt = \tau_x^{-1}(-x + I - b\eta)$, where $\tau_x = 5$ms is the membrane time constant, $b = 2$ is the amplitude of adaptation, and η is the adaptation. The adaptation dynamics are given by, $d\eta/dt = (x - \eta)\tau_\eta^{-1}$, where $\tau_\eta = 30$ms is the adaptation time constant.

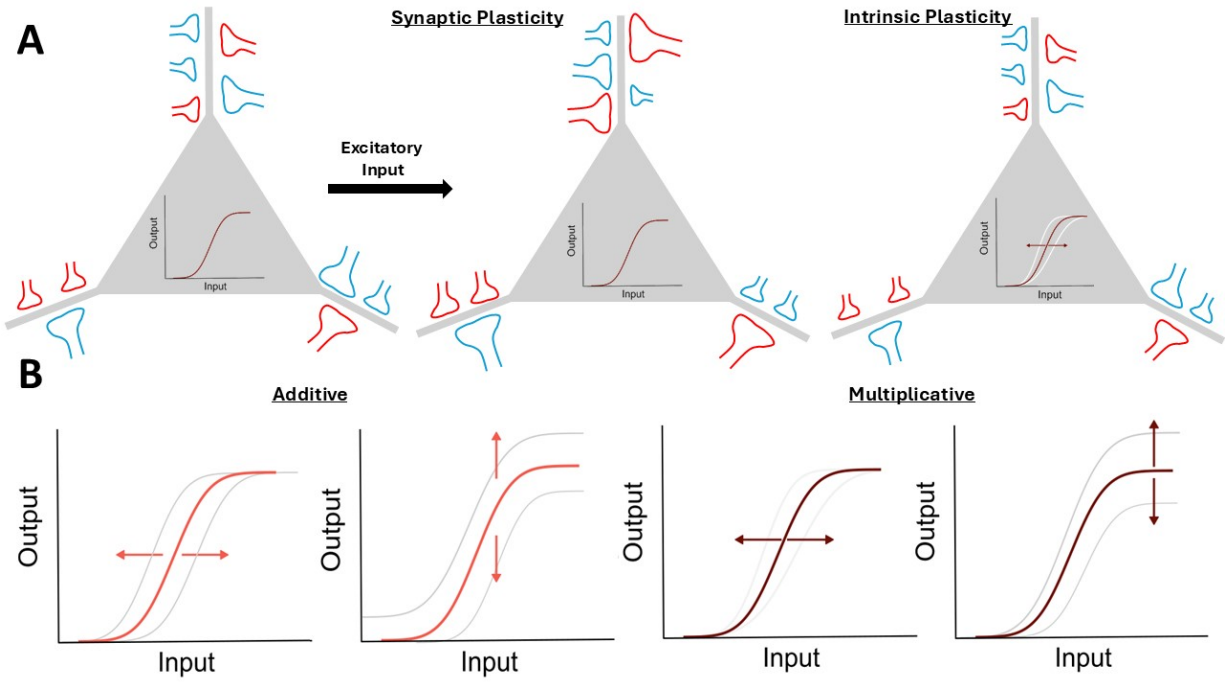

Figure 2.5: **A)** Schematic of the difference between synaptic (middle) and intrinsic (right) plasticity. In response to receiving continuous excitatory input, a neuron (left) may adjust its firing rate through synaptic mechanisms (middle) such as increasing or decreasing specific synaptic strengths, or the neuron may instead modulate its firing rate by changing its excitability via intrinsic plasticity (right). **B)** Intrinsic plasticity can be performed multiplicatively (right and mid-right) or additively (left and mid-left).

being discussed here, synaptic plasticity regulates the response of a neuron to input from a specific connection. Neural adaptation via output-driven mechanisms, as is the adaptation of interest in this thesis, pertains instead to the modulation of the neurons' intrinsic excitability (e.g. intrinsic plasticity) (Fig (2.5B)). This type of activity modulation alters the sensitivity of the neuron to *any* incoming input. As such, synaptic plasticity will not be discussed further in this work (for reviews of synaptic plasticity see [364, 95, 96, 106]).

Phenomenologically, neural adaptation varies considerably between brain regions, both in exact biological contributions (see Section (2.1)) and timescale. This is necessary to accommodate the diverse functionality of those regions, such as the 'slower' adaptation required by the visual system, on the order of hundreds of milliseconds to seconds, compared to the more rapid auditory adaptation that occurs in the milliseconds range [31]. A contributing factor to this stems from the type of input the neurons in different regions receive. Natural stimuli, unlike the rigorously controlled timing of experimental work, are not switched on and off at steady intervals. Rather, they change gradually with time, such as the visual system adapting to the onset of night or the coming dawn. Faster timescales, however, are also necessary as the mean light intensity rapidly changes with, for example, fluorescent lights being switched on and off inside a building. To contend with this variety of timescales, many neurons both gradually and continuously adapt [94]. That is, many neurons first adapt to the slower changes in stimulus mean, filtering out low-frequency contributions, which converts variance changes to changing mean values [31], before adapting again to the resultant mean value, this time by scaling the excitability along the input axis. This two-step system has been observed in both auditory and visual systems [164, 74].

Beyond sensory input, for which it is also critical, flexibility in neurons via adaptation has been implicated in a number of other functions, including more effective information encoding [299, 90, 347], predictive coding [346, 31], feature selectivity [183, 185], and attention and learning [97].

The breadth of biological mechanisms involved in, and models there of, adaptation

far exceeds this thesis (for more comprehensive reviews see [299, 94, 347, 31]). Rather, here we focus on excitability modulation, or intrinsic plasticity, and review two models of adaptation that adhere to the general principles used to model adaptation in neuron models.

2.2.1 Intrinsic plasticity

Intrinsic plasticity is an activity-dependent form of modulation of neural excitability (e.g. gain modulation) [331, 83, 77, 193, 97, 326], at the neuronal level. That is, it modulates the neuron's excitability on the basis of the past activity the neuron received. Unlike the synaptic plasticity described previously, this type of adaptation affects the neuron's sensitivity to any incoming input [350] (Fig (2.5A)). Thus, intrinsic adaptation represents a trade-off between the neuron's responsiveness and its selectivity to specific signals. The modulation of excitability directly regulates the input-output function of the neuron, by changing the slope of the gain or by shifting its rheobase (the minimum amount of current required to evoke an output response) [299, 97]. The adaptations that occur can modulate the input or the output of the excitability (see Fig (2.5B)).

In the case of the input being modulated, the neuron's response can be changed in an additive manner, equivalent to a shift in the rheobase of the neuron. Alternatively, the modulation can be multiplicative, wherein the slope of the excitability is tuned.

If the output is modulated instead, the additive adaptation will manipulate the amplitude of the excitability (e.g. the maximum and minimum output). The mulitiplicative

output adaptation then modulates the slope, as occurred for input adaptation. However, in this case, the altered slope may also yield a higher maximum output. Although formulated here as independent operations, it is important to note that neurons have the ability to perform such adaptations concurrently [299, 97].

The ability of neurons to adapt their excitabilities is crucial for the dynamical range of the brain, as, in the absence of such adaptation, neurons would be capable of responding the same to any incoming stimulus. This would subsequently reduce the maximum encoding capability of the brain, diminishing its overall information. In line with this, intrinsic plasticity has been associated with learning and memory formation [363, 229, 82].

Many contributing factors may trigger intrinsic plasticity, including both input factors such as the excitatory/inhibitory balance, synaptic dynamics, timing/synchrony of inputs, shunting inhibition, and the input amplitude and position (e.g. along the dendrite), and properties of the neuron itself such as its total conductance, depolarization state and fluctuations in the membrane potential. Indeed, the excitability itself can be thought of as an input-output function whereby the input collected and integrated throughout the dendritic arbor is filtered and transformed to the resultant firing rate [350]. As such, any alterations to the input received need to be integrated and, to cope with the wide range of input, neurons must successfully adapt their responsiveness on relatively short time scales.

The availability of this adaptation is of particular importance at the network level, where it has been hypothesized that intrinsic plasticity could modulate cell-to-cell heterogeneity in excitability (Fig (2.6)). Specifically, when receiving statistically different inputs,

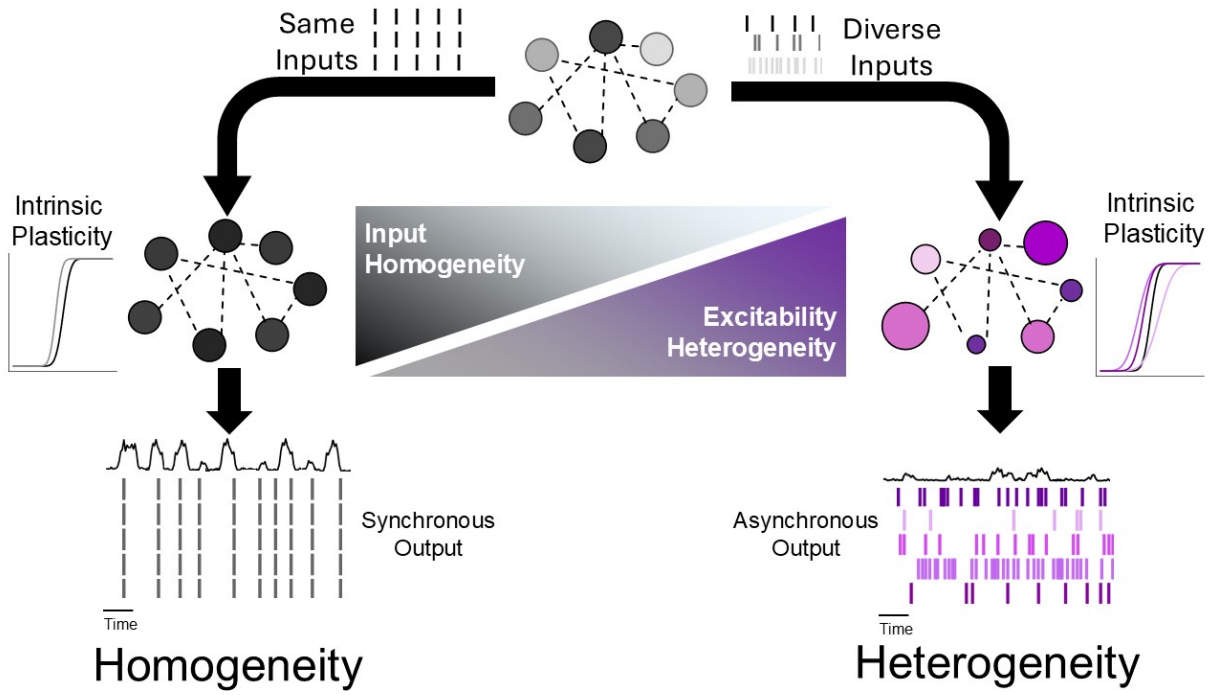

Figure 2.6: Schematic of a candidate hypothesis for the relationship between intrinsic plasticity and heterogeneity. When a network of neurons with heterogeneous excitability (shades of grey; top) is exposed to diverse (the same) inputs will undergo intrinsic plasticity to become heterogeneous (homogeneous) in its cell-to-cell excitability. The heterogeneous (homogeneous) network will display asynchronous (synchronous) output firing activity.

intrinsic plasticity would support individual neuron responsiveness being heterogeneous (and conversely homogenizing if the inputs are statistically similar). This heterogeneity (homogeneity) via intrinsic plasticity then maintains the asynchronous (synchronous) dynamics of the network. A candidate model for this hypothesis is introduced and tested in Chapter 3.

In addition to adapting for the encoding of information, the excitabilities of the neu-

rons must be very precisely tuned moment-to-moment to respond appropriately. This is particularly true in the framework of excitatory and inhibitory cells. For a collection of neurons to respond only for a desired window of time, the excitabilities of both populations of cells must be correctly sensitized.

2.2.2 Models of adaptation

Adaptation has been implemented in models in a variety of ways [188, 2, 185, 246, 31], the extent of which is beyond the scope of this thesis. However, here we review a generalized model of adaptation in a network that is defined completely by the neuron's excitability and the adaptation time constant [33], and describe how the principles used therein are applicable to general adaptation frameworks.

Benda and Herz sought to create a universal model that could describe firing-frequency dynamics of an adapting neuron independently of the specific spike generator or adaptation process involved [33]. To this end, they began by formulating two ordinary differential equations that represent an effective adaptation current, I_A, and its gating variable, a. This effective adaptation current was formulated to encapsulate three primary adapting current sources: i) M-type currents, caused by voltage-dependent, high-threshold K+ channels; ii) afterhyperpolarization (AHP) type currents that are mediated by calcium-dependent K+ channels; and iii) the slow recovery that follows inactivation of fast Na+ channels. The equation for the effective adaptation current is given by,

$$I_A = \bar{g}_A m^p h^q c a (V - E_A)$$

where $\bar{g}_A$ is the maximum conductance of the current, and E_A is the reversal potential. The gating variable, a, is given by,

$$\tau_a(V)\frac{da}{dt} = a_\infty(V) - a$$

where $\tau_a(V)$ is a voltage-dependent time-constant, and $a_\infty(V)$ is a voltage-dependent steady-state. m and h are possible voltage-gated variables raised, respectively, to integer powers p and q. If present, both variables must be much faster than the adaptation variable, a. Finally, c is a proportionality factor for a. Together, these two equations are, in essence, the well-known voltage-gated current equations introduced by Hodgkin and Huxley [144] (see Section (2.1.1)). Indeed, though it is beyond the scope of this thesis, the dynamics of each of the three primary current sources can be written in terms of this effective formalism (see [33]).

By taking a suitable time average of the effective adaptation current and its gating variable (Equations (2.2.2) and (2.2.2)), a phenomenological model of the adapting firing frequency can be written as,

$$f_r = f(I - A[1 + \gamma(f_r)])$$

with an adaptation state, A (e.g. averaged adaptation gating variable, a), and a non-

linear function, γ, to give f an influence on the adaptation state, given by,

$$\tau[1 + \epsilon(f_r)]\frac{dA}{dt} = A_\infty(f_r) - A$$

where ϵ is a term to cover a potential dependence of τ on f_r.

In this formulation, all of the dependencies on the membrane potential are replaced by the firing frequency, f_r, f is the excitability, and A_∞ is the steady-state firing rate. By writing the model this way, the model maps the input current, I, minus its averaged adaptive current, to the excitability to obtain the firing frequency. By linking these properties in such a generalized fashion, Benda and Herz's model can be easily used in a number of different frameworks with little to no modification. Importantly, although this model leverages the excitability for relating the adapted current to the output firing frequency, this is not a model of intrinsic plasticity (Section (2.2.1)). Rather, the utilized excitability is assumed to be unchanged, and the firing rate changes to derive solely from the adaptation of the input current.

2.2.3 Maladaptive adaptation

Adaptation can also lead to undesirable states, such as those observed in pathological states [348]. These changes can result from a failure in the adaptation mechanism itself, that is, where the neuron does not adapt in response to a change in input. Or, the adaptation may serve as the pathway by which a population of neurons reaches an unstable state [28, 69,

275, 153].

In the context of neural excitability and intrinsic plasticity, examples of maladaptations include tinnitus [138], chronic pain [69], and epilepsy [275, 153]. Importantly, unlike in tinnitus and chronic pain, where the malaptation is related only to the incorrect excitability in some subset of neurons, it has been found in epilepsy that the heterogeneity of excitability cell-to-cell is reduced, which has been associated with instability [275, 153].

Example case: Epilepsy

Among the most prevalent neurological pathologies in the world [29], epilepsy is a condition characterized by repeated instances of seizures [214], which present as short (seconds to minutes) intervals of highly synchronous activity. These seizures, despite the variety of pathways through which they can arise [214, 160, 306], have been shown to share many common onset features across different lesions [255]. The frequencies at which seizure activity has been observed, via electroencephalogram (EEG), spans all of the major neural bands (e.g. delta (1-4 Hz), theta (4-8 Hz), alpha (8-12 Hz), beta (12-30 Hz), and gamma (above 30 Hz)) [86]. Recordings of these bands have given insight into the specific types of dysfunctions involved in seizure events, such as the implication of slower delta activity in the post-seizure period and fast, gamma activity in the pre-seizure period that may indicate seizure onset [162, 303, 214]. Moreover, the frequencies can help indicate the type and origin of seizure events, such as the high-frequency activity common to focal seizures (e.g. those originating from a specific cortical area), and generalized seizures (e.g. involving a widespread area or the whole brain) which tend to evoke a greater variety of

frequency bands [303, 214, 86].

Regardless of their type, the dynamics of these seizures are the result of a combination of abnormal membrane potential fluctuations in individual neurons and complex physiological disturbances across populations. Though pre-seizure activity is often indistinct, and hence difficult to identify clinically, patterns emerge with seizure-onset as low-amplitude, fast gamma oscillations (typically > 80 Hz) occur [214, 255]. Alternatively, hypersynchronous patterns are characterized by initially high amplitude spikes oscillating at low frequencies [86]. However, as the seizure progresses, hypersynchrony is also associated with high frequency oscillations. Both types of described patterns can become consistent oscillatory activity as the seizure changes phases (e.g. transition from tonic to clonic) to where the frequency of oscillations decreases and the hypersynchronous dynamics are no longer present [20]. Along with these neurological effects are corresponding bodily outcomes, such as collapse, muscle rigidity, and spasming [214, 29], which have been documented extensively throughout history, with the earliest records appearing around 2500 BC [251].

Importantly, despite its long-standing history, epilepsy is a condition that arises from a number of different pathways [306, 8]. The multifaceted nature of epilepsy thus makes it difficult to treat, as not all patients respond to the same approach(es), and identifying which one is best suited is not easily accomplished. Recent work has shown that heterogeneity in neural excitability is reduced in human and mouse neurons compared to their healthy counterparts [275]. Such changes in excitability could, themselves, arise from a number of pathways. Epilepsy is well documented to involve changes in one or more ion channels [28, 214, 176, 18, 119], as well as morphological changes to dendritic branches [306].

Despite its varied pathological onsets, epilepsy further represents an example of degeneracy in a biological system. That is, it is a condition in which multiple combinations of maladaptation can result in the same qualitative effects.

2.3 Neuromodulation

Interest in probing and controlling brain activity, particularly for medical intervention (e.g. to oppose maladaptive adaptation that yield pathology), through the use of external, or non-invasive, force has a long history. Indeed, the first recorded attempts of using electricity for medical purposes date back to the Greco-Roman period (800 BC - 600 AD) when electric fish were placed on the skull to treat headaches [51]. Though far removed from modern approaches, these attempts leveraged the same overarching principles. That is, a scalar electric potential exists at each point in the brain and can be measured relative to an arbitrary reference and expressed in Volts. An electric field (E-field) is the gradient of this voltage, where all transmembrane currents from nearby neuronal activity contribute to the generation of the E-field [194, 51]. By applying a current to brain tissue, the polarization of the neuron's membrane can be manipulated to alter neuronal excitability. This observation led to the advent of more abrasive techniques, such as the electroconvulsive therapies common in the mid-20th century [51, 308], and ultimately modern approaches collectively referred to as non-invasive brain stimulation.

Non-invasive brain stimulation (NIBS) is a general term used to refer to the group of techniques in which localized regions of the brain are exposed to a low-strength electric or

magnetic field applied at the surface of the skull [263, 73, 341, 260, 322]. Common examples of such techniques include transcranial magnetic stimulation (TMS) [128], transcranial direct current stimulation (tDCS) [236], transcranial alternating current stimulation (tACS) [139], transcranial random noise stimulation (tRNS) [319] and transcranial focused ultrasound stimulation (tFUS) [330], each of which operates over a mesoscopic spatial area, although the timescales between different techniques varies widely [260]. Collectively, NIBS affects neural excitability and allows for widespread, spatially diffuse modulation of superficial cortical activity [253, 267, 341, 277]. This has led to NIBS being of great interest for therapeutic and clinical interventions (e.g. major depressive disorder, schizophrenia, bipolar disorder) [322, 107, 37] as well as for studying the physiology of the central nervous system [80, 73], and brain dynamics [253, 260, 148, 146].

For this thesis, we focus on the transcranial electrical stimulation (TES) subset of these techniques (i.e. not TMS or tFUS) with particular attention to tDCS. TES methods involve applying a weak electric current to the scalp to modulate local, ongoing neural oscillations or influence the excitability of the network [341, 277, 253]. Depending on the exact TES method being used, the waveform of the applied current varies. Examples of this include sinusoids, as in tACS [139, 267], a constant current as in tDCS [236, 39], or noise as in tRNS [319, 253]. Depending on the research objective, and resources available, one technique may be preferable to the others (for a comparative review of these techniques, see [37]). However, all of these methods ultimately allow brain activity manipulation and are generally well tolerated by healthy humans.

Despite increasing popularity over the last three decades [73, 260], there remain many

unknowns and challenges to these techniques. One of the most prominent of these challenges comes from the high dimensionality of available parameters in TES [201, 147] from controllable (e.g. stimulation frequency [230], strength [24], location [225], etc.) and immutable (e.g. age [180], individual cortical geometry [290], attentional state [184], etc.) factors. The dependency of response on such high dimensional space contributes to great patient-to-patient variability [198, 282, 126, 125]. Moreover, many of the initial studies with these techniques were applied to the motor cortex [37] and their efficacy cannot necessarily be extrapolated to other cortical regions. This drastically complicates determining the most influential variables experimentally, leading to the development of a variety of computational models for these frameworks [146, 201] to address these gaps.

2.4 Dynamical systems

The neural activity described in this thesis is an example of a dynamical system. Over the years, a litany of mathematical and computational techniques have been developed and leveraged to study such systems. In their most general deterministic form, dynamical systems are often written as a set of ordinary differential equations. In some instances, these systems of equations can be analytically resolved or analyzed for their properties, such as the mean, variance, and auto- and co-variances. The distribution of these properties across the system (e.g. a population of neurons) and through time can provide insight into the dynamics of the system and its sensitivity to changes in parameters. However, in complex systems, these equations frequently involve nonlinearities that can make resolution

by analytical methods challenging and necessitate the use of computational tools [315]. Indeed, in the last 60 years, much work has gone into understanding the ability of small nonlinearities to induce complex dynamical behaviours [195, 307].

Simulation is one of the most readily accessible ways to study dynamical systems, allowing the progression of the variables to be tracked through time and their dependency on individual parameters assessed. Moreover, many dynamical systems exhibit fixed points, which are asymptotic solutions to the associated differential equations (e.g. equilibria) [307]. The location of these fixed points is dependent on the parameters in the system. If the parameters change through the evolution of time, the system may additionally undergo bifurcations, which represent qualitative changes to the phase space trajectory of the system [195, 261, 315]. The fixed points themselves may be stable, unstable or semi-stable [307]. When the fixed points are stable, they are attracting trajectories where the system will stay at rest upon reaching, unless otherwise perturbed. Unstable fixed points, contrastingly, are repellers. That is, the trajectory of the system will be pushed away. Finally, semi-stable fixed points may have trajectories from some directions that are attracted and others that are repelled. Changes in the parameterization of the system may additionally contribute to stabilization or destabilization by altering the fixed points, which can contribute to drastic changes in the system's dynamics.

Analyzing the fixed points of dynamical systems is a key tool for insight into the behaviour and stability of the systems therein. Indeed, these techniques have been leveraged extensively [81, 155, 307] in the study of neural systems to determine their stability. In particular, techniques from the mathematical field of random matrix theory, such as cir-

cular and elliptical law, have been used extensively to assess the stability of heterogeneous dynamical frameworks. These techniques, although not applied directly in this thesis, serve to determine the stability of the whole network based the lead, or largest, real-component of the eigenvalues for the fixed points in the network (for a more thorough review of random matrix theory see [313]).

In neural systems, these techniques have been applied to probe the relationship between heterogeneity and the long-term persistence and stability of the dynamics. In terms of the excitability (e.g neural excitability; see Section (2.1) and (2.1.1)) of interest to this thesis, it has been theoretically shown to reduce the number of equilibria [152], reduce network volatility [275], linearize the dynamics [153], improve encoding [112] and stabilize against external inputs [5]. Moreover, when cell-type specific connectivity is implemented in a neural network, theoretical work has shown heterogeneous excitability to influence computational capacity [11]. Likewise, the inclusion of heterogeneous connectivity in line with what is anatomically observed was found to non-trivially affect the phase transitions of a network [154]. Together, this strongly supports that, at a minimum, some forms of electrophysiological heterogeneity plays a critical role in supporting healthy dynamics.

2.5 Numerical methods

The brain evolves through many stochastic processes. Not all of these can be appropriately modelled into an analytically tractable form. As such, numerical approaches are utilized to resolve them. Depending on the scale of model, these may take different forms. A

summary of the primary numerical approaches used in this thesis follows.

2.5.1 The Euler-Maruyama Method

One of the methods most commonly used for numerical integration, Euler-Maruyama's method is used to evaluate the majority of systems of stochastic differential equations in this thesis. Given functions g_1 and g_2, X_t is the solution to the stochastic differential equation,

$$dX(t) = g_1(X(t))dt + g_2(X(t))dW(t) \tag{2.12}$$

if $X(t)$ solves the integral equation,

$$X(t) - X(0) = \int_0^t g_1(X(s))ds + \int_0^t g_2(X(s))dW(s) \tag{2.13}$$

where $W(t)$ is a Wiener process used to model white noise; $dW/dt = \xi(t)$ (for a review see [196]).

In the framework of Euler-Maruyama's method, this can, given the initial condition X_o, be resolved over a time interval $[0, T]$. Specifically, it is resolved incrementally for time steps of size dt, such that the total number of steps, $n = T/dt$, where T is the total simulation time [79, 53, 261]. The simulation proceeds in the form,

$$X_{n+1} = X_n + dtg_1(X_n) + \Delta W_n g_2(X_n) \tag{2.14}$$

for the n steps of the simulation where $t_n = t_0 + ndt$. Here, $\Delta W_n = W(t_{n+1}) - W(t_n) = \sqrt{dt}N(0,1)$, where $N(0,1)$ is a Gaussian distribution with mean zero and variance one.

This approach can be expanded to systems of codependent or concurrent differential equations, updating each variable sequentially through time.

2.5.2 Measures of heterogeneity in adaptive models

Including heterogeneity as an adaptable aspect of models poses a considerable challenge. However, along with this comes the question of how to quantify the heterogeneity itself. The choice of metric used to address this issue is, in part, dependent on the scale and type(s) of heterogeneity under consideration. If multiple sources of heterogeneity are present, the contributions of each must be accounted for in the measure. A wide range of similarity metrics exist that can be leveraged to calculate the heterogeneity among a population. The choice of metric may influence the magnitude of heterogeneity that is observed. Here we briefly describe two: i) the Kullback-Leibler divergence, and ii) the Hellinger distance.

Kullback-Leibler divergence

One of the most common similarity metrics is the Kullback-Leibler divergence (KL-divergence), proposed by Solomon Kullback and Richard Leibler in 1951 [175]. Also referred to as the relative entropy or I-divergence, this metric is a statistical distance that measures

the difference between a model probability distribution, Q, and the true one, P. In terms of heterogeneity, particularly in the context of adapting networks, this can be used to compare how the distribution of a given heterogeneous property (e.g. excitability) changes through time or in response to altered network activity. The KL divergence is especially favoured because it has been analytically derived for a number of different distributions, including normal distributions, uniform distributions, and exponential distributions [301]. This then allows for the heterogeneity itself to be considered in terms of relating the changes in distribution mean and variance to what drive them.

The KL-divergence, $D_{KL}(P||Q)$, between two discrete probability distributions P and Q on the same sample space $\mathcal{X}$ is defined as,

$$D_{KL}(P||Q) = \sum_{x \in \mathcal{X}} P(x) \log \frac{P(x)}{Q(x)}$$

Hellinger distance

The Hellinger distance, introduced by Ernst Hellinger in 1909 [136, 235], is a type of f-divergence used to define the difference between two probability distributions, P, and Q [75]. Unlike the KL-divergence, the Hellinger distance is bounded between 0 and 1, and is thus a readily interpretable measure of the network heterogeneity where 0 corresponds to full homogeneity and 1 would indicate heterogeneity with no overlap. In addition to this bounding, similar to the KL-divergence, it has been analytically resolved for normal distributions, thus affording the ability to relate changes in the metric to the heterogeneous

properties underlying it.

For two discrete distributions, $P = (p_1, ..., p_k)$ and $Q = (q_1, ..., q_k)$, the Hellinger distance, $H(P, Q)$, is defined as,

$$H(P,Q) = \frac{1}{\sqrt{2}}\sqrt{\sum_{i=1}^{k}(\sqrt{p_i} - \sqrt{q_i})^2}$$

2.5.3 NEURON Coding Environment

For detailed biophysical models of neurons (e.g. those with comprehensive morphological and electrophysiological properties) where there is spatial inhomogeneity and complex membrane currents, the NEURON simulation environment is often the most flexible, efficient and utilized framework [140, 141]. This coding environment was designed explicitly to maximize the efficiency of integrating the branched nerve equations, leveraging various mathematical simplifications and tricks. Specifically, the environment seeks to resolve the cable equation,

$$\frac{\partial V}{\partial t} + I(V,t) = \frac{\partial^2 V}{\partial x^2} \tag{2.15}$$

where V is a membrane potential, and I is a current. When spatially discretized [140, 141, 232], this can be rewritten as a family of ordinary differential equations in a statement of Kirchoff's current law,

$$c_j \frac{dv_j}{dt} + i_{ion_j} = \sum_k \frac{v_k - v_j}{r_{jk}} \tag{2.16}$$

where j is a compartment index, c is the membrane capacitance, i_{ion} is all currents through ionic channel conductances, and the right hand side of the equation represents all axial currents that enter the compartment. Equation 5.3 involves two approximations: first, that the axial current is specified by a voltage drop between adjacent compartments and second, that the spatially varying membrane current can be represented by its value at the center of a given compartment. These approximations are relatively straightforward in linear cables where all compartments are of identical size, as a Taylor series expansion can demonstrate the error scales proportionally as the square of the compartment size [140, 141]. However, to model biophysically detailed neurons, different compartment sizes and branching must be accounted for. This, in particular, is where NEURON leverages its designs for numerical efficiency.

Indeed, a common dilemma with branched structures in such simulations is that it is often unclear how many compartments should be used for a given branch. This is particularly important as computational accuracy and efficiency are directly related to the number of compartments in a given cable. Additionally, as the number of compartments increases, it then becomes challenging to deal with all of the parameters associated with the many compartments. NEURON, however, addresses this by separating the biophysical properties (e.g. morphology and electrophysiology) from the numerical issues associated with compartment size [141]. This is done through the creation of *sections*, unbranched

portions of cable, that are discretized within themselves. That is, within a given section, many or few compartments, called *segments* and allocated by a parameter $nseg$, can exist and are specified by a normalized distance, $x \in [0, 1]$, along the section.

The internal voltage of each segment is crucially defined at its center, that is, at its node [141], which is the discretization method employed by NEURON. With this, the transmembrane currents over the entire surface area of a given segment are associated with its node, and the nodes of adjacent segments are connected by resistors. Based on the segment position, x, along the section, NEURON specifies internal model parameters (e.g. axial resistance, compartment area, etc) and retrieves state variables as a function of their location. This significantly reduces the amount of tracking required for lower-level details in the model on the part of the user, and allows resolution of section properties without regard for the number of segments that comprise it.

Finally, the sections themselves are then joined to comprise any branched architecture. To allow this, and injection of current, at the precise ends of sections, extra voltage nodes of zero area are defined at the section ends. NEURON then, in its default setting, evaluates the integration using backward Euler approach [81]. This approach is leveraged for its robust numerical stability and availability of extremely large time steps to find the steady-state solution for linear (e.g. passive) systems. Moreover, the backward Euler approach has been previously shown to be well suited to the integration of nerve equations [211], and produces qualitatively good results even with large time steps.

3

Intrinsic plasticity underlies the malleability of neural network heterogeneity

3.1 Abstract

Diversity exists throughout biology, playing an important role in maintaining robustness and stability. The same is true of the brain, as has become increasingly apparent in recent years with the accumulation of datasets of unparalleled resolution. These datasets show widespread neural heterogeneity, spanning cells, circuits and system dynamics, marking it as an unavoidable component of the brain's composition. Recent experiments found declines in heterogeneity amongst neurons may accompany pathological states. While heterogeneity has been linked to stability, robustness and increased computational potential, the loss of biophysical diversity was found conducive to the onset of seizure-like activity, suggesting an important functional role. Despite this, how changes in heterogeneity arise remains unknown. Oftentimes considered a static metaparameter resulting from solely genetic disposition, heterogeneity is, in fact, a highly dynamic property of biological networks arising from various sources. Here, we consider this through the lens of intrinsic plasticity, the activity-dependent modulation of neuron biophysical properties, which we propose allows the degree of biophysical diversity to fluctuate in time. Using a network of Poisson neurons endowed with intrinsic plasticity, we combine analytical and numerical approaches to measure the effect of input statistics on the excitability of individual cells, and how this translates into changes in network heterogeneity at the population scale. Our results indicate that, through intrinsic plasticity, diversity in synaptic inputs promotes heterogeneity in cell-to-cell excitability due to changes in the statistics of presynaptic firing rates, and network topology. In contrast, whenever the statistics of synaptic input between cells

were too similar, intrinsic plasticity promoted the decline in heterogeneity. Further, we show that changes in heterogeneity can coexist with degeneracy in the firing rate between neurons. Taken together, understanding how input statistics affect neuronal network heterogeneity may provide key insights into brain function, resilience and the manipulability of neural diversity through intrinsic plasticity.

3.2 Introduction

A common feature of many complex systems' constitution is the presence of disorder or heterogeneity [110, 213, 12, 312, 338, 203, 168, 189]. This is especially true for the brain, where the sources of heterogeneity are widespread [182, 44], with important consequences on neural circuits dynamics and function[324, 62, 275, 112]. One of the most salient, and studied, forms of heterogeneity arises through diversity in neuronal excitability [226, 58, 220], manifested through neuron-specific, cell-to-cell variations in both the minimal intensity of a stimulus required to elicit a response (i.e., threshold), as well as in the magnitude of this response (i.e., gain) [97]. A confluence of both experimental and theoretical studies have demonstrated that excitability heterogeneity plays multiple important functional roles, such as optimizing coding capacity, promoting efficient learning and information flow, as well as reinforcing the resilience of neural circuits by stabilizing their dynamics away from pathological states [220, 117, 97, 274, 238, 275, 223].

In all likelihood, because neuronal excitability is not static, excitability heterogeneity is also not static and modulated by *intrinsic plasticity* mechanisms that play an important

role in learning and memory [363, 77]. Intrinsic plasticity is the post-synaptic counterpart to synaptic plasticity, whereby a neuron's excitability (e.g. gain) is modulated by its past activity profile [331, 83, 363, 130, 82], including background fluctuations and/or persistent changes in the input statistics (hereafter referred to as the "milieu"). Such modulation of excitability in an activity-dependent manner was first shown by blocking voltage-gated sodium channels to silence neocortical neurons, which triggered an increase in excitability via the upregulation of voltage-gated sodium channels and downregulation of potassium channels [83, 363, 111]. Experimentally, this malleability of excitability not only plays a key role in memory and learning [48, 202, 323, 363, 292], but also in several pathological states of the nervous system [28] including epilepsy [363, 28], tinnitus [192, 138, 69], neuropathic pain [209, 69], and a whole host of neurodegenerative and neuropsychiatric conditions [65, 52, 43, 193, 329, 342, 233, 101].

At a network level, the changes in excitability in pathological states like epilepsy can be seen to alter the diversity of excitability across the population. Indeed, our recent work shows that a loss of excitability diversity accompanies human [275] and rodent [227] epilepsy, and results in network instability that predisposes the brain to slipping into a seizure-like state [275, 153, 152]. However, how such a decline in heterogeneity arises remains unknown, and even of wider important is that how is the excitability diversity we see in the brain [248, 324, 61, 62, 295] maintained for the "healthy" function of the nervous system. Therefore, we pursue the hypothesis that intrinsic plasticity modulates neural circuit heterogeneity, through the regulation of the excitability of individual neurons. We consider this mechanism of particular candidacy as it aligns with recent research highlighting

the importance of degeneracy in explaining the multiple pathways through which epilepsy occurs [306]. Indeed, if intrinsic plasticity enhances variability between neurons, either by diversifying their excitability profiles between each other or by accentuating pre-existing differences, the network's heterogeneity will increase. In contrast, if intrinsic plasticity instead drives a convergence of excitability profiles between cells, this will manifest as a decline in excitability heterogeneity. Given the close relationship between diversity and stability [275, 153, 152], the ability of intrinsic plasticity to promote (or hinder) excitability heterogeneity might provoke important changes in dynamic stability, which may be both physiologically beneficial, or in the extreme predispose neural circuits to pathological states, such as those seen in epilepsy [275, 153, 152].

Inspired by our recent experimental work [227], we here pursue the novel hypothesis that intrinsic plasticity is a critical modulator of neural circuit excitability heterogeneity. This novel perspective is in stark contrast with the pre-existing notions that excitability heterogeneity is a static meta-parameter resulting mainly from genetic predisposition [220, 314, 61, 62, 142, 295, 356, 112]. Herein we propose intrinsic plasticity as a candidate mechanism for time-dependent changes in the heterogeneity expressed by neural populations, thereby influencing the stability of neural circuits. To explore these hypotheses, we use a widely used recurrent neural network of excitatory Poisson neurons with sparse, random connectivity, endowed with intrinsic plasticity. We characterize the dynamics of this model under varying stimulation conditions (e.g. step current, spike trains) and network architecture (e.g. topology and weights). We found that heterogeneity arises naturally among neurons from changes in input statistics, resulting from cell-to-cell variations in connectivity pro-

files. Most importantly, our result indicates that stimuli can be used to manipulate the level of heterogeneity in the network. The increase in heterogeneity was found to enhance network stability. In contrast, diversity decline was alternatively found to promote multistability. Importantly, we found that heterogeneity can coexist with degeneracy: networks of neurons exhibiting similar firing rates can still demonstrate excitability heterogeneity. Taken together, these results imply that heterogeneity is a malleable property of neural networks, supported by the topology of the network and imperative for maintaining stable neural network operation.

3.3 Methods

3.3.1 Network model

We consider an excitatory network of Poisson point neurons with random connectivity. The neurons have a membrane potential, u_i, where $i = 1, ..., N$ is the neuron index. The dynamics of the membrane potential for neurons in this network obey the following system of evolution equations,

$$\tau \frac{du_i}{dt} = -u_i + \frac{1}{N} \sum_{j=1}^{N} w_{ij} X_j, \tag{3.1}$$

where $X_j = \sum_{\{t_k\}} \delta(t - t_k)$ are Poisson spike trains, τ is the membrane time constant, and w_{ij} are synaptic weights. Spiking activity follows a non-homogeneous Poisson process, that is $X_j \to \text{Poisson}(r_j)$, where r_j corresponds to the instantaneous firing rate of neuron

j. This firing rate depends directly on the membrane potential through the excitability curve of that same neuron, that is $r_j = f(u_j)$ where f is defined by the sigmoid [153, 152],

$$f(u_i, \beta_i, h_i) = \frac{1}{2}(1 + \mathrm{erf}(\beta_i(u_i - h_i))), \tag{3.2}$$

where i is the neuron index, and $\{\beta_i, h_i\}$ are the slope and midpoint (or rheobase), respectively. A Poisson spike occurs if $p_{spike} = 1 - \exp(-f(u_i, \beta_i, h_i))$ is greater than a randomly generated uniform probability. The excitability curve hence sets the firing rate, r_i, of neuron i.

3.3.2 Model assumption

The model in Eq. (3.1) and associated analyses below rely on a set of assumptions, validated in previous work [187, 275, 311, 186], and whose purpose is to balance physiological relevance and mathematical tractability. Specifically,

- Neuronal spiking is Poisson, uncorrelated and resides in the high firing rate limit;
- Connectivity is random with probability $\rho = 0.15$, and the network topology is constructed to accommodate any in- and out-degree distributions. To do so, we follow the steps described [166]. In summary, the degree of connectivity to a given neuron, $i = 1, ..., N$, is drawn from a uniform distribution. The connections are then made randomly with the neurons in the network.

- Synaptic weights are positive (purely excitatory network) and uniform across all realized connections: $w_{ij} = w_o > 0$ if a connection exists between neurons i and j and 0 otherwise. This choice is made for convenience, so that the expectation value of the weights across all neurons is $\mathbb{E}_{N\times N}[w_{ij}] = w_o$.

- Intrinsic plasticity is slow compared to membrane potential dynamics. We have assumed that the intrinsic plasticity equations have reached an equilibrium, for which the firing rate of individual neurons has been homeostatically normalized to a set value r^o (see below).

These assumptions play an instrumental role in the analysis that follows. Notably, they set the network in a dynamical regime in which individual membrane potentials can be assumed to be Gaussian, a key requirement in the mean field analysis pursued below. These assumptions also enable the use of adiabatic approximations, in which intrinsic plasticity has reached an equilibrium, where firing rates remain constant on the shorter time scales defined by the membrane time constant (i.e., $\tau_{IP} \gg \tau$). While seemingly restrictive, analyses relying on these assumptions have been shown to agree well with simulations, both here and in our previous work[187, 275, 311, 186].

3.3.3 Regulation of excitability via intrinsic plasticity

Thus far, the excitability described for each neuron in the network is static. To introduce intrinsic plasticity in this framework, we allow the parameters β_i and h_i in Eq. (3.2) to

fluctuate in time to normalize the firing rate of individual neurons in an activity-dependent manner. Specifically, we allow the excitability curve of each neuron to adapt so that, over long time scales, its firing rate is drawn towards a value r^o, hereafter referred to as the *homeostatic target rate*. For simplicity, this target rate is chosen to be equal for each neuron in the network. To implement intrinsic plasticity, Eq. (3.1) and (3.2) are complemented by an additional set of differential equations accounting for the dynamics of the parameters β_i and h_i,

$$\tau_{IP}\frac{d\beta_i}{dt} = \epsilon_\beta(f(u_i, \beta_i, h_i) - r^o)\Theta(\beta_i), \tag{3.3}$$

and

$$\tau_{IP}\frac{dh_j}{dt} = \epsilon_h(f(u_i, \beta_i, h_i) - r^o), \tag{3.4}$$

respectively. Combined, Eqs. (3.1), (3.3) and (3.4) form a system of $3N$ differential equations, in which the parameters defining the excitability of individual neurons adapts to fluctuations in its membrane potential. The constant τ_{IP} refers to the time constant of intrinsic plasticity, and is assumed to be slow compared to the dynamics of the membrane potential in Eq. (3.2) i.e. $\tau_{IP} \ll \tau$. The parameters ϵ_β and ϵ_h correspond to learning rates ($\epsilon_\beta < 0$ and $\epsilon_h > 0$), scaling the direction of the rate of change, while compensating for the vastly different range of values the parameters β_i and h_i can take. The function Θ in Eq. (3.3) is defined by $\Theta(\beta_i) = 1$ whenever $0 < \beta_i < \beta_{max}$ and zero otherwise, and is included to ensure that the slopes β_i remain positive, and bounded within a physiologically plausible range, where $\beta_{max} = 50$.

3.3.4 Excitability and cellular milieus

To characterize how intrinsic plasticity influences the activity of individual cells in Eq. (3.1), one can examine the asymptotic dynamics of the parameters β_i and h_i for an arbitrary neuron i. Since the membrane potential u_i is a stochastic state variable (due to Poisson spiking), it is more appropriate to consider the temporal averages of Eq. (3.3) and (3.4), that is

$$\tau_{IP}\frac{\langle d\beta_i\rangle_T}{dt} = \epsilon_\beta\langle(f(u_i,\beta_i,h_i) - r^o)\rangle_T, \tag{3.5}$$

$$\tau_{IP}\frac{\langle dh_i\rangle_T}{dt} = \epsilon_{h_i}\langle(f(u_i,\beta_i,h_i) - r^o)\rangle_T, \tag{3.6}$$

where $\langle\cdot\rangle_T$ represents an average over a long time window i.e., $T \gg \tau_{IP}$ and $T \gg \tau$ and where we assumed $\Theta(\beta_i) = 1$. At equilibrium, these equations possess steady states β_i^* and h_i^* that satisfy the same implicit expression

$$\langle f(u_i,\beta_i^*,h_i^*)\rangle_T - r^o = 0, \tag{3.7}$$

which simply indicates that asymptotically, the average individual firing rate of a neuron i will converge towards the homeostatic target rate r^o. This can equivalently be written for $T \to \infty$ as,

$$\int f(u_i,\beta_i^*,h_i^*)p(u_i)du_i = r^o. \tag{3.8}$$

Note that one obtains an identical expression for each neuron in the network, although the values of β_i^* and h_i^* may differ. The above expression depends directly on the a priori

unknown probability density function $p(u_i)$ for the membrane potential of neuron i, as defined in Eq. (3.1). Determining this distribution exactly represents a challenge, but approximations are possible. Indeed, in the limit of high firing rates, and assuming that spiking activity in the network is uncorrelated, one may replace the spike trains, X_j, in Eq (3.1) by $X_j \approx r_j + \sqrt{r_j}\xi_j$, where r_j is the firing rate of neuron j, and ξ_j is a Gaussian white noise process such that $\langle \xi_j(t)\xi_k(s)\rangle_T = \delta_{jk}(t-s)$ [310]. Using these approximations, Eq. (3.1) becomes,

$$\tau \frac{du_i}{dt} = -u_i + \frac{1}{N}\sum_{j=1}^{N} w_{ij}(r_j + \sqrt{r_j}\xi_j) \tag{3.9}$$

As per the steady state analysis of the intrinsic plasticity equations performed above, we now examine the adiabatic regime in which the individual firing rates r_j asymptotically converge towards their homeostatic target rate r^o (i.e., Eq. (3.7)) and remain constant within the time window T. Hence, at equilibrium, one obtains [311, 186]

$$\tau \frac{du_i}{dt} \approx -u_i + \frac{1}{N}\sum_{j=1}^{N} w_{ij} r^o + \frac{1}{N}\sum_{j=1}^{N} w_{ij}\sqrt{r^o}\xi_j. \tag{3.10}$$

One may simplify this expression further, recalling synaptic weights are assumed to be random and the same for all connections i.e., $w_{i,j} = w_o$ with probability ρ, and zero otherwise. Note that we will break this assumption later on. In this case, the degree distribution $P(k)$ of the network connectivity adopts a Binomial distribution i.e., $P(k) = \binom{N-1}{k} p^k (1-p)^{N-1-k}$. Both in-degree (i.e., k^{IN}) and out-degree (i.e., k^{OUT}) are identically distributed, with $\mathbb{E}_N[k_i^{IN}] = \mathbb{E}_N[k_i^{OUT}] = \rho(N-1)$. As such, one may rewrite Eq. (3.10)

as

$$\tau \frac{du_i}{dt} \approx -u_i + \frac{1}{N} k_i^{IN} w_o r^o + \frac{1}{N} k_i^{IN} w_o \sqrt{r^o} \zeta_i \tag{3.11}$$

where k_i^{IN} corresponds to the in-degree associated with neuron i. By independence, the second sum on the right hand side of Eq. (3.10) also conforms to a zero mean Gaussian white noise process [109], and has thus been replaced by independent, identically distributed Gaussian white noise processes ζ_i, also satisfying $\langle \zeta_j(t) \zeta_k(s) \rangle_T = \delta_{jk}(t-s)$ [310]. Following these approximnations, Eq. (3.11) is fully decoupled from the dynamics of other neurons in the network. It further shows that the dynamics of the membrane potential of individual cells depend directly on the neuron's *milieu* - here defined as the environment or local conditions that impact a neuron's membrane dynamics [336] - resulting from the combination of passive properties, synaptic inputs (i.e., via the in-degree, and also external stimuli (see below). Following the assumptions highlighted above, the membrane potential u_i in Eq. (3.11) of each neuron can be approximated by an Ornstein-Uhlenbeck process whose probability density function $p(u_i)$ has the shape of a normal density with mean

$$\mu_{u_i} = \frac{1}{N} k_i^{IN} w_o r^o, \tag{3.12}$$

and variance

$$\sigma_{u_i}^2 = \frac{1}{2N^2} (k_i^{IN} w_o)^2 r^o, \tag{3.13}$$

where we assume $\tau = 1$. We highlight that the mean and variance differ between between cells within the network, here as a result of variability in synaptic connectivity.

With an approximation for the probability density function $p(u_i) = N(\mu_{u_i}, \sigma^2_{u_i})$ in hand, we can now return to Eq. (3.8) and determine the conditions on the excitability parameters β^*_i and h^*_i by computing the integral on the right hand side, that is

$$\int f(u_i, \beta^*_i, h^*_i)p(u_i)du_i = \frac{1}{2\sqrt{2\pi\sigma^2_{u_i}}} \int_{-\infty}^{\infty} (1 + \text{erf}(\beta^*_i(u_i - h^*_i)))e^{\frac{-(u_i-\mu_{u_i})^2}{2\sigma^2_{u_i}}} du_i, \tag{3.14}$$

which can be separated into two integral terms,

$$\int f(u_i, \beta^*_i, h^*_i)p(u_i)du_i = \frac{1}{2\sqrt{2\pi\sigma^2_{u_i}}} \int_{-\infty}^{\infty} e^{\frac{-(u_i-\mu_{u_i})^2}{2\sigma^2_{u_i}}} du + \frac{1}{2\sqrt{2\pi\sigma^2_{u_i}}} \int_{-\infty}^{\infty} \text{erf}(\beta^*_i(u_i - h^*_i)))e^{\frac{-(u_-\mu_{u_i})^2}{2\sigma^2_{u_i}}} du_i. \tag{3.15}$$

The first term of this equation resolves to 1/2. The second term can be solved using the known integral solution of a normal distribution with an error function [234], yielding

$$\int f(u_i, \beta^*_i, h^*_i)p(u_i)du_i = \frac{1}{2} + \frac{1}{2\sqrt{2\pi\sigma^2_{u_i}}} \sqrt{\frac{\pi}{(1/2\sigma^2_{u_i})}} \text{erf}\left(\frac{-\beta^*_i(\mu_{u_i} - h^*_i)}{\sqrt{2\sigma^2_{u_i}}\sqrt{\beta^{*2}_i + (1/2\sigma^2_{u_i})}} \right). \tag{3.16}$$

$$\int f(u_i, \beta_i^*, h_i^*) p(u_i) du_i = \frac{1}{2} + \frac{1}{2} \operatorname{erf}\left(\frac{-\beta_i^*(\mu_{u_i} - h_i^*)}{\sqrt{2\sigma_{u_i}^2}\sqrt{\beta_i^{*2} + (1/2\sigma_{u_i}^2)}} \right). \tag{3.17}$$

Simplifying this equation, we obtain an expression for the average firing rate of individual neurons, which at equilibrium must correspond to the homeostatic rate as per Eq. (3.7), that is,

$$F(\mu_{u_i}, \beta_i^*, h_i^*) \equiv \frac{1}{2}\left(1 + \operatorname{erf}\left(\frac{-\beta_i^*(\mu_{u_i} - h_i^*)}{\sqrt{1 + 2\beta_i^{*2}\sigma_{u_i}^2}} \right)\right) = r^o. \tag{3.18}$$

Equation 3.18 shows that the excitability of individual neurons changes in an activity-dependent manner to normalize the neuron(s) firing rate: it defines a self consistent, yet implicit expression for values of β_i^* and h_i^* reached at equilibrium, which result from Eqs. (3.3) and (3.4). It further confirms that the shape of the excitability curve (which is parametrized by the parameters β_i^* and h_i^*) depends directly on the statistics of the membrane potential of individual cells. Variability in membrane potential statistics result in different excitability profiles, reflected as heterogeneity in the network.

3.3.5 Excitability degeneracy

As defined, the equilibrium of Eqs. (3.5)-(3.6) both satisfy Eq. (3.7): these form an underdetermined system and, by extension, the model displays *degeneracy*. That is, Eq. (3.18) admits multiple equivalent solutions, where multiple combinations of β_i^* and h_i^* satisfy the equilibrium conditions of the intrinsic plasticity equations. That is, within the available $h - \beta$ parameter space there exists a set of equivalent pairs of β_i^* and h_i^* that parameterize an excitability curve with the same qualitative excitability profile. These define a curve, which we call the *degeneracy curve* $h^*(\beta^*)$, towards which values of β and h will converge to maintain the neuron at a set homeostatic target firing rate (see Fig (3.1C)).

The degeneracy curve arises directly from Eq (3.18), where $F(\mu_{u_i}, \beta_i^*, h_i^*) = r^o$. Assuming that $\sigma_{u_i}^2 > 0$ and performing the appropriate rearrangement to isolate h_i, we hence obtain an expression for the degeneracy curve,

$$h_i^*(\beta_i)^* = \mu_{u_i} - \frac{1}{\beta_i^*}\left(\sqrt{1 + 2\beta_i^2\sigma_{u_i}^2}\,\mathrm{erf}^{-1}(2r^o - 1)\right) \tag{3.19}$$

The degeneracy curve depends on the homeostatic target firing rate, as well as the mean and variance of the membrane potential of individual neurons, which themselves depend on the weights and firing rates within the network (i.e., Eq. (3.12 and (3.13)). The presence of degeneracy in the plasticity of our model differentiates it from other adaptation models [115, 34, 31, 347, 346, 174, 270] as there are equivalent parametric pairs that can

arise from inputs with the same statistics. Further, in cases where the neurons have non-identical input statistics (from e.g. degree distribution, connections weights) the presence of degeneracy allows for elevated levels of heterogeneity in the network. This degeneracy allows neurons to have different parameterizations, increasing the available parameter space beyond what a non-degenerate model can access. This is particularly important, as it is consistent with neuronal adaptations that occur via the complex interaction of multiple biophysical properties [266, 8].

3.3.6 Network simulations

Manipulating network heterogeneity: stimulation

The input statistics of each neuron regulate the network's level of heterogeneity by way of the membrane potential mean and variance (Eq (3.12) and (3.13)). As such, we would expect that heterogeneity will be modulated by exogenous stimulation. To explore how different types of stimulation affect network heterogeneity, we apply stimulation, S_i, to every neuron in the network such that Eq (3.1) becomes,

$$\frac{du_i}{dt} = -u_i + \sum_{j=1}^{N} w_{ij} X_j + S_i(t) \tag{3.20}$$

where S_i is representative of different kinds of stimulation:

$$S_i(t) = \begin{cases} I_o & \text{Fixed input} \\ \eta(t) & \text{Ornstein-Uhlenbeck process} \\ Y_i(t) & \text{Spike trains} \end{cases} \tag{3.21}$$

These correspond to different stimulus types regularly observed in experimental protocols and *in vivo* [169].

Starting with the case of fixed input, S_i corresponds to regimes of persistent high or low activity whereupon every neuron receives the same injected input. This kind of persistent stimulation is modelled in Section 3.4.2, where three different simulations are performed: one with persistently high activity where $I_o > 0$, one with persistently low activity where $I_o < 0$, and a baseline case where $I_o = 0\ \forall t$. The networks are initialized with random values of $\beta_{i,o}$, $h_{i,o}$ from uniform distributions of β and h for neurons $i = 0, ..., N$.

At the end of these simulations, the obtained parameterizations of the excitability curves (e.g. $\beta_{i,f}, h_{i,f}$) for each of the three networks are kept to investigate the dynamics these curves would evoke in a static network. That is, *without* intrinsic plasticity to adjust the excitability curves, what dynamics may result from the new levels of excitability and homogeneity. This no-plasticity version of the network is then simulated with an Ornstein-Uhlenbeck process, η, such that every neuron receives the same slow-varying signal. This variety of stimulation allows us to investigate the influence of heterogeneity on the stability of the network dynamics.

Finally, in the case where the network is stimulated by impinging spike trains each

train, $Y_i, i = 1, ..., N$, is independent of the $N-1$ other trains and has a rate, $r_{i,s}$, drawn from a uniform distribution of rates. The rates are non-identical between neurons with the objective of increasing the heterogeneity in the population. Simulations using this kind of stimulation are initialized with random $\beta_{i,o}, h_{i,o}$, the spike trains are applied over a window Δt, to induce heterogeneity in the network.

Manipulating network heterogeneity: In-network properties

In addition to exploring the effect of stimulation, we sought to investigate the effect of the network's properties on excitability and heterogeneity. Specifically, we consider the impact of i) the topology and ii) the connectivity weights. These quantities are of particular interest due to their role in setting the mean (see Eq(3.12)) and variance (Eq(3.13)) of the membrane potential. To do this, rather than stimulating, we alter the input statistics of the neurons by changing i) the degree distribution of the topology or ii) the weights.

Specifically, to explore the effect of the topology on the network heterogeneity, we fix the mean connectivity to 15%, but replace the distribution the number of connections is drawn from (see Methods - Section (3.3.1)) with a uniform one. In subsequent simulations, the variance of the uniform distribution is increased to observe the effect on network heterogeneity. For all of these simulations, the weights are maintained at a constant value, $w_{i,j} = w_o$.

For the contribution of the weights, the topology is kept to the initial degree distribution with 15% random connectivity. However, the weights are no longer constant ($w_{i,j} \neq$

w_o). Instead, the weights are drawn from uniform distributions and multiplied by the connections ($C_{ij} = 0$ or 1), to obtain the realized weight matrix W. As the network is all excitatory, the weights are all chosen to be $w_{ij} \geq 0$.

In both cases, it is of interest to know what level of heterogeneity these in-network properties create and their ability to retain any induced heterogeneity. Thus the simulations for each case are first allowed to run until a baseline level of heterogeneity is achieved, after which spike trains of different rates (Y_i in Eq (3.20)) are applied for an interval $t = 3000$ to induce elevated heterogeneity in the network. When the stimulation ends, it can then be observed in each framework if, and to what extent, the induced heterogeneity is successfully retained.

3.4 Results

3.4.1 Intrinsic plasticity and neural excitability

To explore the relationship between intrinsic plasticity and heterogeneity, we considered a simple and well-studied [115, 305] excitatory network endowed with a phenomenological model of intrinsic plasticity, whereby the excitability of individual neurons changes in an activity-dependent manner. Similar to other forms of adaptation [34, 35, 31, 115, 347, 346], homeostatic intrinsic plasticity was implemented by allowing the slope, β, and rheobase, h, of each neuron's excitability curves to change as a function of membrane potential fluctuations (see Fig (3.1A,B)), while preserving a target homeostatic firing rate.

A key difference between the myriad of other models of neural adaptation [115, 305, 174, 347, 346, 34, 35, 31, 270] and ours stems from the presence of degeneracy, a phenomenon where multiple unique sets of solutions can produce a highly similar performance. Importantly, this differs from redundancy, where multiple sets of the same elements perform the same function [262, 119, 306]. While long understood in theory, it is only more recently that degeneracy has been understood as a pervasive property of biological systems, including in the brain where neurons with widely varying ion channel conductances can nonetheless exhibit remarkably similar electrophysiological properties [246, 13, 266, 104, 8]. This is particularly true for excitability, as multiple forms of contextual, environmental, and neuromodulatory perturbations may cause changes in input statistics to trigger intrinsic plasticity, ranging from variations in synaptic dynamics, synchrony, input amplitude and position, shunting inhibition, total conductance, depolarization state, and fluctuations in the membrane potential [97]. Leveraging this in our model, we implement degeneracy by allowing the neurons to possess different excitability profiles while sharing a common target firing rate (see Methods). By this, numerous combinations of β and h satisfy the equilibrium conditions of the intrinsic plasticity equations, which define a curve which we call the *degeneracy curve*, $h(\beta)$. Over time β and h converge to the degeneracy curve maintaining the cell at a set target firing rate (see Fig (3.1C)). As the statistics of the neuron's membrane potential change, the combinations of β and h required to preserve the target firing rate change too, repositioning the degeneracy curve in parameter space.

To demonstrate how intrinsic plasticity shapes the excitability profile of neurons (Fig (3.1)), simulations were performed in which individual neurons were exposed to different

inputs (resulting from both connectivity and external stimuli). From these simulations, three categories (classed by ad hoc thresholds of impinging firing rate to each neuron) of excitability emerged as a result of neuron exposure to persistent high-, mid- or low-amplitude activity (Fig (3.1D)). For those neurons receiving high-amplitude activity, compared to baseline, the intrinsic plasticity-driven excitability changes in h (Fig (3.1E)) and β (Fig (3.1F)), yielded hypoexcitability. In contrast, low-amplitude activity did the opposite and yielded hyperexcitability. Despite displaying the same target firing rate, such changes in excitability result in an important difference in the neuron's response to forthcoming stimuli, as both the rheobase (i.e., h) and slope (i.e., β) of the resulting excitability curve had changed significantly. These results echo the experimentally observed homeostatic responses of neurons to low and high activity [331, 83, 111], supporting the qualitative behavior of this model of intrinsic plasticity.

3.4.2 Intrinsic plasticity supports changes in cell-to-cell heterogeneity and network dynamics

Our central hypothesis is that, within an active network, the tuning of cellular excitability through intrinsic plasticity will modulate population diversity. To investigate this potential relationship between diversity and activity, we placed our network of neurons into three distinct activity level regimes by applying a constant input equally to all neurons (i.e., $+/-I_o$) reflective of three different physiological/experimental states (see Fig (3.2A)): 1) a baseline state, where the network receives no external stimulation, and thus the activity

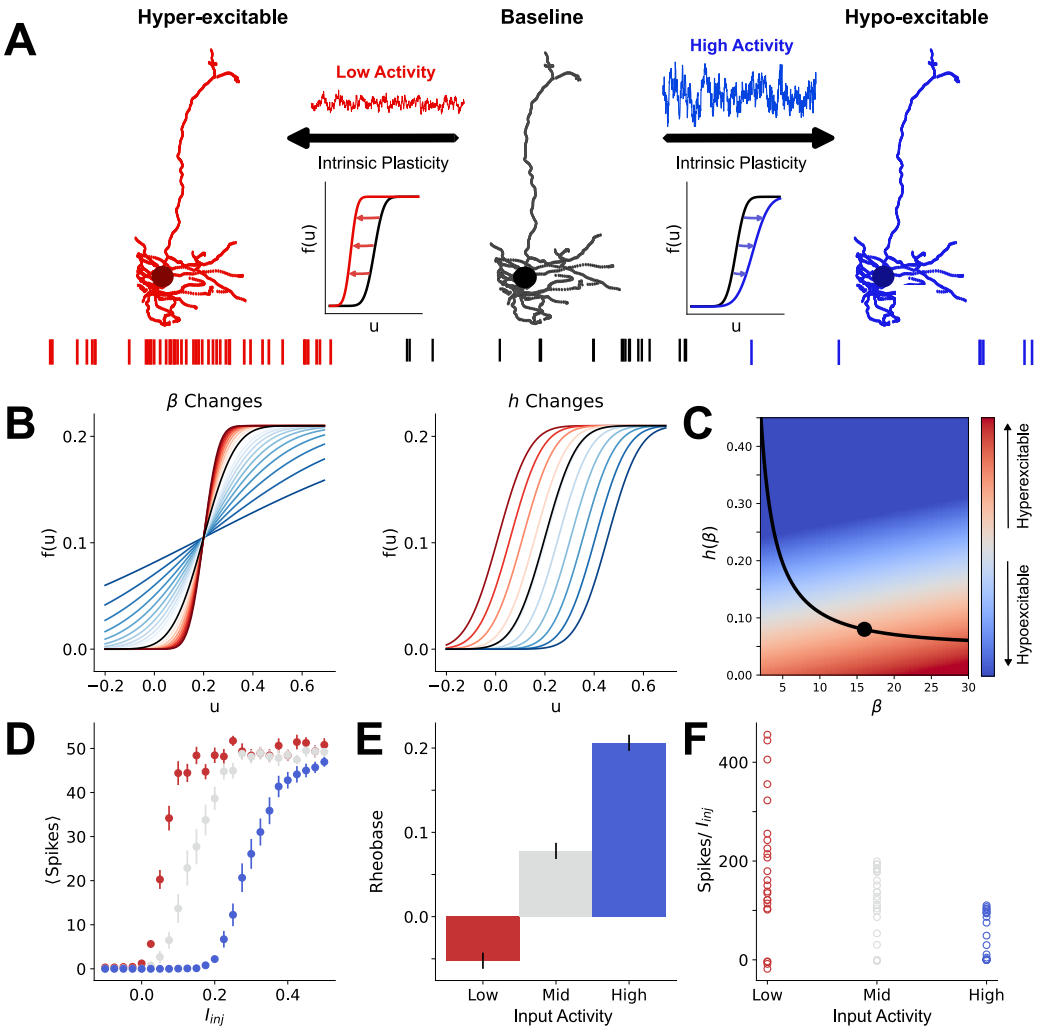

Figure 3.1: **Intrinsic plasticity regulates neuron excitability in response to input statistics.** Caption continued on next page.

Figure 3.1: **A)** For a given neuron, its excitability is altered by the input statistics it receives via intrinsic plasticity. Changes in input statistics can result from multiple factors, including connectivity and weights. In response to an increase in activity (such as from a high amount of input; blue), a neuron becomes hypoexcitable. Conversely, a low activity (red) will yield hyperexcitability. Both of these directions of change are facilitated by intrinsic plasticity. **B)** Intrinsic plasticity adapts the slope, β (left) and rheobase, h (right) of the excitability in response to high (blue) and low (red) input activity. **C)** The slope and rheobase the excitability adopts are directly influenced by the intensity of input received, where high (blue) intensity yields hypoexcitable low slopes and high rheobase values, and low (red) intensity the opposite. The black line is the degeneracy curve, and the black circle acts as an exemplar initial parameter set for a given neuron. When the input intensity changes to lower or high activity, the neuron will adopt new parameters via intrinsic plasticity that are more hyperexcitable (low activity) or hypoexcitable (high activity), the relative parameter spaces for which are demonstratively shown as a heat map. In a simulated network of $N = 100$ excitatory neurons, the varied statistics of their presynaptic firing rates will cause a heterogeneous population of excitabilities to emerge. By assigning thresholds, these excitabilities can be grouped into three broad categories of the amount of activity the neurons receive (low (red), mid (grey), and high (blue)). Correspondingly, this results in neurons that are hyperexcitable (red) and hypoexcitable (blue) with the mid group having excitability between these extremes. **D)** This excitability is shown as the average number of spikes produced by neurons in each grouping when stimulated by step currents, I_{inj}, for $t = 700$ ms intervals with increasing current amplitude (see Methods). Error bars are SEM. The spikes evoked by the step current are recorded and reflect the rheobase, h, **E)** and gain, β, **F)**.

of the population is entirely dictated by the recurrent connectivity of the network; 2) a high activity state similar to what is observed in the upstate of the cortex [304, 320] or in a region receiving feed-forward drive [76]; and 3) a low activity state similar to what is found in slice culture [108], or deafferented cortex [21] where the population receives a scarcity of excitatory drive. Thereafter, a second stimulation protocol, *without plasticity*, is leveraged to demonstrate the dynamical differences between the three excitability levels obtained (see Fig (3.3A)).

The top row of Fig (3.2E) shows that persistent high and low activity states cause shifts in excitability compared to baseline, Fig (3.1), that one would expect experimentally [331, 83]. In the network, these changes are reflected in the shape of the mean network response function, $\langle f(u, \beta_{eff}, h_{eff})\rangle_N$. This mean network response function was computed by assuming that intrinsic plasticity operates over long time scales compared to ongoing membrane potential fluctuations, rendering the excitability profile of individual neurons essentially constant on shorter time scales. The mean response function is characterized by an effective parameterization (β_{eff} and h_{eff}) of the network excitability, where the effective rheobase, h_{eff} is the midpoint of the population-average excitability curve (e.g. $\langle f(u_j, \beta_j, h_j)\rangle_N = 1/2$) and the effective slope, β_{eff}, can be determined from the derivative of this curve (see Methods). The value of these parameters reflects the heterogeneity in excitability found in the network and was determined numerically. We found that receiving persistent high-level input activity caused the excitability to be suppressed homeostatically (Fig (3.2Ei)), whereas receiving persistent low level input activity caused the neurons to become more excitable (Fig (3.2Eiii)) [83] before returning to baseline after the persistent

high and low activity stops (bottom row of Fig (3.2Ei-iii)).

The parameterizations of the excitability, expectedly, change in opposing ways to adapt to the strength of the persistent activity they receive (Fig (3.2F)). In line with Fig (3.1A-C), the neurons exposed to high activity (and hence requiring to become *less* sensitive to maintain their target firing rate) adopt more hypo-excitable curves, characterized by lower β and high h values, and the neurons exposed to low activity (and hence requiring to become *more* sensitive to maintain their target firing rate) adopt more hyper-excitable curves, with higher β and lower h values (Fig (3.2F)). Concurrent with these excitability changes, the population firing rate also rose or dropped in response to high and low drive, respectively, but normalized over time back towards their homeostatic target via intrinsic plasticity (see Methods; Fig (3.2B,C)). Likewise, when the induced activity was turned off, the networks experienced opposing deviations in their firing rate before being driven back toward their homeostatic target again. The amount of time required for a given neuron in the network to regain the target firing rate is dependent on the excitability it possessed at the onset of high- or low-activity (Fig (3.2B)).

Beyond these predictable network-level excitability changes, surprisingly, these shifts in excitability were accompanied by a remarkable amount of malleability in heterogeneity (Fig (3.2Ei-iii)). Heterogeneity was quantified by computing the population-averaged Hellinger distance, $\langle H^2 \rangle_N$, (a similarity metric; see Methods) to track the variability in excitability profiles among cells. Using this metric, the network demonstrated a decline in heterogeneity for both activity states. However, in the high-activity state, this initial loss recovers to an overall increase in heterogeneity as the activity persists (Fig (3.2D)). The initial nominal

drop in heterogeneity in the hypo-excitable case occurs as the sudden increase in activity induces intrinsic plasticity, and all the neurons start moving toward more hypo-excitable parameterizations. However, as the high activity persists, the inter-neuron variance in activity (e.g. from differing connectivity degree) brings the recovery and eventual overtake of the baseline heterogeneity. Moreover, the cessation of the high-activity state induces further heterogeneity. This differs from the hyper-excitable case, which experiences a profound decline in diversity, where the inter-neuron variability in activity becomes small owing to the suppressing nature of the applied input (see Methods). Interestingly, this lost heterogeneity is readily recovered when the low activity stops.

In the hyper-excitable case modelled here, and paralleled by our recent human slice culture experiments [227], a substantial reduction in diversity is accompanied by shifts in mean excitability. These features are similarly reproduced in our simulations (Fig (3.2Eiii)). While a simplified representation, our model effectively captures the adaptive regulation of diversity and its relationship to excitability through intrinsic plasticity mechanisms observed in biological neural networks, thus highlighting how diversity is maintained by activity, declining without it.

Recent experimental evidence, corroborated by numerical and analytical work, has associated reduced heterogeneity in neuron excitability with pathological states [275], and found it broadly destabilizing for brain activity [153, 152]. The results presented in Fig (3.2) support these findings, showing that stimulation can be used to manipulate the excitability (i.e., Fig (3.2E)) and level of heterogeneity (i.e., Fig (3.2D)) of a population of neurons. It remains to explore the consequences of these heterogeneity changes on the

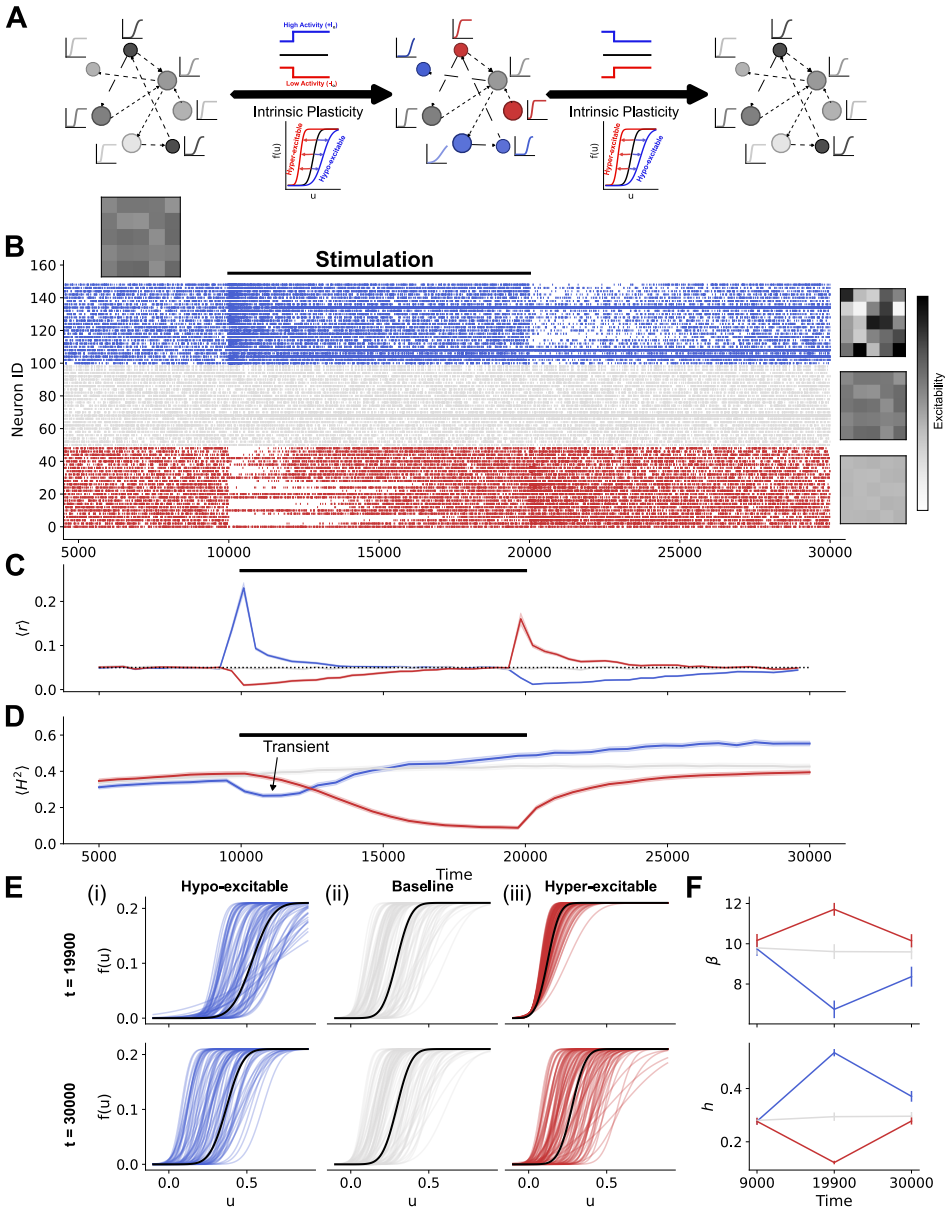

Figure 3.2: **Persistent high and low activity states modulate both excitability and heterogeneity via intrinsic plasticity.** Caption continued on next page.

Figure 3.2: **A)** To explore our network we initialized it to have heterogeneous excitability by randomly sampling $\{\beta_{o,i}, h_{o,i}\}$ for each neuron $i = 1, ..., N$ from independent uniform distributions. For this protocol, the simulation proceeds as follows: after a transient period to allow the randomized excitability parameters to adapt their equilibrium values via intrinsic plasticity (e.g. $r_i = r^o \ \forall \ i = 1, ..., N$), the neurons are all stimulated with a fixed current, I_o. This is considered in three independent simulations, i) $I_o > 0$ (high activity), ii) $I_o = 0$ (baseline), and iii) $I_o < 0$ (low activity). After a time, the stimulation is stopped. Intrinsic plasticity adapts the excitabilities in response to the stimulus's on- and off-sets. **B)** A raster of the firing rate of a random sample of $n = 5$ neurons from the network stimulated with persistent high activity (blue), baseline activity (grey) and persistent low activity (red). The heatmaps are schematic representations of the heterogeneity in excitability obtained in the simulated networks. **C)** The population average firing rate, $\langle r \rangle$, throughout the simulations. The black bar indicates when stimulation is applied to provide persistent high (blue) and low (red) activity. The horizontal dashed line is the target rate, $r^o = 0.05$. **D)** The heterogeneity level in the network, calculated as the population average Hellinger distance, $\langle H^2 \rangle_N$, (see Methods) is calculated as the pairwise average across all neurons. The black bar indicates exposure to stimulation. A window of transient behaviour, indicated by the arrow on the plot, occurs with the onset of high activity (blue) resulting in a temporary decline in heterogeneity as intrinsic plasticity is induced. **E)** Top: The coloured curves represent the excitabilities obtained by the $N = 100$ individual neurons connected with mean degree 15, and the black curve is the mean network response function, $\langle f(u, \beta_{eff}, h_{eff}) \rangle_N$, from simulations of a network initialized with random $\beta_{o,i}$ and $h_{o,i}$ at Top: $t = 19900$ ms following 9900 ms of exposure to stimulation of (i) persistent high activity, $+I_o$ (blue), (ii) continued baseline activity, $I_o = 0$ (grey), and (iii) persistent low activity, $-I_o$ (red). Bottom: plots of the excitabilities at $t = 30000$ ms, 10000 ms after exposure to persistent high (i) and low (iii) activity has stopped. **F)** The average population value of β (left) and h (right) before ($t = 9000$), during ($t = 19900$) and after ($t = 30000$) persistent activity. The error bars are SEM.

network's dynamics. To do this, we exposed networks endowed with the hypo-, hyper- and baseline excitabilities as a result from exposure to different activity levels (Fig (3.3A) and Fig (3.2E), top row) to a slow, time-varying stimulus (i.e., $\eta(t)$) in the form of an Ornstein-Uhlenbeck process selected to interrogate the system's dynamics (see Methods, Section 3.3.6). To avoid confounds, and because it occurred on a much slower time scale, intrinsic plasticity was temporarily turned off for this analysis.

The network response to the applied stimulus is shown in Fig (3.3B). In the baseline case, the neurons' responses varied smoothly, mirroring the stimulation applied. Variability in spiking was observed amongst neurons, as a direct consequence of high excitability heterogeneity (Fig (3.2E)). However, both other regimes had stereotyped network responses: In the hypoexcitable case, the network remained mostly silent and unresponsive, revealing reduced heterogeneity. In the hyperexcitable case, the network dynamics were characterized by sharp, network-wide (i.e., identical between cells) fluctuation alternating between states of full quiescence and states of saturation. This is the signature of heterogeneity decline depicted in Fig (3.2E). Such transitions emerged as the direct consequence of the increased non-linearity of the network mean response function. This homogenization-induced nonlinearity was especially important when the network was in the hyperexcitable regime, wherein bursts of intense activity resulted from small perturbations, suggestive of multistability. That is, in line with what has been observed in previous studies of pathological states [275], reduced heterogeneity results in network dynamics with sharp transitions between alternate states, displaying highly nonlinear behavior. Conversely, heterogeneity prevents such dynamics and replaces them with smooth, more linear responses. To further

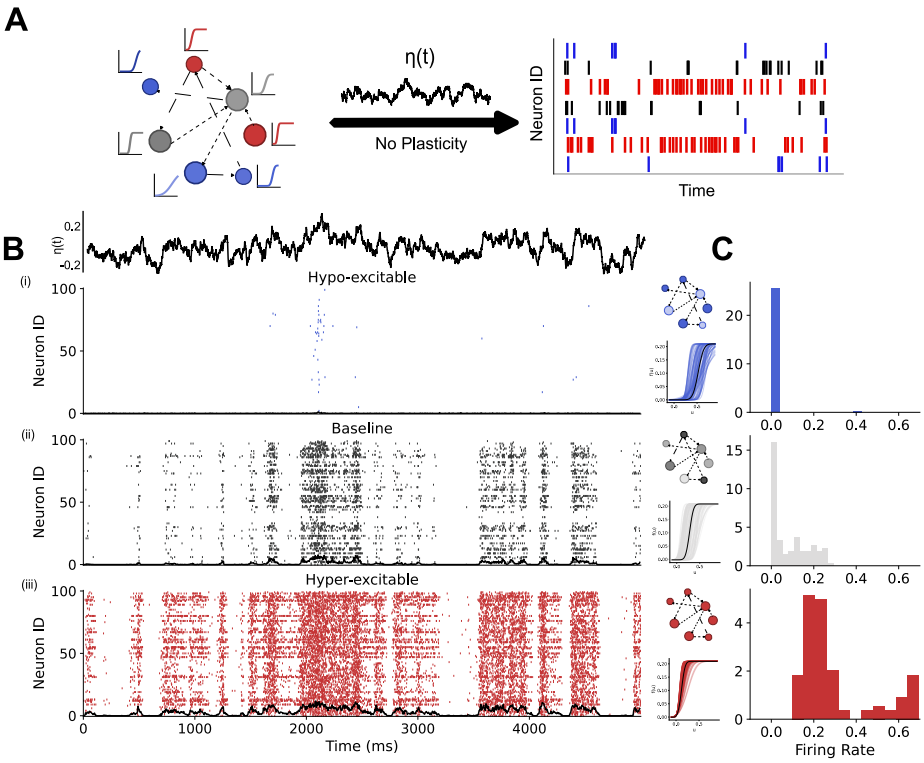

Figure 3.3: **High- and low- activity induced excitability alterations yield aberrant network dynamics.** To explore the dynamics of the different regimes of excitability that are obtained during persistent stimulation in Fig (3.2), we consider a separate stimulation protocol. **A)** In this case, three separate networks are considered. Each is endowed with the excitabilities obtained during the persistent stimulation (e.g. $+/-I_o$)) of Fig (3.2). Importantly, for this protocol, the *plasticity is off*. Instead, the neurons of each network are exposed to a low amplitude, slow Ornstein-Uhlenback input, $\eta(t)$, to demonstrate the differences in network activity for each level of excitability. **B)** Raster of a subset of the neuron responses to the new slow stimulus η (see Eq (3.20)). **C)** Distribution of the firing rates of the $N = 100$ neurons simulated in each network in (B).

interrogate this result, we performed linear stability analysis on the network (see Methods and Supplementary Fig (1)).

Further in line with the spiking behaviour exhibited by the different networks, the hypoexcitable neurons had the lowest firing rates, and the mean of the hyperexcitable neurons was highest (Fig (3.3)C)). The differences in these excitabilities is reflected in the firing rates, showing the high (red) through low (blue) firing rates that result when such hyperexcitable or hypoexcitable populations receive input different from the persistent activity. In addition to the OU process applied here, we further verified the response patterns of the three levels of excitability were robust to more complex stimulation by applying: i) sine waves with uncorrelated noise and ii) partially correlated noise (see Supplementary Fig (2)).

Beyond promoting dynamical stability, our results further demonstrate that heterogeneity enhances the network's computational capabilities. Specifically, in agreement with an extensive number of existing works on the subject [68, 248, 219, 324, 199, 85, 361, 153, 152], mutual information between stimuli and network response is amplified in heterogeneous networks compared to homogeneous networks (see Supplementary Fig (3)), scaling with stimulation amplitude. The mutual information is found to be maximal when the stimulus amplitude is close to the population effective excitability threshold. These results confirm that heterogeneity promotes the encoding of stimuli.

3.4.3 Network heterogeneity reflects variability in cellular milieus

Our results indicate that excitability heterogeneity is an activity-dependent, malleable property of our network model. This malleability arises directly from the intrinsic plasticity equations through an implicit dependence on the membrane potential of individual cells. The impetus for any alteration in the heterogeneity is thus supported by changes to its membrane potential statistics (e.g. $\langle u_i \rangle_T$ and $\sigma^2_{u,i}$ - Eqs (3.12,3.13)) that define the neuron's *milieu* - here defined as the environment or local conditions that impact a neuron's response [336] - resulting from the combination of passive properties (e.g., membrane time constant, leak term), synaptic inputs, and external stimuli. Thus, as has been hypothesized for cells in organ tissue [250, 88], we postulate that heterogeneity is a direct consequence of variability in cellular milieu wherein the neurons adapt to their local conditions. In our model, this is then obtained through intrinsic plasticity. To challenge this claim, we first considered factors that influence the firing rate, r_i, and connectivity weights, w_{ij}. Specifically, we consider these factors as they directly influence the neuron's milieu via the membrane potential statistics to individual neurons (see Eqs (3.12) and (3.13)). Importantly, the inputs to a given neuron are dictated by the excitability (i.e. β_i, h_i) of the presynaptic neurons as well. That is, the milieu is not easily de-tangled from excitability and its heterogeneity itself. However, owing to the regularized firing rates across the network in the steady state (e.g. r^o), we here quantify the heterogeneity (see Methods) in the network and its relationship with the milieu. This analysis, and all hereafter, have

the intrinsic plasticity once more engaged and, unless otherwise stated, have membrane potential dynamics obeying Eq (3.1).

To highlight the effects of different milieu, we simulate a network of neurons each receiving stimulation via a spike train whose rate is drawn from a uniform distribution. The steady-state excitability parameters (β_i, h_i) of each neuron, i, will be at a point along its degeneracy curves (Fig (3.4A; see inset for corresponding excitability curves). To characterize how unique each neuron is from the population, we calculated its Hellinger distance $(\langle H_{ij}^2 \rangle, i \neq j = 1, ..., N)$, which represents the difference of neuron i's excitability profile from those of the $N-1$ other neurons in the network. This was performed on the network in its baseline regime (one where no stimulation is present; $I_o = 0$). This resultant "uniqueness" metric was plotted with respect to the first two moments of the membrane potential of individual cells, that is the temporal mean, $\langle u_i \rangle_T$ (Fig (3.4B)), and variance, $\langle \sigma_{u,i}^2 \rangle_T$ (Fig (3.4C)).

We found that the neurons with the most unique excitability profiles were those with the most unique milieus - characterized by statistics far from the population average (dashed lines in Figs (3.4B,C)). This was also reflected in their degeneracy curves (Fig (3.4A)), where those of high $\langle u_i \rangle_T$ and $\sigma_{u,i}^2$ were positioned far from the population average curve (dashed line). The separation of these degeneracy curves from those around the population average will, via intrinsic plasticity, lead to very different parameterizations of their excitability (Fig (3.1A)) and hence contribute to amplify heterogeneity in the network. These results indicate that factors which increase the variability of membrane potential statistics between cells - i.e., diversify the milieus - promote heterogeneity.

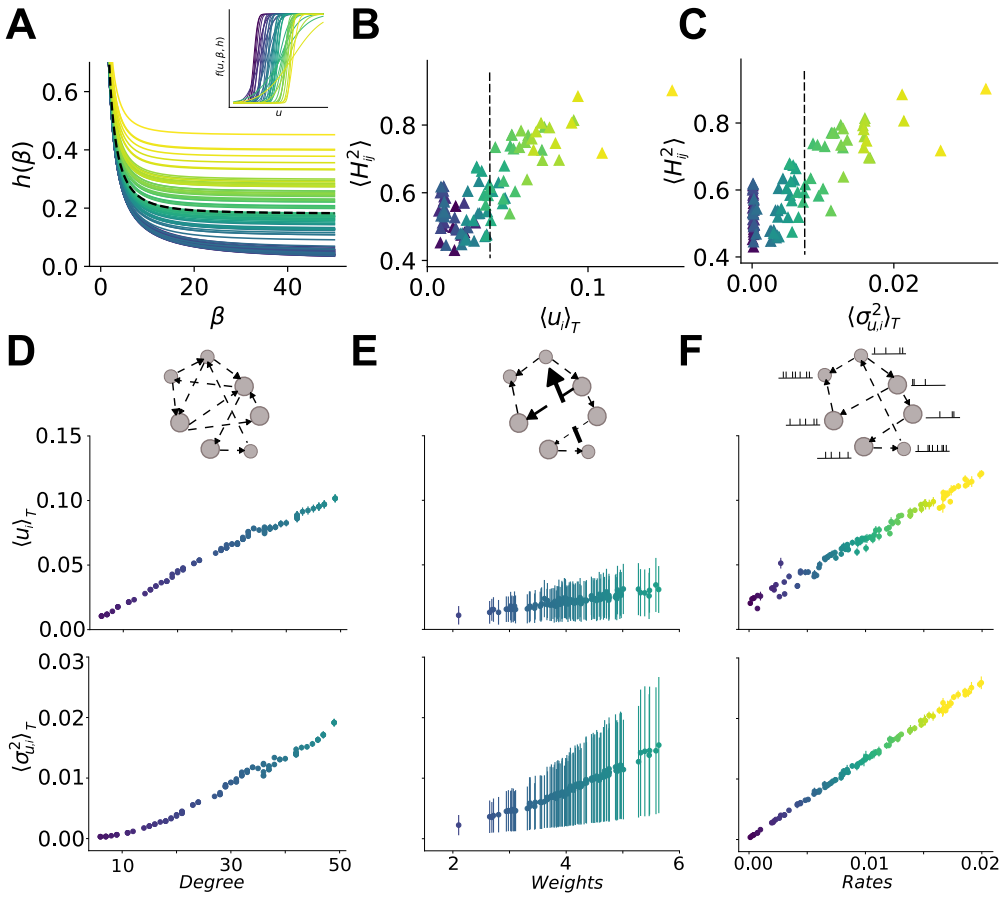

Figure 3.4: **Network properties affecting membrane potential statistics regulate population diversity** Caption continued on next page.

Figure 3.4: For a network simulated with each neuron, $i = 1, ..., N$, receiving stimulation via a Poisson spike train of rate, r_i, drawn from a uniform distribution of rates (see Methods), we plot **A)** the degeneracy curve (Eq. (3.19)) of each neuron using its membrane potential mean, $\langle u_i \rangle$ and variance, $\sigma^2_{u_i}$, colouring the curves such that darker (e.g. more purple-blue) curves correspond to lower membrane potential mean and variance. The corresponding excitability curves (Eq (3.2)) are plotted in the inset. The dashed degeneracy curve is found using the population mean and variance ($\langle u \rangle_N$ and $\langle \sigma^2_u \rangle_N$). The average of the pairwise Hellinger distance for each neuron, $\langle H^2_{ij} \rangle, i \neq j, j = 1, ..., N$ as a function of the membrane potential **B)** mean, $\langle u_i \rangle_T$, and **C)** variance, σ^2_u, of each neuron, $i = 1, ..., N$. The colour of a given point matches its degeneracy curve in (A). The population membrane potential mean, $\langle u \rangle_N$ and variance, $\langle \sigma^2_u \rangle_N$ are shown as dashed vertical lines in each plot. In subsequent simulations, the mean (top) and variance (bottom) of the membrane potential of neurons for varying **D)** in-degree, **E)** sum of the realized weight, W, and **F)** rate of stimulation is calculated for 10 trials each. Error bars are SEM across trials.

To understand the underpinning factors that influence the mean and variance of the membrane potential, which define the milieu, we considered three factors that have major influence on single cell milieus as per Eq. (3.12) and (3.13): the network topology via input degree (Fig (3.4D)), the connectivity weight (Fig (3.4E)), and the presynaptic firing rate, r_s, (Fig (3.4F)). The latter acts as a proxy for a case where the impinging firing rates could be directly manipulated. In line with their theoretical relationship, the mean of the membrane potential was found to scale linearly with the degree of connectivity, synaptic weights and presynaptic firing rate, and scaled non-linearly with the variance of the synaptic weights and connectivity.

Having characterized a relationship between milieu features and the excitability of individual neurons, we sought to elucidate the contributions of these features to network heterogeneity. To do this, we performed a series of simulations where the variances of each trait were systematically increased for different distribution means. At the end of

the simulation, the network's effective excitability (Fig (3.5), top row) and heterogeneity (Fig (3.5), bottom row) were calculated as the population-average Hellinger distance (see Methods).

Beginning with the degree of connectivity (Fig (3.5A)), we found that regardless of the mean degree, increasing the variance of the degree distribution increased the heterogeneity of the network. Specifically, because the presynpatic weights are not scaled with respect to the degree, increasing the variance of the degree distribution results in a perturbation to the milieu of the postsynaptic neurons, driving intrinsic plasticity. As the distribution of the degrees widens, and hence the cell-to-cell degree becomes more heterogeneous, the milieus of individual neurons become correspondingly different (Fig (3.4D)), and the excitability heterogeneity increases. The observed increase in heterogeneity from high $\langle Degree \rangle$ and σ^2_{Degree} was in agreement with our analytical predictions, where $\langle u_i \rangle_T$ (Eq (3.12)) and $\sigma^2_{u,i}$ (Eq (3.13)), and hence the milieu, were related to degree as it controls the number of local synaptic connections. In contrast, Fig (3.5B) showed that changes in effective excitability scaled mostly with the mean synaptic weight, $\langle w \rangle$, but did not vary significantly with the distribution's variance, $\sigma^2_{Weights}$. Not unexpectedly increasing the mean of the degree distribution, $\langle Degree \rangle$, produced a more hypoexcitable effective excitability. Increasing the mean of the weight distribution similarly increased the network heterogeneity. However, increasing the variance of the weight distribution had no such effect (Fig (3.5B)). Finally, we investigated the influence of the presynpatic firing rate on excitability and heterogeneity. As with degree, the heterogeneity of the network increased with higher variance in the distribution of presynpatic firing rates (Fig (3.5C)). Taken together, these results suggest

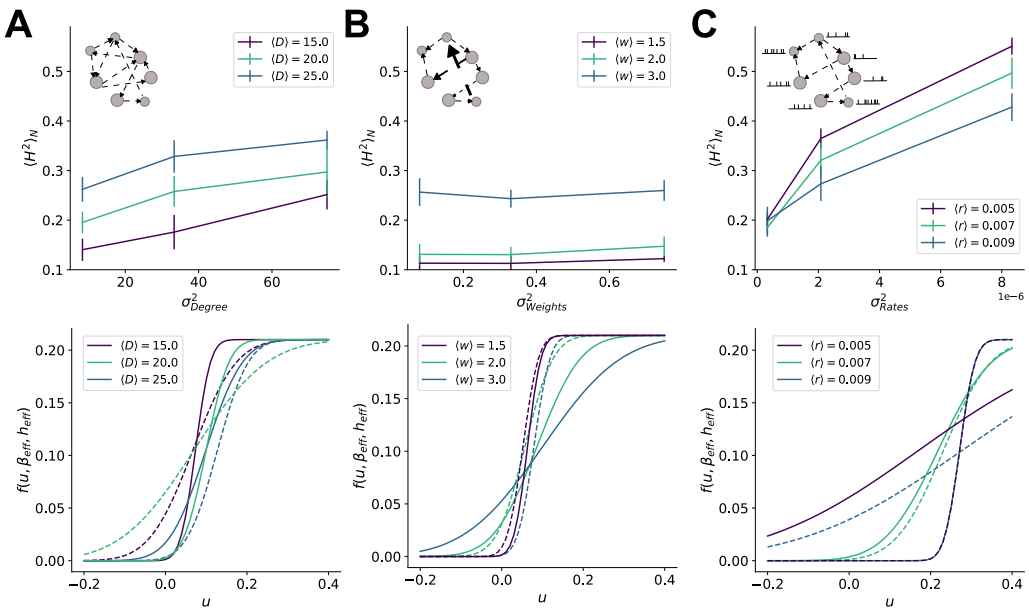

Figure 3.5: **Increased variance of degree distributions and stimulation rate but not weights yields elevated heterogeneity.** For networks of increasing variance in **A)** the degree distribution, σ^2_{Degree}, **B)** the weight distribution, $\sigma^2_{Weights}$, and **C)** the rates of Poisson spike trains that act as surrogates for presynatpic firing rate (see Methods), σ^2_{Rates}, population-average heterogeneity, $\langle H^2 \rangle_N$ (top), and the effective excitability profiles (bottom) are plotted for three different means. For the effective excitability profiles, the dashed lines correspond to the lowest variance cases and the solid lines to the highest variance cases. Error bars are the standard deviation across ten independent simulations at each variance level. When not otherwise stated, the network for all subsequent simulations has a degree distribution with mean 15 connections and fixed weight, $w_{ij} = w_o$, for all connections. The network is simulated for $T = 20000$ ms, during which intrinsic plasticity allows the evolution of each neuron's excitability in response to the neuron's milieus.

that degree and presynaptic firing rate are the most influential on the neurons' milieus, and hence the heterogeneity of the network.

3.4.4 Application: external stimulation as a candidate for stabilizing changes in heterogeneity

Collectively, the previous results indicated that: 1) intrinsic plasticity makes heterogeneity malleable; 2) variability in milieu features promotes increased diversity in the network; and 3) such increased diversity is activity-dependent. We therefore sought to explore the malleability of heterogeneity in the context of neuromodulation, where exogenous stimulation may be a potential therapeutic intervention. Specifically, we wished to verify 1) whether external stimulation may be used to modulate the heterogeneity of our network model and 2) if such induced changes in heterogeneity might persist in time (i.e., whether networks can retain such stimulation-induced heterogeneity). To this end, we repeated the simulations of networks with different variances in the degree distribution (Fig (3.5A)), but included a fixed input, I_o, injection for an epoch of duration $\Delta t = 10000$ ms in the middle of the stimulation. From these simulations, we compare the heterogeneity in the network in three epochs: before (pre; $\Delta t = 15000$ ms), during (stimulation; $\Delta t = 10000$ ms), and after (post; $\Delta t = 10000$ ms). The pre-stimulation duration is longer to allow the network excitabilities to reach a steady state from their randomized initialization. The heterogeneity of each of these epochs is measured by calculating $\langle H^2 \rangle_N$ for the network at a time point near the end of each epoch ($t = 14000, 24500$ and 34000 ms, respectively).

This process was repeated for injections of input with increasing amplitude.

As can be seen in Fig (3.6A), heterogeneity increases with stimulation, I_o, of sufficiently high amplitudes. This was true across a range of degree distribution variances. However, increasing variance of the degree itself had only limited effect, contributing only when stimulation was a moderate amplitude (Fig (3.6B)). This suggests, in agreement with Fig (3.5A,C), that more heterogeneity is recruited by the manipulation of presynaptic input than the variance of degree. Interestingly, the induced heterogeneity was found to persist after stimulation offset when the amplitude of stimulation was sufficiently large (Fig (3.6B)). In line with Fig (3.2), this suggests that the network, perhaps by recruiting the pre-existing heterogeneity from the distributed degree of connectivity, has enough variability to sustain the heterogeneity induced by stimulation.

In fact, for stronger stimuli, there is a net increase in the mean population membrane potential, $\langle u \rangle_N$ (Fig (3.6C)) that results in a more hypoexcitable effective excitability post-stimulation (Fig (3.6D)). This occurs because, as the stimulation amplitude increases, neurons in the network that were quiescent pre-stimulation are induced to fire. When this occurs for sufficient neurons (e.g. the majority or all of the neurons in the network), the baseline activity of the network increases. However, while the population's effective excitability becomes more hypoexcitable, some of the neurons with a low degree of connectivity maintain relatively similar excitabilities to their initializations and thus alters the heterogeneity. When the pre- (and hence post-) stimulation excitabilities of the lower degree neurons are more excitable, they fire at a high rate whenever the limited neurons connected to these neurons are active, which is more frequent with the elevated network

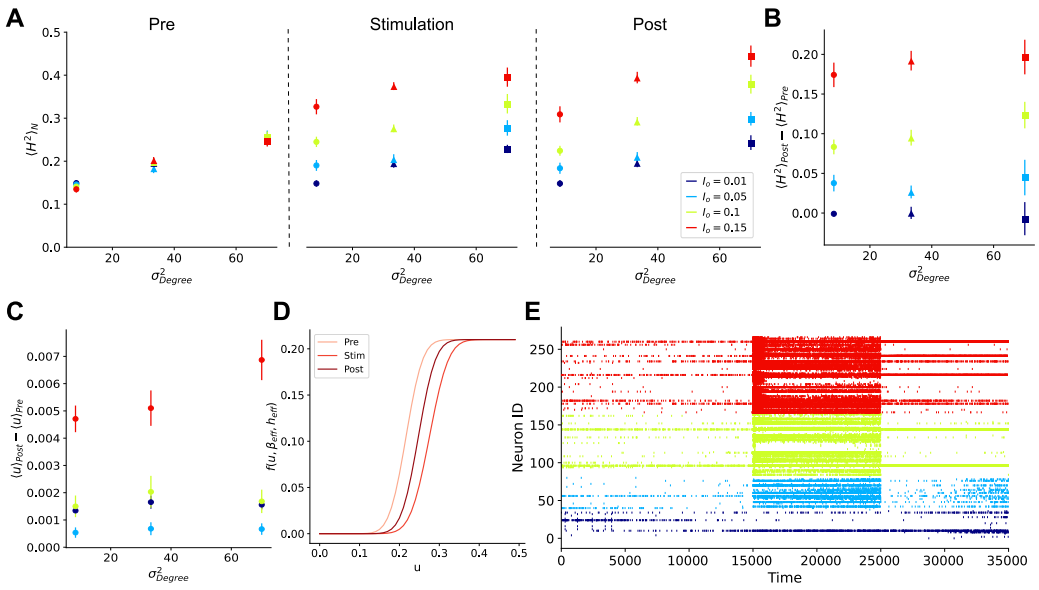

Figure 3.6: **High amplitude stimulation induces heterogeneity across multiple variances in degree distributions. A)** Three networks with increasing variances in their degree distributions and a mean $\langle Degree \rangle = 15$, were simulated for $T = 35000$ ms. Each network received fixed-input injections, I_o, at four different amplitudes (indicated by colour) for $\Delta t = 10000$ ms ($t = 15000$ ms to $t = 25000$ ms). This was repeated 10 times, with the connectivity randomly drawn at the start of each trial. The heterogeneity of each simulation was calculated at three different time points: $t = 14000$ ms (pre-stimulation), $t = 24500$ ms (during), and $t = 34000$ ms (post-stimulation), as the population-average Hellinger distance, $\langle H^2 \rangle_N$. Error bars are SEM. **B)** The difference in the population-average Hellinger distance pre- and post- stimulation obtained in (A). **C)** The difference in the average membrane potential before, $\langle u \rangle_{pre}$, and after, $\langle u \rangle_{post}$, stimulation is calculated for the different degrees of connectivity and strengths of stimulation. **D)** The effective excitability of the highest variance network ($\sigma^2_{Degree} = 70$) under the strongest stimulation ($I_o = 0.15$) is plotted before (pre), during (stim), and after (post) stimulation. **E)** A raster plot showing one simulation of each of the degrees of network receiving stimulation $I_o = 0.1$.

activity (Fig (3.6E)). This subsequently supports the continuation of the post-stimulation elevated population mean membrane potential, and hence the maintenance of the attained heterogeneity.

3.5 Discussion

Our computational modelling and mathematical analyses reveal that neuronal activity "milieus" interacting with degenerate homeostatic intrinsic plasticity rules can actively modulate neuronal diversity. Herein, our work animates the conceptually static image of transcriptomic and electrophysiological diversity [61, 314, 62, 147, 226, 295, 58, 298], towards understanding within cell-type diversity as a homeodynamic process. In this light, rather than a fixed monolithic property of neuronal populations, within-cell-type diversity takes on an adaptive property of networks dependent on activity statistics, connectivity, and intrinsic plasticity rules. This has particularly salient implications, as recent genetics research has found that neurons receiving different inputs (e.g. baroreceptor versus catecholaminergic) form unique clusters in reduced dimensional anaylsis [250]. That is, differential inputs to individual cells drive population variability at the phenotypic level.

Crucially, in our network model, this occurred in neurons endowed with a degenerate intrinsic plasticity mechanism, wherein qualitative similarity of their dynamics (e.g. firing rate) is achieved with diverse excitability curves. Such degeneracy has been observed throughout the nervous system, including at the level of ion channels [8, 266, 208], which directly relates to the plasticity rule implemented here. Including degeneracy in our frame-

work distinguishes the approach from existing adaptation models [34, 35, 31, 174, 346, 305, 115, 347], where neurons exposed to the same input statistics reach identical parameterizations. The intrinsic plasticity in the model serves to modulate the level of diversity in response to the milieus the neurons experience. However, in actual neurons, changes in excitability manifest as biophysical alterations such as upregulation of ion channels [336, 305, 97, 306]. By including the ability to capture these differences in our model, we obtained a much more biophysically plausible model [119, 357, 208, 8], supporting the candidacy of intrinsic plasticity as a mechanism by which diversity is actively maintained, and which can be lost under pathological conditions.

Importantly, here, we were interested in exploring the malleability of excitability heterogeneity as a result of intrinsic plasticity in a homeostatic context. This neglects heterogeneity that may be observed in more non-equilibrium regimes, such as from firing rate heterogeneity [288]. Rather, we limit our results to those about an equilibriated firing rate, in part, due to the simplistic nature of our network model (Eq (3.1)), and all of the neurons being excitatory, which limits the dynamical regimes available to the model. However, while beyond the scope of this work, there remain many interesting questions about the role of this mechanism in non-equilibrium states.

Within this framework, our finding that the hyperexcitable state gives rise to seizure-like dynamics through diversity decline is particularly compelling, as it supports the emerging view that network 'silence' may serve as a convergent pathway to seizure generation across diverse neurological and neurodegenerative disorders [320]. Although such silence is thought to destabilize network dynamics through homeostatic increases in excitability

alone [320, 83, 331], our previous work suggests the associated diversity decline is equally culpable in allowing pathological dynamics to emerge [275, 153, 152].

Aside from its utility for pathological explorations, our model's relative simplicity allowed us, with analytical motivation, to interrogate what network properties support heterogeneity. Specifically, we consider those features that effect the membrane potential statistics, $\langle u_i \rangle_T$ and $\sigma^2_{u,i}$, (Eq. (3.12) and (3.13) and Fig (3.4)) that comprise each neuron's milieu. In our analysis, we found each neuron's milieu was defined by the presynaptic firing rate, connectivity, and weights. Increasing the mean of any of the three properties and increasing the variance of the degree or presynaptic firing rate directly increased network heterogeneity (see Fig (3.5)). The network weights having less influence on the ability of the network to induce heterogeneity implies that the local milieu differences between neurons acquired by varying the weights are small compared to those created by topology (e.g. degree). This is of particular interest as it has been reported in recent years that the probability of connectivity within and between different cortical layers and regions is variable [58, 70]. This may then serve a purpose in bolstering the heterogeneity within the brain. That is, in line with transcriptomic work [250] and theory in non-neuronal cells [88], increasing the variability in input to individual neurons shifts the network into near-subclasses reflective of the milieus the neurons experience (e.g. separation of neurons with low degree and hence membrane potential mean and variance from those with a high degree). This separation of milieus begins to cause increased diversity in the excitability analogous to what is observed under different activity levels as was simulated (see Fig (3.1D-F)) and aligns with experimental manipulation of presynaptic firing rate [111].

In this context, it is well established that the number of synaptic connections a neuron receives — its degree — is log-normally distributed, reflecting the heavy-tailed structure of cortical and hippocampal networks[55]. Interestingly, transcriptomic levels of many ion channel genes also exhibit log-normal distributions. Our work here provides a parsimonious explanation for this convergence via intrinsic plasticity [358]. Neurons with high synaptic degree tend to fire more frequently and with higher burst probability, engaging calcium-dependent signalling cascades and transcriptional regulators such as CREB and Fos, which in turn modulate ion channel gene expression [197]. Because both synaptic input and transcriptional output are shaped by multiplicative, synergistic processes—rather than linear summation—their resulting distributions naturally follow log-normal statistics [55]. This link provides a mechanistic bridge from network topology to cellular identity, suggesting that intrinsic plasticity may serve to reinforce or even amplify the functional stratification imposed by the log-normal architecture of connectivity.

The malleability of heterogeneity observed in our model shares a remarkable convergence with our previously reported experimental papers [275]. This is particularly true in the hyperexcitable state (see Fig (3.2Eiii)), which paralleled our recent human slice culture experiments [227] where a substantial reduction in diversity is accompanied by shifts in mean excitability. In our computational approach, the hyperexcitable state is induced by applying a negative fixed input (see Methods). Similar to a slice experiment, wherein the neurons are deafferented, this pushes the neurons in our network to a $\sim$ homogenous, near-zero mean that will move the target parameters of the neurons into the hyperexcitable regime (see Fig (3.1C) and Methods). That is, the milieus of the neurons become

aggressively similar. This differs from the hypoexcitable state, where applying a positive fixed input yields an initial transient decline in heterogeneity (see Fig (3.2D)). However, ultimately, the baseline variance in the milieus created by the network connectivity is preserved (unlike the large quenching experienced in the low activity regime) and pushes the neurons to new, greater levels of heterogeneity across the hypoexcitable regime. Compared to physiological regimes, which are constrained by factors such as energy expenditure, our model has no upper bound in parameteric space.

From a functional perspective, our current work positions the work of Tripathy et al. [324] in a "dynamic" light, suggesting that heterogeneity can be tuned by the statistics of afferent input. Their results show that population coding is optimized not by maximal heterogeneity, but by an intermediate level tailored to the structure of the stimulus. This suggests that intrinsic plasticity mechanisms could adapt the diversity of a neuronal population to match its functional demands. For example, a population exposed to highly periodic, low-dimensional input — such as a rhythmic oscillation — may converge toward similar intrinsic properties, effectively homogenizing the population to encode redundant temporal/spatial features efficiently. In contrast, exposure to more asynchronous, high-entropy input, rich in temporal or spectral complexity, could diversify the population, broadening its receptive field space to enhance coding capacity. An excellent example of this is the visual system that is pluri-potent in the activity it can generate in reponse to stimuli of varying spatial statistics. We have provided computational evidence of how, within the same network, visual input of low spatial variance generates gamma oscillations, whereas stimuli with high spatial variance generate broadband power changes indicative

of asynchronous (high-entropy) population activity [54]. Thus, stimulus-driven patterns of activity may shape population heterogeneity through intrinsic plasticity, enabling neural circuits to flexibly allocate variability in service of efficient coding.

3.5.1 Limitations

Due to the mobile nature of the degeneracy curves in response to increases in $\langle u \rangle$ and σ_u^2, and the equations which regulate the intrinsic plasticity (Eq (3.3) and (3.4)), the network is sensitive to its initialization conditions. If the initialization of β and h starts a sizable portion of the neurons on or near the multistable region (see Fig (3.7C) shaded region) or in the hyperexcitable regime it may result in initially high activity that will prompt a period of hypoexcitability in the network by causing a large upward migration of the degeneracy curves. Further, the lack of inhibitory activity in the model predisposes the network to bursts of high activity if a sufficient portion of the neurons occupies the hyperexcitable parameter space at the same time. Such states result in intermittent fluctuations in the rate, as any sudden burst of high activity induces the network's plasticity to adapt toward hypoexcitability. Additionally, as β_i are restricted to positive values for all neurons (Eq (3.3)), initializations placing neurons near the minimum and maximum (e.g. 0 or β_{max}) risk neurons reaching those boundaries and becoming stuck.

To quantify the amount of heterogeneity in the networks here, we use the Hellinger distance as a metric (see Methods). We use this in order to have a metric by which we can directly, analytically relate the parameters β and h to the heterogeneity, in this case

via their relationship to the mean and variance of the derivative of the excitability curve. Importantly, though both parameters contribute to the heterogeneity measured by this metric, there is a disproportionate weighting to heterogeneity in β compared to h. This is due to the scale difference in the parameters and the variance of β being accounted for by a squared term (see Eq (3.38)). As a result of this, if the heterogeneity is increased, for example, before and after stimulation predominantly in h, it may appear small in $\langle H^2 \rangle$ for such cases. This can be verified, visually, instead by looking at the standard deviations of the excitability curves when overlaid.

3.6 Conclusion

We have demonstrated that a degenerate intrinsic plasticity rule is a viable mechanism for dynamically regulating heterogeneity in an excitatory network. Specifically, we showed that intrinsic plasticity can sustain, increase, or decrease diversity. Such "dynamic diversity" is dependent on the milieus experienced by the neurons in the network as a function of the input statistics to each neuron, which are manipulated by external stimuli, and amount of diversity itself. These results thus form the framework for future investigation into how the statistics that arise in more complex networks may influence the heterogeneity and hence functional capacity [324] and resilience of neuronal networks [275].

3.7 Appendix

3.7.1 Mean field analysis

To formally relate intrinsic plasticity and heterogeneity at the network scale in Eq. (3.1) we leverage an approach inspired by mean field theory [153, 152]. Taking the mean of Eq (3.1) yields

$$\left\langle \tau \frac{du_i}{dt} \right\rangle_N = -\langle u_i \rangle_N + \left\langle \frac{1}{N} \sum_{j=1}^{N} w_{ij} X_j \right\rangle_N, \tag{3.22}$$

where $\langle \cdot \rangle_N = \mathbb{E}_N[\cdot]$ corresponds to the ensemble average taken across all neurons in the network. Recalling that in a regime of high firing rates and uncorrelated spiking, $X_j \approx r_j + \sqrt{r_j}\xi_j$ [311], and that $r_j = f(u_j, \beta_j, h_j)$, one may write

$$\tau \frac{d\bar{u}}{dt} = -\bar{u} + \rho w_o \langle f(u_j, \beta_j, h_j) \rangle_N \tag{3.23}$$

since $\langle \xi_j \rangle_N = 0$. In the above, we assumed independence between the firing rates and synaptic weights i.e. $\mathbb{E}_N[w_{ij} r_j] = \mathbb{E}_N[w_{ij}]\mathbb{E}_N[r_j]$, which holds whenever the degree distribution is relatively uniform, and introduced the population mean membrane potential (i.e., the mean field) defined by

$$\bar{u} \equiv \langle u_i \rangle_N = \mathbb{E}_N[u_i] \tag{3.24}$$

Equation (3.23) warrants further examination of the population-averaged response function at a given moment in time, defined by

$$\mathbb{F} \equiv \langle f(u_j, \beta_j, h_j) \rangle_N, \tag{3.25}$$

which for $N \to \infty$ may be written as

$$\mathbb{F} = \int \int \int f(u_j, \beta_j, h_j) p(u_j) p(\beta_j) p(h_j) du_j d\beta_j dh_j. \tag{3.26}$$

The above expression depends on the priori unknown membrane potential probability density function $p(u_i)$ (which differs between neurons), as well as the distributions for the slopes $p(\beta_i)$ and rheobases $p(h_i)$ found across the network.

To the best of our knowledge, Eq. (3.26) does not possess a well-defined analytical solution for arbitrary distributions. However, whenever $\rho(u_i^\alpha)$ and $\rho(h_{\alpha,i})$ are normally distributed, Eq.(3.26) is also often sigmoidally shaped. The slope and rheobase of this resulting sigmoid depend on the mean and variance of the distributions $p(u_i)$ and $p(h_i)$, and hence scales with network heterogeneity in those parameters [153, 152]. Motivated by these findings as well as robust numerical observations (i.e., see Figs 3.2,3.5), we assume the population-averaged response function in Eq. (3.25) is also sigmoidally shaped and write

$$\mathbb{F} \approx f(\bar{u}, \beta_{eff}, h_{eff}), \tag{3.27}$$

where β_{eff} and h_{eff} are the effective slope and rheobase of the population averaged re-

sponse. The value of these parameters reflected the heterogeneity in excitability found in the network, and will be determined numerically. It is indeed known that increased heterogeneity will generally decrease the slope β_{eff} of the mean response function [153, 152], effectively making the system behave more linearly. Combining the steps above, we may recast Eq. (3.23) and obtain the dynamics of the mean field,

$$\tau \frac{d\bar{u}}{dt} = -\bar{u} + \rho w_o f(\bar{u}, \beta_{eff}, h_{eff}). \tag{3.28}$$

Steady state. At equilibrium, intrinsic plasticity and network dynamics have both stabilized. There, the parameters β_i^* and h_i^* lie on the degeneracy curve (i.e., Eq. (3.19)) and one has $f(u_j, \beta_j, h_j) \approx r^o$, $\forall j$ as per Eq. (3.7). Hence, Eq. (3.25) reduces to

$$\mathbb{F} \approx r^o. \tag{3.29}$$

Thus, within the scope of the approximations above, the steady state of Eq. (3.28) is found to be

$$\bar{u}^* \approx \rho w_o r^o. \tag{3.30}$$

The steady state $\bar{u}^*$ above is furthermore unique. Indeed, since the derivative of Eq. (3.2) with respect to u_i is always positive, Eq. (3.7) possesses a single root. We further highlight that this steady state does not depend explicitly on the excitability of individual neurons in the network, and results directly from homeostasis, by which the firing rate of each cell

is normalized.

Stability. To characterize the effect of excitability heterogeneity on network stability, we rely on an adiabatic approximation. We first assume that under the action of the intrinsic plasticity equations, which operate on a slower time scale, the system has reached equilibrium: neurons adopt their individual excitability profiles (i.e., β_i^* and h_i^*), leading the network towards its steady state activity $\bar{u}^*$ defined above. Over short time scales ($\ll \tau_{IP}$), the excitability profile of individual neurons can be assumed to be constant: the value of the parameters β_i and h_i do not change, even the membrane potential of neurons is perturbed. As such, in this adiabatic regime, the stability of the system depends only on the membrane potential (i.e., Eq. (3.1)), and we may thus restrict our analysis to the mean field equation. While approximate, this approach allows us to relate heterogeneity with stability resulting from the parameters β_{eff} and h_{eff} over short time scales.

Systems such as those in Eq. (3.28) are known to exhibit multistability. The following steady state equation

$$\bar{u}^* = w_o f(\bar{u}^*, \beta_{eff}, h_{eff}), \tag{3.31}$$

may indeed admit one or three solutions, depending on the values of the parameters β_{eff} and h_{eff} [187, 221, 311]. Linear stability analysis indicates that the stability of these fixed points is determined by the following characteristic equation for the eigenvalues $\lambda \in \mathbb{R}$,

$$\lambda + 1 - w_o f'(\bar{u}^*, \beta_{eff}, h_{eff}) = 0, \tag{3.32}$$

with $f'(\bar{u}^*, \beta_{eff}, h_{eff}) = \frac{\beta_{eff}}{\sqrt{\pi}} e^{-\beta_{eff}^2 (\bar{u}^* - h_{eff})^2} > 0$. For the fixed point defined in Eq. (3.30),

this equation becomes

$$\lambda = -1 + \frac{w_o \beta_{eff}}{\sqrt{\pi}} e^{-\beta_{eff}^2 (w_o r^o - h_{eff})^2}. \tag{3.33}$$

The above equation indicates that stability of the steady state $\bar{u}^*$ decreases whenever β_{eff} increases and h_{eff} approaches the value $w_o r^o$, conditions in which the second term on the right hand side of Eq. (3.33) becomes large. We note that this analysis is only valid over short time scales. Over longer time scales, perturbations of the membrane potential will be compensated for by intrinsic plasticity, driving the system back to its baseline steady state $\bar{u}^*$ defined above. Thus, strictly speaking, the steady state $\bar{u}^*$ is stable over long time scales, but allows for brief periods of instability.

3.7.2 Table of parameters

3.7.3 Quantifying heterogeneity

To discuss the heterogeneity of the excitability curves within the network, we first require a metric to quantify it. In choosing a metric for this, we capitalize on the fact that the derivative of the excitability curves is normally distributed, for which there exists a number of established similarity metrics [334, 175, 38]. The derivative of the excitability curve is given by,

$$f'(u, \beta, h) = \frac{\beta}{\sqrt{\pi}} e^{-\beta^2 (u-h)^2} \tag{3.34}$$

Symbol	Definition	Value
u_i	Membrane potential of neuron i	N/A
β_i	Slope of the excitability curve	0.1-50
h_i	Rheobase of neuron i	0-0.7
N	Number of neurons in the network	100
τ_{IP}	Time constant of intrinsic plasticity	$>> \tau$
r^o	The target firing rate of the neurons	0.05
ϵ_β	The learning rate of β	-0.05
ϵ_h	The learning rate of h	0.001
τ	Membrane time constant	1
r_i	Firing rate of neuron i	N/A
dt	Integration time step	0.1
w_{ij}	Weight of connection between neuron i and j	0-0.4
w_o	Fixed connection weight of all w_{ij} unless otherwise stated	0.21
ρ	Connection probability	0.15
X_i	Poisson spike train	N/A

Table 3.1: Model parameters.

where we have dropped the index i for convenience, and further adopts the form of a normal distribution of mean, μ, and variance, σ^2 which can be written in terms of β and h. Specifically, $\mu = h$ and $\sigma^2 = 1/(2\beta^2)$. We use these values to calculate the Hellinger distance, H^2 (Eq (3.38)). The Hellinger distance is a type of f-divergence used to define the difference between two probability distributions [75]. We chose it as our heterogeneity metric because, leveraging the normally distributed shape of the derivative of the excitability (Eq (3.34)), it can be fully resolved in terms of β and h (Eq (3.38)) allowing for a more direct relationship to our excitability. Moreover, the Hellinger distance is bounded between 0 and 1, and is thus a readily interpretable measure of the network heterogeneity where 0 corresponds to fully homogeneous and 1 would indicate heterogeneity with no cell-to-cell overlap. Between any two probability distributions P and Q, the Hellinger distance is defined on measure space χ as,

$$H^2(P,Q) = \frac{1}{2}\int_{\chi}(\sqrt{P(dx)} - \sqrt{Q(dx)})^2 \tag{3.35}$$

for a discrete distribution $P = (p_1, ..., p_k)$ and $Q = (q_1, ..., q_k)$, this is,

$$H^2(P,Q) = \frac{1}{\sqrt{2}}\sqrt{\sum_{i=1}^{k}(\sqrt{p_i} - \sqrt{q_i})^2} \tag{3.36}$$

This measure is bounded between 0 and 1, where the maximum distance 1 is achieved if there is no positive overlap whatsoever between the two distributions. For the special case where the distances are calculated between two normal distributions, $P \sim N(\mu_p, \sigma_p^2)$

and $Q \sim N(\mu_q, \sigma_q^2)$, we can write H^2 as,

$$H^2 = 1 - \sqrt{\frac{2\sigma_p\sigma_q}{\sigma_p^2 + \sigma_q^2}} e^{-\frac{1}{4}\frac{(\mu_p - \mu_q)^2}{\sigma_p^2 + \sigma_q^2}} \tag{3.37}$$

where μ's and σ^2's are the mean and variance of the respective distributions, as noted earlier, these can be written in terms of β and h for the excitability curves. This then yields,

$$H^2 = 1 - \sqrt{\frac{2\beta_p\beta_q}{\beta_p^2 + \beta_q^2}} e^{-\frac{1}{2}\frac{\beta_p^2\beta_q^2(h_p - h_q)^2}{\beta_p^2 + \beta_q^2}} \tag{3.38}$$

where $\beta_p, \beta_q > 0 \; \forall \; p, q$. To quantify the heterogeneity within the network, this value is calculated pairwise for each neuron, and the result is then averaged.

3.7.4 Random walk approach and alternate excitability functions

Prior to the candidate mechanism ultimately used in this work, attempts were made at other approaches. In particular, for the excitability itself, more mathematically simplistic functions were considered, including an exponential function,

$$f(u_i, \beta_i, h_i) = e^{\beta_i(u_i - h_i)}$$

and a standard sigmoid (similar to that used in [275]),

$$f(u_i, \beta_i, h_i) = \frac{1}{1 + e^{-\beta_i(u_i - h_i)}}$$

However, both alternate excitability formulations were discarded due to difficulties with analytical resolvability (sigmoid) or yielding solutions that diverged toward infinity (exponential).

In addition to different excitability formulations, we also considered an alternative adaptation rule for β and h. Specifically, based on the exploratory adaptation model of Schreier et al.'s work [296], a random walk-like approach was considered. Within this framework, each neuron in the network has an excitability curve (Eq 3.2) defined by a randomly assigned slope, β_i, and midpoint, h_i. The readout of the excitability is, as always, the instantaneous firing rate, r_i, of a given neuron. Within this framework, we define a tolerance level, ϵ_{r^o}, around the target firing rate, r^o. Whenever the value of r_i is greater than $r^o + \epsilon_{r^o}$ or less than $r^o - \epsilon_{r^o}$, a random walk is initiated for β_i and h_i. Otherwise, within the tolerance, β_i and h_i stay constant.

In more detailed terms, we define a function $M(r_i - r^o)$, where M is called the mismatch level between the instantaneous firing rate and the target firing rate. The mismatch function, taken directly from Schreier's work [296], is given by,

$$M(r_i - r^o) = \frac{M_o}{2}\left(1 + \tanh\left(\frac{|r_i - r^o| - \epsilon_{r^o}}{\mu}\right)\right)$$

which is a sigmoid centred around the target firing rate, r^o. μ is the sigmoid's steepness,

and $M_o = 2$ its maximum value. Whenever a random walk is triggered for the parameters (e.g. the instantaneous firing rate is outside the tolerance level around the target firing rate), the walk follows,

$$d\beta_i(t) = \sqrt{DM(r_i - r^o)}dN_t(0, \sigma^2_{u_i})$$

and

$$dh_i(t) = \sqrt{DM(r_i - r^o)}dN_t(0, \sigma^2_{u_i})$$

where D is the scale parameter, and dN_t is the stochastic noise associated with the walk. Importantly, unlike the Weiner process conventionally used for random walks [232], here we instead draw from a normal distribution centred around zero with a variance equal to that of the membrane potential, $\sigma^2_{u_i}$. This was done to tie the random walk to the activity of the neurons.

Ultimately, this approach was unsuccessful as a candidate mechanism, as the network was poorly behaved, frequently exiting the tolerance region unless the region itself was made overly broad. Additionally, in instances where the membrane potential variance, $\sigma^2_{u_i}$, was large, there was an increased likelihood of a given step in the walk overshooting the tolerance region. Conversely, for low variance cases, the steps were often so small that it would take an exorbitant amount of time for any steady state to be reached.

3.7.5 Supplementary Figures

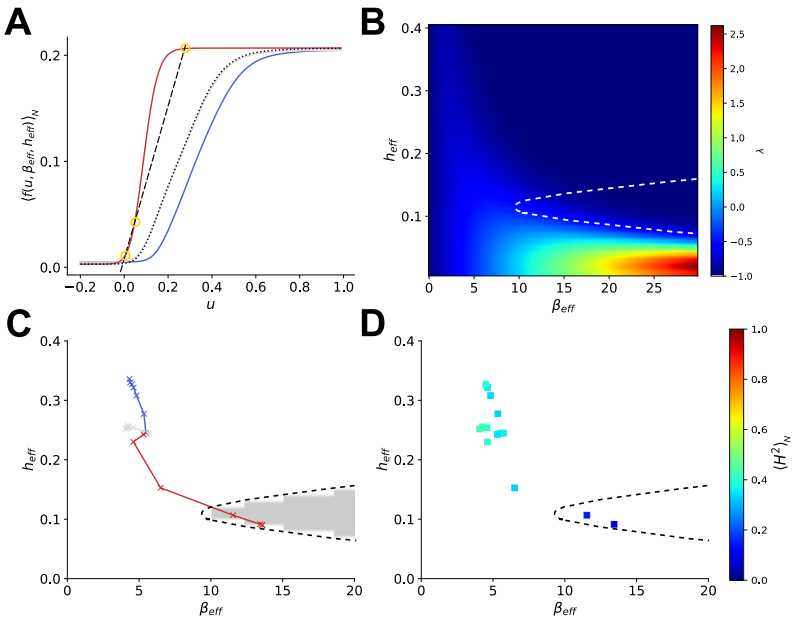

Figure 3.7: **Linearization and stability analysis. A)** The population average excitability profile, $\langle f(u, \beta, h) \rangle_N$, for the network under chronic over- and under-stimulation and at baseline as simulated in Fig (3.2A). The dotted line is $\langle f(u, \beta, h) \rangle_N$ pre-stimulation. Yellow circles indicate fixed points of the red excitability curve. The dashed line in these plots represents the graphical intercept indicating the fixed-point location(s) on each excitability curve. **B)** The effective parameterizations of $\langle f(u, \beta, h) \rangle_N$ over the time course of the simulation. The shaded region is the graphically determined multistable regime. The dashed line around this region is replicated on (C) and (D) for visualization. **C)** The eigenvalue of the network, λ, as calculated from the mean field predictions of the model (see Methods; Eq (3.33)) for combinations of β_{eff} and h_{eff} when the weights of the network are $w_o = 0.21$ and the target firing rate is $r^o = 0.05$. **D)** Relationship of the heterogeneity level in the network, measured as $\langle H^2 \rangle$ (see Eq (3.38)), to the effective excitability.

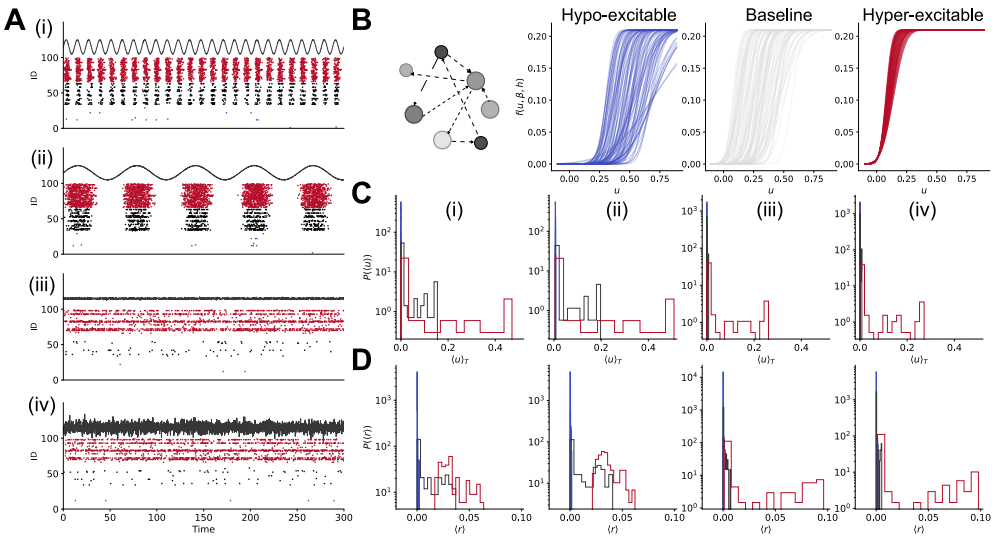

Figure 3.8: **Characterization of fixed network dynamics.** Building on the simple OU process dynamics demonstrated in the hypo- (blue), baseline (grey) and hyper-(red) excitable networks in Fig (3.3), we follow the fixed excitability protocol (Fig (3.3A)) in the three networks for more complex stimuli. **A)** The response of a subset of neurons ($i = 1, ..., N$) in a network for each excitability type is plotted in response to (i) high ($\omega_s = \pi/6$) and (ii) low frequency ($\omega_s = 0.1$), noisy ($D = 0.05$) sine waves ($S_i(t) = S_o \sin(\omega_s t) + \sqrt{2D}\xi_i(t)$), and (iii) uncorrelated ($c = 0$) and (iv) partially correlated ($c = 0.5$) noise ($S_i(t) = \sqrt{2D(1-c)}\xi_i(t) + \sqrt{2Dc}\ \xi_c(t)$) stimulations. **B)** Each network has sparse, random connectivity with probability $\rho = 0.15$. The excitabilities for each of the networks are plotted. We subsequently plot **C)** the distribution of average membrane potentials and **D)** average firing rates for each network type and stimulation (i-iv).

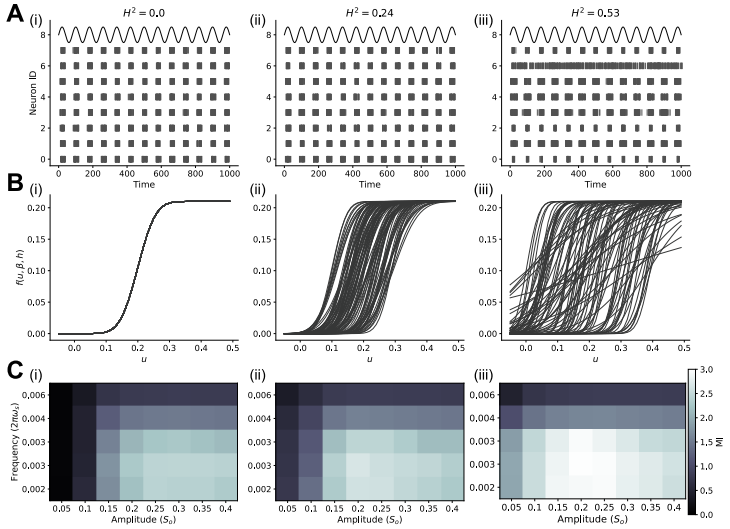

Figure 3.9: **Heterogeneity improves encoding of input signals.** Heterogeneous excitability has been linked to improved coding by numerous experimental and computational works [68, 248, 219, 324, 199, 85, 361, 153, 152]. To validate that this holds in our own framework, we consider the network *without plasticity* in three different levels of heterogeneity: (i) homogeneous excitability ($H^2 = 0$), (ii) partially heterogeneous excitability ($H^2 = 0.24$), and (iii) highly heterogeneous excitability ($H^2 = 0.53$). The neurons in the network are each stimulated with a sine wave, $S(t) = S_o \sin(2\pi\omega_s t)$, for various amplitudes, S_o, and frequencies, ω_s. **A)** An example raster for a few neurons from each level of heterogeneity receiving sine waves ($S_o = 0.25; \omega_s = 0.0125$) are shown. **B)** The excitabilities of the neurons in each level of heterogeneity are shown. The heterogeneity is increased by increasing the variance of uniform distributions of β and h about fixed means ($\langle\beta\rangle = 16, \langle h\rangle = 0.2$). To assess the relationship between heterogeneity and encoding, we calculate **C)** the mutual information (MI) between the average firing rate, $\langle r\rangle$, and the applied stimulation, S, to reflect how well the stimulus modulates the network activity. In line with what has been done in previous work ([311]) we calculate the MI as MI $= \frac{1}{2}\log_2(1 + \text{SNR})$, where SNR is the signal-to-noise ratio, SNR$= \omega/(1-\omega)$ and ω is the zero-lag cross-correlation of $\langle r\rangle$ and S. Calculating this across simulations of varied stimulus amplitudes and frequencies, we found that for a majority of signal parameterizations, networks with heterogeneous excitability encoded the stimulus as well or better than the homogeneous case.

4

Exploring the influence of cell-type-specific human cortical excitability on network dynamics

4.1 Abstract

Neural excitability captures the transformation and encoding of neural input to output firing rate, thus allowing neurons to flexibly and selectively respond to the wide range of inputs they receive. When experimentally measured, excitability has recently been found to be heterogeneous both within and between cell types. Indeed, interest in cell-type heterogeneity has steadily grown as increasingly more detailed datasets have highlighted the prevalence of heterogeneity throughout the brain. However, most modelling efforts to explore the dynamical consequences of heterogeneity in neural excitability have used only the variability in threshold of activation and further assumed similar distributions of excitability between excitatory and inhibitory populations. Here, leveraging openly available data from the Allen Institute for Brain Science on the excitability of human cortical excitatory and inhibitory neurons, we built an augmented Wilson-Cowan model network, whose connectivity and excitabilities are constrained by human cortical data. We find the excitatory and inhibitory neurons to have quantifiably different excitabilities. Exploring both between- and within-cell-type excitability heterogeneity, we find that such sources of variability contribute to modulating the population firing rates and their correlations. Further, the within-cell-type excitability heterogeneity promotes network insensitivity to changes in the inhibitory weights, while retaining excitatory weight sensitivity.

4.2 Introduction

The human cortex has a complex and heterogeneous organization on multiple scales, from genes and synapses to cells, neural circuits, and regions [335, 324, 63, 42, 226, 58, 182]. Despite this multiscale heterogeneity, the dynamics of the cortex, which have been extensively studied in both experimental and theoretical contexts [352, 92, 81, 155, 7], are surprisingly robust. In fact, heterogeneity has recently been linked to stability [153, 152], improved encoding [219, 112], the absence of synchrony [349, 120, 22], and avoidance of pathological states, such as autism, schizophrenia and epilepsy [237, 275, 227].

Many of the rich dynamics observed in the cortex arise from the interactions between excitatory and inhibitory (E and I) neurons. These two types of cells are, both between and within themselves, heterogeneous. This includes their physical properties, such as their morphologies (e.g. branching, cell size, etc.) [42], electrophysiological properties (e.g. rheobase, sag, input resistance, etc.) [182, 67], connectivity motifs [93, 58], and genes [295, 298, 44]. In the context of electrophysiological heterogeneity, of particular interest in recent decades has been the neural gain, or *excitability*. The excitability of a given neuron, which reflects its past activity [331, 77], characterizes its sensitivity to incoming electrical input with respect to the rate of its output firing rate. Within a population of neurons, the excitability heterogeneity then reflects the variability in features of those neurons [326]. The excitabilities are often characterized in terms of the threshold of activation (e.g. rheobase), slope, and amplitude [163, 299, 229, 97]. When measured

experimentally, in both mice and humans, neural excitability has been shown to differ both between-cell-type (e.g. E vs I cells) and within-cell-types [237, 226, 58, 182]. What is less clear from these datasets is what, if any, effect the heterogeneity between- and within-cell-type excitability heterogeneity has on cortical dynamics. Indeed, in addition to pathologies associated with aberrant excitability - such as tinnitus [192, 138], chronic pain [69] and epilepsy [275] - understanding the heterogeneity of excitabilities has been proposed as an avenue for elucidating the differences underlying pathologies associated with aberrant excitation [237, 36].

Models of heterogeneity in neural excitability have often focused on the one particular parameter: the threshold of activation [121, 120, 219, 220, 275, 153, 152, 112]. Studies of this variety of heterogeneity have shown it to affect synchrony and firing rate and increase the stability of the dynamics [220, 153, 152]. However, these models often treat heterogeneity across neurons as similarly distributed in excitatory and inhibitory neurons. As such, the effects of between- and within-cell-type excitability heterogeneity on network dynamics are largely unknown. Moreover, this neglects the contributions of the slope and amplitude of excitability, which have their own contributions to neural excitability [229].

To address this, we implement an augmented Wilson-Cowan network of excitatory and inhibitory neurons with subtype-specific excitabilities. These excitabilities are taken from recent datasets of human cortical neurons made freely available by the Allen Institute for Brain Science. Characterizing these excitabilities, we determine the between-cell-type-specific differences in effective excitability and explore how this influences the network dynamics. Thereafter, we incorporate the excitability heterogeneity within cell-types and

interrogate its influence on the population firing rates and their correlations, finding it to attenuate the firing rate in comparison with homogeneous frameworks. Finally, we find that within-cell-type excitability heterogeneity makes the network sensitive to changes in the excitatory, but not inhibitory, weights. Together, these features suggest that the heterogeneous, subtype-specific excitability found in cortical neurons impacts the dynamics of our network model.

4.3 Methods

4.3.1 Model network

The model network, a data-informed adaptation of the Wilson-Cowan network [352, 87], has N neurons of which K^E are excitatory (E) and K^I are inhibitory (I). The neurons are sparsely connected with probability, ρ, based on the average connectivity of human cortical cells from [58] with synaptic weights $(w^{EE}, w^{EI}, w^{IE}, w^{II})$ from the same dataset (see Section (4.3.1)).

Each neuron, $i = 1, ..., N$, is given an excitability curve, f, with slope, β_i^α, and threshold, h_i^α, drawn at random from the distribution for their subtype $\alpha = \{E, I\}$ (see Section (4.3.2)). For both populations, f is a sigmoidally shaped function given by,

$$f(A_{,i}^\alpha, \beta_i, h_i) = \frac{1}{2}\left(1 + \text{erf}(\beta_i^\alpha(A_i^\alpha - h_i^\alpha))\right) \tag{4.1}$$

where the activity, A, is a proxy for the membrane potential of each neuron i.

The dynamics of the neurons' firing rates, r_i^α, in the two populations are given by,

$$\tau^E \frac{dr_i^E}{dt} = -r_i^E + f_i\left(\frac{1}{\rho K^E}\sum_{j=1}^{K^E} w_{ij}^{EE} X_j^E + \frac{1}{\rho K^I}\sum_{j=1}^{K^I} w_{ij}^{IE} X_j^I + I^E + \sqrt{2D(1-c)}\xi_i^E + \sqrt{2Dc}\xi_c\right) \tag{4.2}$$

and

$$\tau^I \frac{dr_i^I}{dt} = -r_i^I + f_i\left(\frac{1}{\rho K^E}\sum_{j=1}^{K^E} w_{ij}^{EI} X_j^E + \frac{1}{\rho K^I}\sum_{j=1}^{K^I} w_{ij}^{II} X_j^I + I^I + \sqrt{2D(1-c)}\xi_i^I + \sqrt{2Dc}\xi_c\right) \tag{4.3}$$

where I^α are the baseline currents for the E and I populations; ξ_i^α and ξ_c are, respectively, uncorrelated and correlated Gaussian white noise, with both populations receiving fraction c of their total noise as the same correlated noise; D is the noise amplitude; $X_i = \sum_{\{t_k\}} \delta(t - t_k)$ are Poisson spike trains; and $\tau^{E,I}$ are the membrane time constants. Spiking activity follows a non-homogeneous Poisson process, $X_i^\alpha \to \text{Poisson}(r_i^\alpha)$, where r_i corresponds to the instantaneous firing rate of neuron i. This firing rate depends directly on the membrane potential through the excitability curve (Eq (4.1)) of that same neuron, that is $r_i^\alpha = f_i(A_i^\alpha)$. The values of the parameters can be found in Section (4.3.3).

Connectivity

As we wish to explore the role of heterogeneity in human cortical excitability, we sought to keep our network as data-informed as possible. To this end, we leverage additionally available human cortical data from the Allen Institute for Brain (see [58]) to determine the degree of connectivity and synaptic weights in our model. Within the dataset, the probabilities of connectivity between pre- and post-synaptic connections of human cortical neurons are given by layer for the excitatory neurons, and as a generalized value for the inhibitory neurons. The excitatory neuron probabilities include cortical layers $2, 3, 4$ and 5. For our purposes, we calculate the average of all of the probabilities together (e.g. pooling all layers and both excitatory and inhibitory connections) and use the result as our network connection of probability, ρ. In each initialization, the neurons in the network are randomly connected with this probability.

For the synaptic weights, we leverage the post-synaptic potential amplitudes from the same dataset as the connection probabilities [58]. These are likewise organized by pre- and post-synaptic cell types. Taking the average of each type of connectivity (e.g. EE, EI, IE, and II), we find that the ratios are such that $w^{EI} > w^{IE} \approx w^{II} > w^{EE}$. The values of these weights from the post-synaptic potential amplitudes are then scaled while maintaining this ratio in the model. Specifically, we choose a realized weight value for the largest weight, w^{EI}, and compute the factor, q, required for the dataset weight to equal this value,

$$w^{EI} = q\left(\frac{w^{EI}_{data}}{\rho}\right)$$

The remaining weights for the IE, II and EE connections are then scaled by the same factor, q.

4.3.2 Human cortical excitabilities

The Allen Institute for Brain Science has made publicly available an electrophysiology dataset [317, 58, 182] that includes, among many other properties, the threshold (i.e. rheobase; h in our model), and excitability curve slope (β in our model; see Eq (4.1)), for 413 human cortical neurons. This includes both excitatory and inhibitory neurons from layers $1-6$ across brain regions, including: medial temporal gyrus, frontal lobe, medial frontal gyrus, angular gyrus, inferior temporal gyrus, inferior frontal gyrus, temporal lobe, and superior frontal gyrus (see Supplementary Fig (1)). These neurons were obtained from slices of human cortical tissue of patients with epilepsy or tumors, taking only those far enough from the affected zone to be considered representative of healthy neurons. The neurons were subsequently characterized electrophysiologically in slice experiments (see [58, 182] for details).

To inform our model with these data, we first linearly rescale both the thresholds and slopes to constrain them to the parameter space of our model. Specifically, we rescale the thresholds such that $h_{unscaled} \to h_{model} \in [0, 0.3]$ and the slopes such that $\beta_{unscaled} \to \beta_{model} \in [3, 15]$ (Eq (4.7)). We choose these value ranges for our rescaled parameters $(h_{model}, \beta_{model})$ because of their qualitative similarity to the excitabilities observed in the unscaled data. To fit the parameters to these ranges, we linearly rescale each parameter

in the dataset according to,

$$h_{model,i} = m_h h_{unscaled,i} + b_h \tag{4.4}$$

and

$$\beta_{model,i} = m_\beta \beta_{unscaled,i} + b_\beta \tag{4.5}$$

where m_h and m_β are the slopes needed to rescale h and β to their respective ranges, and b_h and b_β are the intercepts for the rescaling. To determine the values of $\{m_k, b_k\}$ for $k = [\beta, h]$, we pool the excitatory and inhibitory unscaled data for each parameter and set the maximum and minimum equal to the bounds of our desired range. From this we obtain $(m_\beta, b_\beta) = (12, 3)$ and $(m_h, b_h) = (9.5 \times 10^{-5}, 0.014)$. The scaling for h and β are thus, respectively, calculated as,

$$h_{model,i} = 9.5 \times 10^{-5}(h_{unscaled,i}) - 0.014 \tag{4.6}$$

and

$$\beta_{model,i} = 12(\beta_{unscaled,i}) + 3 \tag{4.7}$$

In our network, each neuron receives a $\{h^\alpha_{model,i}, \beta^\alpha_{model,i}\}$ pair randomly drawn from the rescaled dataset to parameterize its excitability curve. Hereafter, we will use β_i and h_i to

mean the model parameters.

Mean excitability

In a few instances, it is of interest to consider the mean excitability, $\langle f(A_i^\alpha, \beta_i^\alpha, h_i^\alpha)\rangle_{K^\alpha}$, taken over a population, $\alpha = \{E, I\}$. For $K^\alpha \to \infty$ the mean excitability may be written as

$$\langle f(A_i^\alpha, \beta_i^\alpha, h_i^\alpha)\rangle_{K^\alpha} = \int\int\int f(A_i^\alpha, \beta_i^\alpha, h_i^\alpha)\rho(A_i^\alpha)\rho(\beta_i^\alpha)\rho(h_i^\alpha)dA_i^\alpha d\beta_i^\alpha dh_i^\alpha. \tag{4.8}$$

The above expression depends on the priori unknown membrane potential probability density function $\rho(A_i^\alpha)$ (which may differ between neurons), as well as the distributions for the slopes $\rho(\beta_i^\alpha)$ and rheobases $\rho(h_i^\alpha)$ found across the network.

To the best of our knowledge, Eq. (4.8) does not possess a well-defined analytical solution for arbitrary distributions. However, whenever $\rho(A_i^\alpha)$ and $\rho(h_{\alpha,i})$ are normally distributed, Eq.(4.8) is also often sigmoidally shaped. The slope and rheobase of this resulting sigmoid depend on the mean and variance of the distributions $\rho(A_i^\alpha)$ and $\rho(h_i^\alpha)$, and hence scales with network heterogeneity in those parameters [153, 152]. Motivated by these findings as well as robust numerical observations (i.e., see Figs (3.2) and (3.5)), we assume the population-averaged response function in Eq. (4.8) is also sigmoidally shaped and write

$$\langle f(A_i^\alpha, \beta_i^\alpha, h_i^\alpha)\rangle_{K^\alpha} \approx f(\bar{A}^\alpha, \beta_{eff}^\alpha, h_{eff}^\alpha), \tag{4.9}$$

where β_{eff}^{α} and h_{eff}^{α} are the effective slope and rheobase of the population-averaged response. These parameters reflect the heterogeneity in excitability found in each subtype population in the network and will be determined numerically.

4.3.3 Table of Parameters

Parameter	**Name**
r_i^{α}	Firing rate of neuron i in population α
τ^{α}	Membrane time constant for neurons in population α
β_i^{α}	Slope of excitability curve for neuron i in population α
h_i^{α}	Threshold (rheobase) of excitability curve for neuron i in population α
K^{α}	Number of neurons in population α
ρ	Probability of connectivity
$w_{ij}^{\alpha\alpha}$	Synaptic weight between two neurons (ij) in populations α
I^{α}	Baseline current to population α
D^{α}	Noise amplitude for population α
ξ_i^{α}	Additive uncorrelated noise to neuron i in population α
ξ_c	Additive correlated noise
c	Fraction of total noise that is correlated

Table 4.1: Parameters used in the network model. In all cases $\alpha = \{E, I\}$.

4.4 Results

4.4.1 Characterizing the excitability of excitatory and inhibitory cortical neurons

Neuron excitability, which defines the reactivity of a given neuron to the incoming electrical activity it receives, varies between neurons both within- and between-cell-types. At its extrema, a neuron's excitability can range from hyperexcitable (e.g. highly reactive to even small input) to hypoexcitable (e.g. low reactivity unless very large input is received) (Fig (4.1A)). In cases of hyperexcitability, this elevated sensitivity can be characterized by a low rheobase and steep slope (Fig (4.1B,C)). Conversely, more hypoexcitable neurons will have high rheobases and less steep slopes. Collectively, these properties will influence the dynamics of both individual neurons and the networks they form. If the average of the excitabilities of all of the neurons in a network is calculated, the effective excitability is obtained (see Methods), and will indicate the relative excitability of the overall network. Populations of neurons with more heterogeneous excitabilities have been shown to have more linear effective excitabilities and dynamics [275, 153], and, in contrast, the nonlinear effective excitabilities in homogeneous networks have been shown to promote unstable dynamics [152, 326].

Data from the Allen Institute for Brain Science [58, 182] show that the excitability of human cortical neurons is not randomly distributed. Rather, there are distinctive excitabil-

ities for the excitatory (E) and inhibitory (I) neurons. Here, we sought to characterize the excitabilities of these subtypes. The dataset includes cortical layers $1-6$ however no significant difference was found between the layers (see Supplementary Fig (1,2)): we thus pool them all and separate only by subtype. Following rescaling to fit the data to our parameter space (see Section (4.3.2)), we plot the slopes (β) and rheobases (h) of the excitabilities. We observe that two groups emerge: one for the excitatory neurons and another for the inhibitory neurons, displaying overall little overlap (Fig (4.1D)). This arrangement of excitabilities is of particular interest as it sets the excitability parameters on an approximately $y = 1/x$-shaped curve. That distribution is similar to the degeneracy curve that arose from our previous modelling of heterogeneous excitability [326], where different parameterizations yielded the same firing rate. This distribution of excitabilities suggests that a level of degeneracy is present between the E and I cells. Regardless, the placement of the cell-types in the parameter space also indicates the type of excitability they possess. Specifically, the inhibitory population has a wider variance in its slopes and smaller threshold variance, and the excitatory population demonstrates the opposite.

Whenever the parameters of the excitabilities (i.e., β, h) are plotted according to Eq. (4.1), a qualitative visualization of the differences in excitability can be observed (Fig (4.1E)). This qualitative visualization further highlights the difference in shape of the excitabilities between-cell-types and the heterogeneity within-cell-type, as well as indicating their relative type (Fig (4.1A)) of excitability. In line with their higher thresholds, we see that the E cells are mostly between mid-range (Fig (4.1A)) and hypoexcitable, whereas the I cells are more hyperexcitable: We thus expect E cells to require larger input to respond,

and I cells to respond strongly whenever they receive input.

To interrogate the dynamics resulting from this particular arrangement of excitabilities, we use them to inform an adapted Wilson-Cowan model (see Methods). Specifically, each neuron in the network is assigned a pair of parameters $\{\beta_i^\alpha, h_i^\alpha\}$ ($\alpha = \{E, I\}$), randomly sampled from the rescaled dataset distribution (Figs (4.1D-F)). We will then use this model to explore the impact of E and I heterogeneity, both within- and between-cell-types, on network dynamics.

Before investigating the consequences of the excitability more broadly, we used the asynchronous state as a baseline for our simulations to observe the difference in activity between the cell types. As can be seen in Fig (4.1G), the differences in excitability between the two populations can be seen in the distribution of firing rates evoked from the neurons through time. While the E population a unimodal one, the I population has a more bimodal firing rate distribution. Said otherwise, the between-cell-type firing rate differences are reflective of the larger effective slope (e.g. increased non-linearity) and smaller variance in threshold of the I cell excitability distribution (Fig (4.1F)). The non-linearity of the effective I cell excitability makes the cells respond strongly or not at all, which manifests as the bimodality of firing rates. The distributed thresholds and more linear slopes of the E cells, conversely, yield a relatively constant, but lower, firing rate.

Despite the differences in the between-cell-type firing rates and largely asynchronous dynamics, the network displays irregular instances of highly coincident spiking (Fig (4.1H)). In these brief, irregular instances of synchrony, the sharp increase in excitatory activity

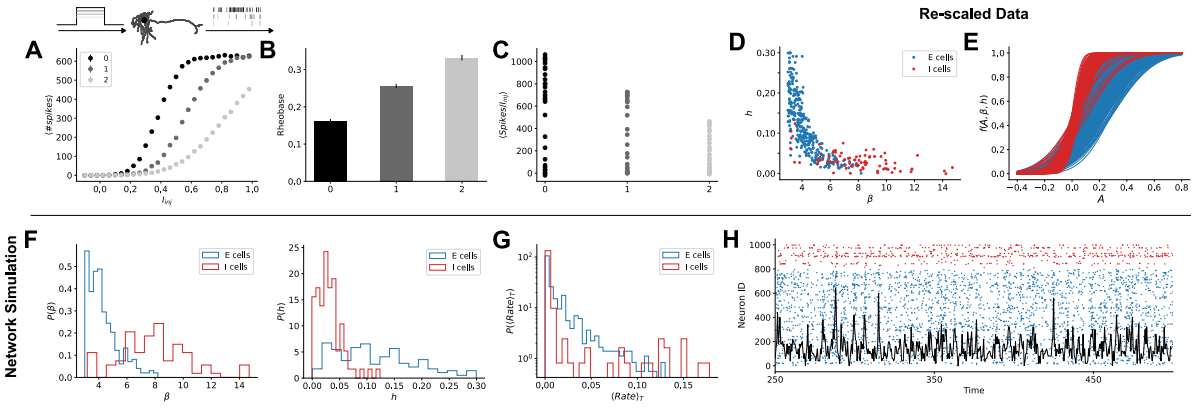

Figure 4.1: **A)** The activity of a single point neuron is simulated for increasing amplitudes of fixed current, I_{inj}. The average number of spikes evoked for each current amplitude is plotted under three different excitability conditions: hyperexcitable (0), midrange excitable (1), and hypoexcitable (2). **B)** The mean rheobase of a neuron with the excitabilities shown in (A) across 10 trials. Error bars are SEM. **C)** The average number of spikes evoked per injected current strength as a function of the excitability of the neuron as shown in (A). **D)** The linear-rescaled (see Methods) slopes, β, and thresholds, h, for the excitatory (blue) and inhibitory (red) neurons in the Allen Institute for Brain Science dataset [58, 182]; **E)** the excitability curves for each $\{\beta,\ h\}$ pair in (D). A network of $N = 1000$ neurons is parameterized with $\{\beta, h\}$ per (D), and randomly connected with probability $\rho = 0.133$. **F)** the probability distributions of (left) the β and (right) h values for the excitatory (blue) and inhibitory (red) neurons. Simulating this network with low-amplitude, uncorrelated noise ($D^E = D^I = 0.01;\ c = 0$) yields **G)** histograms of the excitatory (blue) and inhibitory (red) temporal-average population firing rates. A subset of the activity ($\Delta t = 250$ ms) is shown in **H)** a raster plot. The black line is the population-average firing rate ($\langle r \rangle_N$).

rapidly recruits inhibition. With the more hyperexcitable profile of the inhibitory population, this yields a rapid, strong response, and thus halts the activity before prolonged coincident activity can emerge. This irregular asynchronous regime is of particular interest as a baseline of activity for the network as it represents a state that is stereotypically observed in experimental data [49, 291, 272, 199, 191].

4.4.2 Between-cell-type excitability heterogeneity yields higher firing rates and promotes correlation in excitatory neurons

To explore the dynamical consequences of between-cell-type excitability, we first consider the effective excitability (see Section (4.3.2)), which differs between the E and I cells (Fig (4.2Ai)). Specifically, we seek to investigate the consequences of their specific arrangement on the dynamics of our model network. For simplicity, we exclude the within-cell-type heterogeneity for this part of our investigation, and instead assign all of the cells in each subtype the effective excitability (e.g. $f_i^E = f_{eff}^E$ for all excitatory neurons $i = 1, ..., K^E$ and likewise for the I cells). We do this under three different conditions: (i) The dataset effective excitability (Control case) (Fig (4.2Ai)); (ii) all neurons having the same effective excitability (Mixed case) (Fig (4.2Aii)); and (iii) reversing the effective excitability of the dataset (Reversed case) (Fig (4.2Aiii)). The mixed case is referred to as such because we mix the excitabilities of both cell types to find the effective excitability.

We find that the control case (Fig (4.2Ai)) corresponds to the highest average popula-

tion firing rates, with the reversed case (Fig (4.2Aiii)) having the lowest (Fig 4.2B). The low firing rate in the reversed case shows that when we have more hyperexcitable excitatory neurons and more hypoexcitable inhibitory neurons, we have a regime in which the inhibitory neuron activity prevents the excitatory neurons from firing easily. In the firing rates, this manifests as the average inhibitory firing rate for the reversed case becoming close to the excitatory firing rates of the control and mixed cases. However, the same is not true for the excitatory population in the reversed case, which yields a near-zero firing rate. Thus, from the similarities of the control and mixed cases, we find that making E cells hypoexcitable or I cells hyperexcitable drives an increase in the firing rate.

Beyond the firing rates, we consider the correlation of the firing rates in these networks by calculating the average Pearson correlation coefficient between them, $\langle R_c \rangle_N$ (Fig (4.2C)). This was done for each different connection-type within the networks (e.g. EE, EI, II), as well as for the whole network. From this analysis, we find that the correlation in the EE and EI connections of both the control and mixed cases is significantly higher than in the reversed case. That is, we find cases where the excitatory population is has more linear, hypoexcitability promotes more correlation in E cell firing rates. However, reversing the effective excitabilities led to more correlation in the II connections (reversed case).

Unlike the reversed case, the control and mixed cases show no significant difference in their correlation. This aligns with previous literature, which has shown homogeneous excitability across neuron populations, as is seen in the mixed case, to promote increased correlation in the firing rate [275, 153]. Thus, we would expect this case to have as much, if

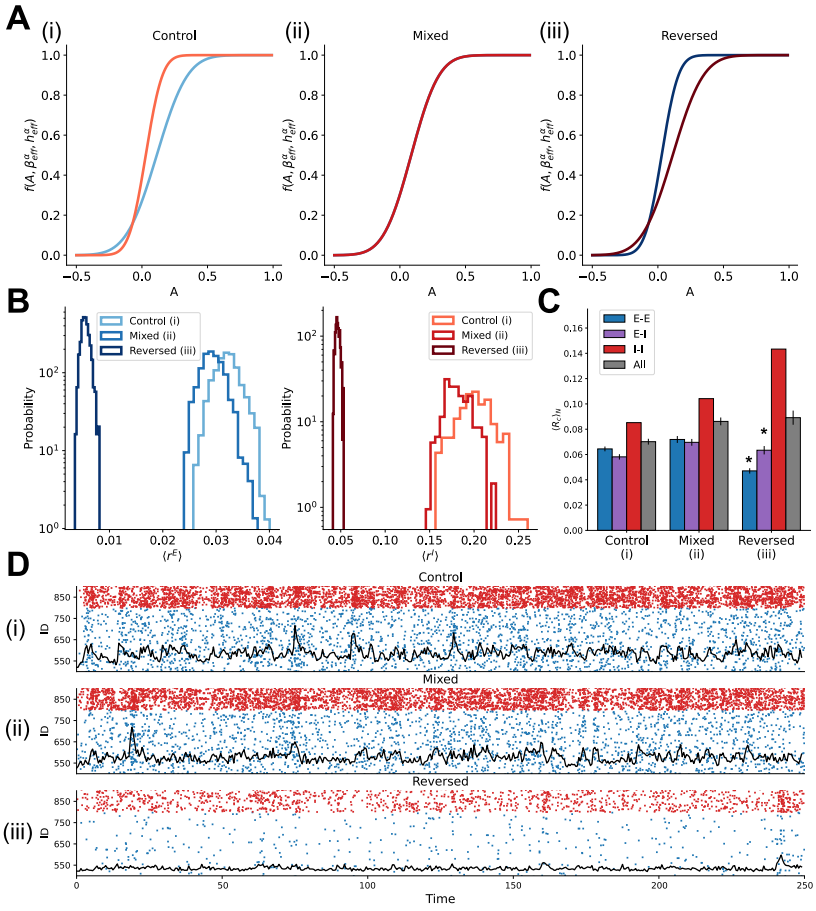

Figure 4.2: Network simulations are performed such that each excitatory (E) and inhibitory (I) neuron is endowed with the effective excitability of that population. This is considered under three conditions: **A)** the control (i.e. true dataset), a mixed case (i.e. E and I are considered to have one distribution), and a reversed case (i.e. switching the distributions of the true dataset). Simulating each network of $N = 1000$ neurons for $N_{trials} = 5$ with low correlation, low amplitude noise ($c = 0.2$; $D^E = D^I = 0.01$), **B)** the population mean firing rates (in ms^{-1}) for the excitatory (left) and inhibitory (right) neurons are shown. **C)** The average correlation of the firing rates is calculated as the average Pearson correlation, $\langle R_c \rangle_N$, for each type of connectivity. Asterisks above the bars for the reversed condition indicate a significant difference from the control and mixed cases, calculated by a Mann-Whitney U test. Asterisks indicate that $p < 0.05$. Error bars are SEM. **D)** An example raster for one simulation of each condition. The black line indicates the average firing rate.

not more, correlated activity as the control case. Moreover, the effective excitability of the mixed case is qualitatively similar to the excitatory population excitability in the control case (compare Fig (4.2Ai) and (4.2Aii)), which may further contribute to the similar levels of correlation they beget.

The effects of the different cases on firing rate and their correlations are likewise observable in the example raster plots for the three cases, where firing rates and irregular, brief instances of highly correlated activity in the control and mixed cases (Fig (4.2Di,ii)) far exceed that of the reversed case (Fig (4.2Diii). Together, this suggests that the between-cell-type heterogeneity observed in the cortex contributes to allowing increased correlation among excitatory neuron activity and elevates the firing rates.

4.4.3 Within-cell-type heterogeneity decreases population firing rate

Having examined the effects of between-cell-type excitability on the network dynamics, we now consider within-cell-type excitability heterogeneity. To do this, we explore two different networks: one where each neuron in the network is initialized with an excitability from the relevant E or I distribution (Fig (4.1G)), and the other where all of the excitatory and inhibitory neurons have the effective excitability of their subtype (analogous to the control case in Fig (4.2)). We simulate these networks for different values of noise correlation, c, and probe the firing rates and their correlations.

In doing this, we find that the heterogeneous network consistently yields a significantly

lower mean firing rate regardless of the noise correlation, c, (Fig (4.3A)). This is true of both the E and I cell populations. In line with what was observed in Fig (4.2), the I cells have a higher average firing rate. Although the mean firing rate of the subpopulations remains constant in both the heterogeneous and homogeneous networks, the noise correlations do affect the variance of the population firing rate over time (Fig (4.3B)) in both the heterogeneous and homogeneous networks.

The introduction of within-cell-type heterogeneity additionally influenced the firing rate correlations of the network (Fig (4.3C,D)). Interestingly, whether the heterogeneous network firing rates were more or less correlated, particularly in the excitatory (EE) connections, was dependent on the correlation of the additive noise, c. Moreover, although statistically significant in their difference at low and high noise correlation levels, the difference between the heterogeneous and homogeneous $\langle R_c \rangle_N$ values is small. The stronger effect on the correlation, instead, being the value of c, with fully correlated input resulting in the highest firing rate correlations in both the homogeneous and heterogeneous cases. Example raster plots of the heterogeneous and homogeneous networks further highlight the completely asynchronous activity when the input is fully uncorrelated as compared to when the noise is fully correlated (Fig 4.3E).

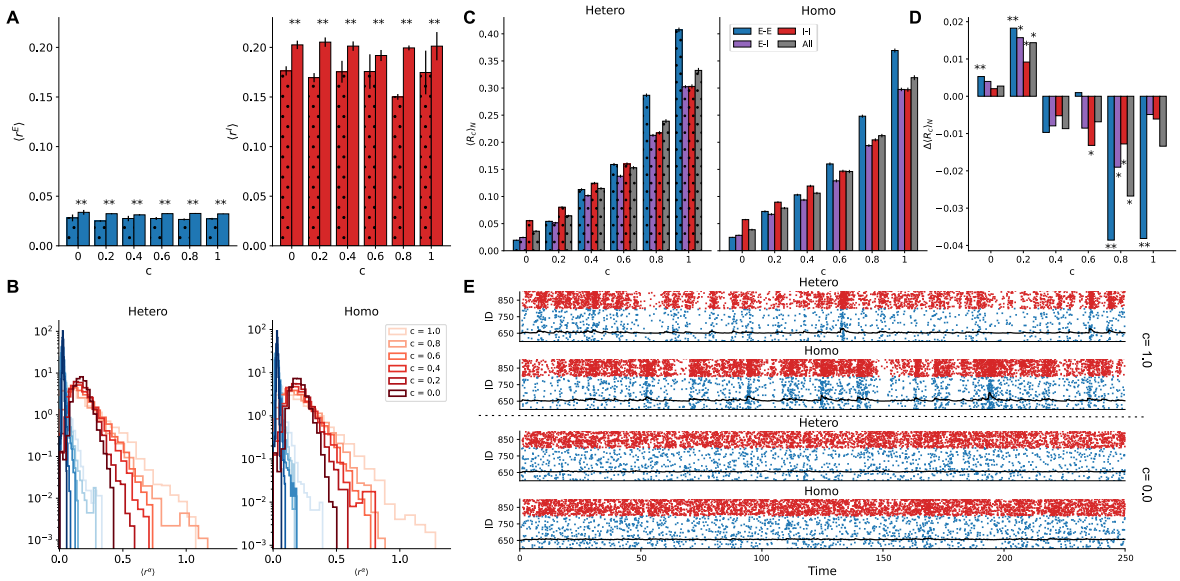

Figure 4.3: The **A)** mean population firing rates of the excitatory (left) and inhibitory (right) neurons in a heterogeneous (dotted bars) and homogeneous (solid bars) network receiving varying levels of noise correlation, c ($D^E = D^I = 0.01$). Each simulation is carried out for $N_{trials} = 5$. Error bars are variance and asterisks indicate $p < 0.01$ for a MannWhitney-U test. **B)** The temporal average firing rate of the excitatory (blues) and inhibitory (red) neurons in a network with heterogeneous (left) and homogeneous (right) excitability. Lighter shades are higher levels of noise correlation. **C)** The correlation of the neurons' firing rates, $\langle R_c \rangle_N$, is measured as the average Pearson correlation coefficient across each type of connectivity in a heterogeneous (left; dotted bars) and homogeneous (right; solid bars) network across varied input correlation levels, c. **D)** The difference, $\Delta\langle R_c \rangle_N = \langle R_c \rangle_N^{Homo} - \langle R_c \rangle_N^{Hetero}$, in the firing rate correlations measure between the two networks as a function of increasing noise correlation. Asterisks indicate the p-value ($* : p < 0.01; ** : p < 0.001$) for a MannWhitney-U test of the type of connectivity between the heterogeneous and homogeneous cases. **E)** Example raster plots of a heterogeneous (upper) and homogeneous (lower) network receiving completely correlated noise ($c = 1.0$) and completely uncorrelated noise ($c = 0.0$). Black lines are the average firing rate.

4.4.4 Within-cell-type heterogeneous excitability increases network sensitivity to weight changes

Beyond the effects of the correlation of the inputs, we now seek to explore the influence of within-cell-type excitability heterogeneity on the network's sensitivity to changes in the synaptic weights. To do this, we consider again the heterogeneous network described in Fig (4.3), and simulate it with one of the synaptic weights changed. For each simulation, the synaptic weights of the connections not being explored are held fixed at their control values.

From these simulations, we find that when the excitatory weights (w^{EE}, w^{EI}) are modulated, the firing rates of the E and I cell populations are highly sensitive to the change across combinations of baseline currents, I^E and I^I (Fig (4.4)Ai,ii). Specifically, the firing rates in both the E and I populations increase well beyond the physiological range with increasing w^{EE}. Conversely, both population firing rates decrease with higher w^{EI}. In line with the sensitivity to w^{EE}, when w^{EI} is very small, the firing rates blow up toward non-physiological levels. Taken together, these sensitivities to changes in the excitatory weights show that the network is highly responsive to excitatory weight perturbations across the full range of weights and at all baseline current strengths.

Unlike the changes to the excitatory weights, when the inhibitory weights (w^{IE}, w^{II}) are modulated, there is generally low sensitivity of the network firing rates (Fig (4.4Aiii,iv)). In the case of w^{IE}, firing rates arose only under conditions of high baseline currents, and when

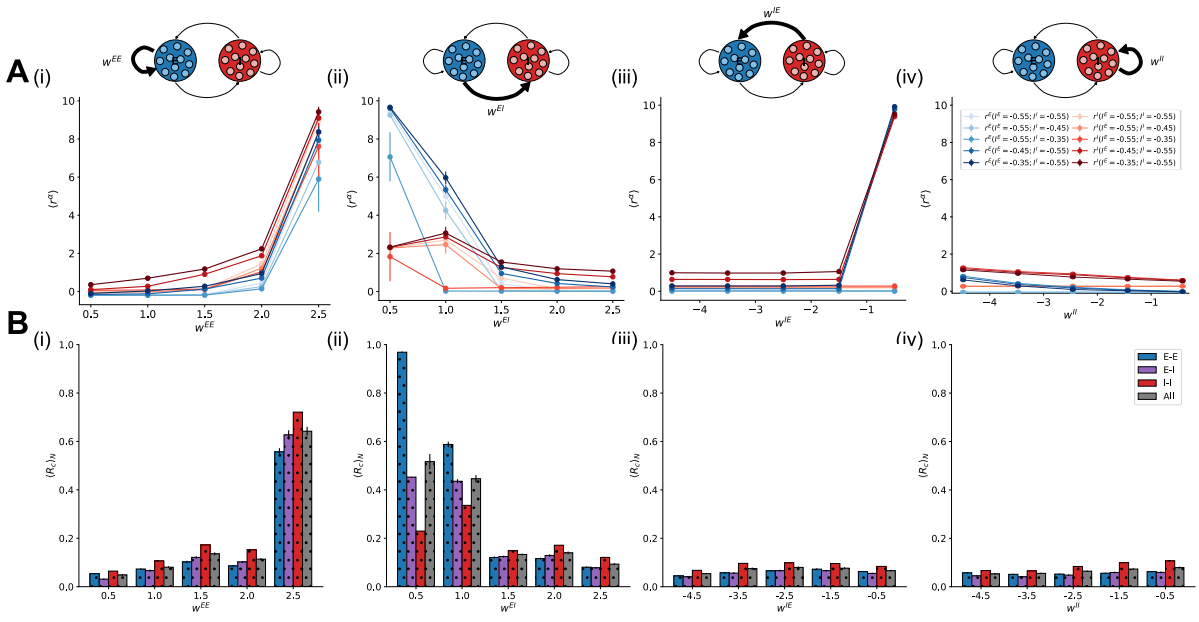

Figure 4.4: The network is simulated with a partially correlated additive noise ($c = 0.2$) for $N_{trials} = 5$. **A)** The average firing rate in ms^{-1} of the E and I cells is plotted for various levels of baseline current (I^E, I^I) are plotted for changing the magnitude of the excitatory to excitatory weights (left), excitatory to inhibitory weights (mid-left), inhibitory to excitatory weights (mid-right) and inhibitory to inhibitory weights (right). Keeping the network in the regime used for the Figures (4.2 and 4.3) (e.g. $I^E = I^I = -0.55$), we plot **B)** the average firing rate correlation, $\langle R_c \rangle_N$, is calculated for each of the weight changes and types of connectivity.

the weight decreased to effectively zero, resulting in an abrupt increase to non-physiological levels of firing. The network was insensitive to changes in w^{II} across all baseline currents. That is, based on this and the excitatory-weight results (Fig (4.4A)), we see that inhibitory control over both excitatory and inhibitory firing rates is preserved across a broader range of inhibitory weights. The contrast with the more gradual firing rate changes observed under excitatory weight perturbations may stem from differences in the within–cell-type heterogeneity between the two populations (Fig (4.1D,E)). Specifically, the inhibitory neurons exhibit less within–cell-type excitability heterogeneity than the excitatory neurons. Combined with their more hyperexcitable baseline state, this reduced heterogeneity produces higher firing rates (Fig (4.3A)) and more all-or-none dynamics compared to the excitatory population

In addition to the firing rates, we also investigated the correlations of the connection types under changes to the synaptic weights. In line with the effects on the firing rates, modifications to the excitatory (Fig (4.4Bi,ii)), but not inhibitory (Fig (4.4Biii,iv)), weights affected the firing rate correlations of the networks. However, as the jumps in firing rate correlation observed in response to the excitatory weights at which the network blows up to non-physiological firing rates (Fig (4.4A-Bi,ii)), this increase largely reflects the firing rate change rather than a more complex change in firing rate correlation, such as would emerge in oscillatory behaviour.

4.5 Discussion

Heterogeneity in neural excitability, as the source of interest here, has been found in a variety of experimental and computational works to contribute to avoiding pathological onset [275, 153, 152], optimal decoding [219, 112], and synchronization [121, 349, 120, 220, 46]. However, many of these approaches have examined this heterogeneity broadly. That is, models of heterogeneous excitability have often assumed similar distributions between neuron subpopulations. Here, we endowed a network with biophysically constrained excitabilities and explored the influence of between- and within-cell-type heterogeneity on the network dynamics.

From our investigations, we find that between-cell-type (Fig (4.1)) and within-cell-type excitability heterogeneity (Fig (4.3)) both affect the neuron firing rates and correlation. In the case of the correlation, previous work has shown that heterogeneity contributes to increased decorrelation of neural activity [248, 149]. However, in our work, we find that comparing the heterogeneous network (within-cell-type excitability heterogeneity) with the homogeneous network (between-cell-type excitability heterogeneity) paints a less clear picture (Fig (4.3C)). Rather, as the correlation of the additive noise changed, it differed whether the heterogeneous or homogeneous network was less correlated. Moreover, the relative difference of correlation between the two networks is small (Fig (4.3D)). This may be, in part, because our homogeneous case uses the between-cell-type heterogeneity rather than an arbitrary excitability.

The modulation of firing rates by human cortical cell-type-specific excitability aligns with recent research using mouse cortical cell-type-specific excitability, which demonstrated that excitatory-inhibitory balance alone was insufficient to account for the correlation and firing rate differences observed in pathologies [237]. Importantly, our exploratory work here does not further subdivide the neurons into types of excitatory or inhibitory neurons. This is particularly important as, within the dataset we use to inform our model, there are fewer inhibitory than excitatory neurons, which may result in an underestimation of the overall inhibitory excitability heterogeneity.

The fact that inhibitory neurons in the dataset show lower excitability heterogeneity is particularly important, because it may help explain why our network is less sensitive to changes in the synaptic inhibitory weights (Fig (4.4A)). Specifically, the insensitivity we observed may be related to the relative homogeneity of the inhibitory neurons, along with their hyperexcitability, as compared to the more hypoexcitable and heterogeneous excitatory neurons. Further investigation into the role of inhibitory neuron excitability in network dynamics will be of importance to future works, as inhibitory activity has been found crucial in neural circuits for decorrelation [272, 285, 7], generating oscillations [302], and learning [106, 115].

4.6 Appendix

4.6.1 Supplemental Figures

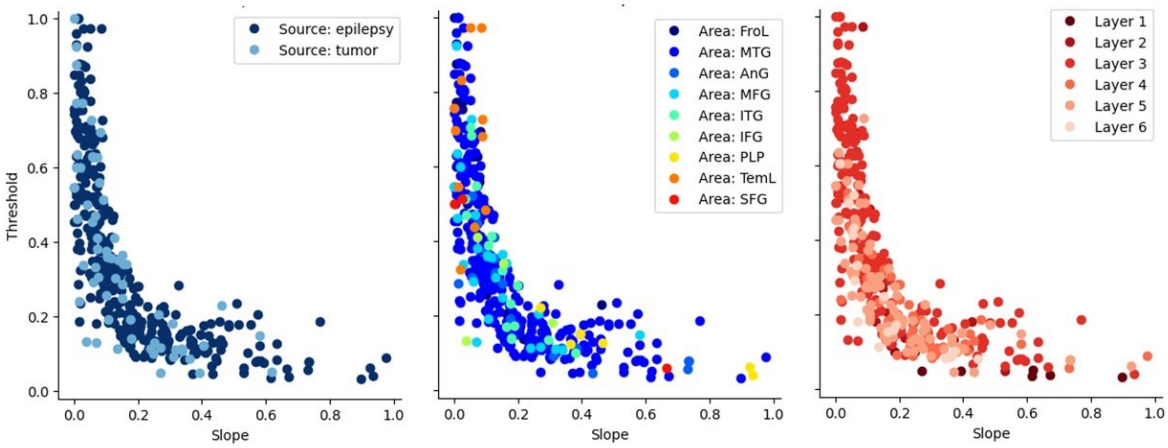

Figure 4.5: Normalized threshold and slope values for all human cortical neurons in the dataset from the Allen Institute for Brain Science coloured according to: patient condition (left), brain region (center), and cortical layer (right).

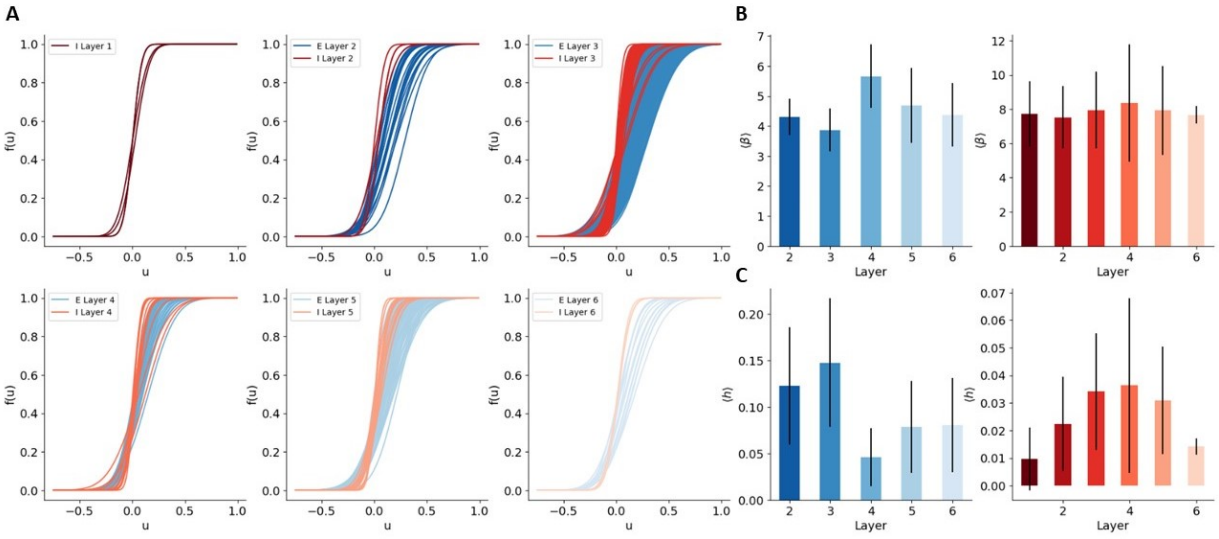

Figure 4.6: **A)** The excitability curves of the rescaled (see Methods) dataset for neurons in each cortical layer. Shades of blue are excitatory, shades of red are inhibitory. **B)** The average slope, β, of the excitatory and inhibitory excitabilities by layer. **C)** The average threshold, $\langle h \rangle$, of the excitatory and inhibitory excitabilities by layer. Error bars in (B) and (C) are standard deviation.

5

Morphological variability may limit single-cell specificity to electric field stimulation.

5.1 Introduction

Non-invasive brain stimulation (NIBS) paradigms are used for a variety of purposes, including attempted treatment of several psychiatric conditions (e.g. major depressive disorder [278, 127], schizophrenia [131], bipolar disorder [258]), and investigating neural oscillation properties and controllability [148, 253, 146]. Despite reported clinical efficacy, many questions remain about the mechanisms involved [194] as well as how to optimize their use. The high variability in brain response to NIBS protocols represents a major limitation in these efforts. Such variability has been attributed to genetic and neurophysiological factors, but evidence suggests that the brain state during stimulation may further impact the response [282, 126, 184]. Many contributing factors to response variability are immutable (e.g. subject age, skull thickness, etc), but others, such as the placement of the apparatus (e.g. electrodes or coil), are malleable [126, 322]. The immense combination of free parameters in these protocols greatly complicates parsing which ones are crucial. This has led to the development of a variety of computational models in efforts to improve the efficacy of experimental approaches and our overall understanding of NIBS [146, 201].

Despite widespread utility, comparatively little is known about the effects of NIBS at the level of single neurons [194]. It is known experimentally, although not widely investigated, that NIBS techniques can modulate the activity of individual cells [172, 171, 322]. Along with this awareness has come an acute interest in parsing the limits of *specificity* of these techniques: That is, the extent to which neuron traits (e.g. subtype, morphology)

govern the ability of a single NIBS protocol to acutely activate or suppress the response of neurons sharing similar characteristics. Preliminary efforts have been made to elucidate a relationship between response variability and neuron morphology via intermediate morphological models (that is, models with a limited set of stereotyped, structural components) with nominal success [359, 19, 170, 4, 17]. One such simplified model examined the relationship between many physical traits (e.g., branching, compartment widths and lengths, etc.) of a basic neuron and found that, on a trait-by-trait basis, they alter the strength of electric field (E-field) necessary for the neuron to fire [359]. Moreover, even for the most simplified case of a straight-cable neuron model [19], changing a single property, such as the length of the cable, was found to influence the response. Collectively this supports the consensus that physical morphology acts as an avenue for layer- and cell-type NIBS specificity.

However, experimental work in alert non-human primates, at field strengths typically applied to humans, has shown transcranial electrical stimulation is capable of recruiting individual neurons and, in some cases, controlling the timing, but not firing rate, of their spikes [172]. That experimental study found no notable difference in phase locking between putative interneurons and putative pyramidal cells. This result is at odds with what has historically been expected of individual neurons, which are long theorized to have subtype- and layer-specific differences in NIBS response [264, 170, 146]. In light of this, it may then be purported that other neuron traits (e.g. morphology) that vary widely across neuron populations may in fact limit layer- and cell-type specificity to NIBS paradigms.

Here, we put these results to the test using detailed morphological multi-compartment

models from real mouse neurons. The present work employs computational methods to evaluate the effects of NIBS on membrane potential polarization of neurons of different types (PV, PC) populating various cortical layers via the application of a uniform E-field. We specifically examined which, if any, physical characteristics might be involved in generating cell-type and/or layer-specific responses. To do so, we developed metrics quantifying various aspects of cellular morphology, both at the level of whole cells and the compartments they are modelled from, ranging from cell volume to compartment lengths, diameters, number of branches, cellular orientation as well as interneuron myelination [316, 317, 57]. Using field strengths commensurate with those used in non-invasive experimental settings, such metrics were used as a benchmark for evaluating how polarization varied as a function of cellular morphology, linking single-cell morphological characteristics to response specificity. Axonal, dendritic, and somatic compartments could be modulated reliably through changes in E-field amplitude and orientation, and both subtype and layer-specific responses could be observed. Yet, none of these results could be attributed to morphology: the aforementioned metrics didn't show any statistically significant influence in supporting subtype- and/or layer-specific responses. These null results suggest that the interplay between stimulation parameters and physical neuron characteristics is complex in its direction of neuron excitability and that other biophysical features, such as ion channel density and membrane time constant, might be more relevant. Yet, the abundant variability of these traits both within and between neuron subtypes [249, 226, 62] may limit layer- and subtype specificity of non-invasive stimulation paradigms. We believe reporting such null results represents a crucial step for the optimization, scope of applicability, and

replicability of NIBS studies.

5.2 Results

5.2.1 Characterizing neuron morphology variability

The neuron models created by the Allen Institute are based on the morphologies of pyramidal (PC) and parvalbumin (PV) neurons from layers (L) 23, 4, and 5 of mouse primary visual cortex [316, 317] (see Methods). A collection of example morphologies of these models from each layer and subtype are shown in Figure (5.1A). Seeking to investigate the effects of morphology on the response of such neurons to NIBS is a very high-dimensional problem due to the high variability seen between neurons. We quantified the variability in physical properties between neuronal subtypes at the level of 1) whole cells (i.e., vector magnitude, length, volume, myelin; see Methods); and 2) compartments (i.e., axonal/dendritic compartment lengths, diameters, branches; see Methods) and evaluated the contribution of each on membrane potential polarization from uniform electric fields.

At the whole-cell level, vector magnitude refers to the mean of the square root of the summed squared cartesian coordinates of each compartment. The length refers to the maximum length of the neuron in the z-direction and volume is the maximal elliptical volume it occupies. Separating the mean vector magnitude for each neuron subtype and layer, the PV neurons generally had smaller vector magnitudes, and so were less spatially spread, than their PC counterparts, with L2/3 having the smallest difference between the

two subtypes (see Figure (5.1B), top). In line with this, the PV neurons were on average shorter than their PC counterparts in the same layers, with L2/3 having the minimal difference between subtypes (see Figure (5.1B), top and middle panels). Similarly to the vector magnitudes and lengths of these cell models, the volumes occupied by neuron subtypes in the same layers were similar, with the exception of L4 where the PV neurons occupied substantially less volume (Figure (5.1B), bottom). Within subtypes, these macroscopic characterizations were correlated with each other, such that longer neurons tended toward a larger vector magnitude and by extension elliptical volume.

In addition to these whole-cell characterizations, compartment-level variability may also be considered (see Methods). These can be separated further into characteristics and organization of dendritic and/or axonal components for each subtype (see Figure (5.2) top and bottom rows, respectively). This scale of breakdown for the model properties is important as it has been demonstrated that, in isolation, each of these features may affect the field strength required to evoke depolarization [359]. For these models, the compartment lengths show more variability across the layers and subtypes in the axonal compartments than in the dendritic ones (Figure (5.2A)). Further, the dendritic compartments are on average longer than the axonal compartments, however, there are exceptions such as in L5 PC models where axonal and dendritic compartments were around the same length.

By contrast, diameters are relatively similar between the dendritic and axonal compartments (Figure (5.2B)). The diameters observed between subtypes and layers are also, on average, relatively similar to each other. Branching is, generally, observed to be much more prevalent in the dendritic compartments than the axonal ones (Figure (5.2C)). However,

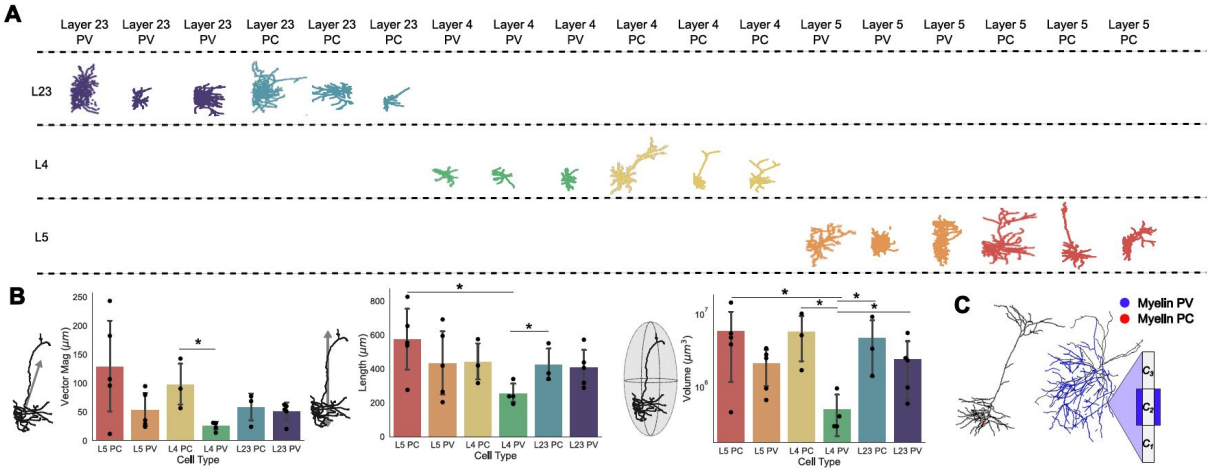

Figure 5.1: **Whole-cell morphological characterization. A)** Example morphologies of one model neuron each for pyramidal (left) and parvalbumin (right) neurons in layers (L) 23, 4, and 5. **B)** (top) Vector magnitudes of all neuron models split by layer and type; (middle) Length in the z-direction of all neuron models; (bottom) ellipsoid volume occupied by neuron models. Error bars are standard deviations. All bars are colour-matched to the morphologies shown in the example column of panel A). Significance determined using Mann Whitney U tests; single star represents $p < 0.05$. **C)** Example morphologies and schematic for a PC and a PV neuron model with representative myelination on their axons. In (C), $C_i, i = 1, 2, 3$ represent the axonal compartment and the blue sheet over C_2 is myelin.

there are exceptions to this, such as in the L5 and L2/3 PV models where the axons are very densely branched. Indeed, the PV models generally have more branching than their PC counterparts in the same layer regardless of whether the branching is considered at an axonal or dendritic level.

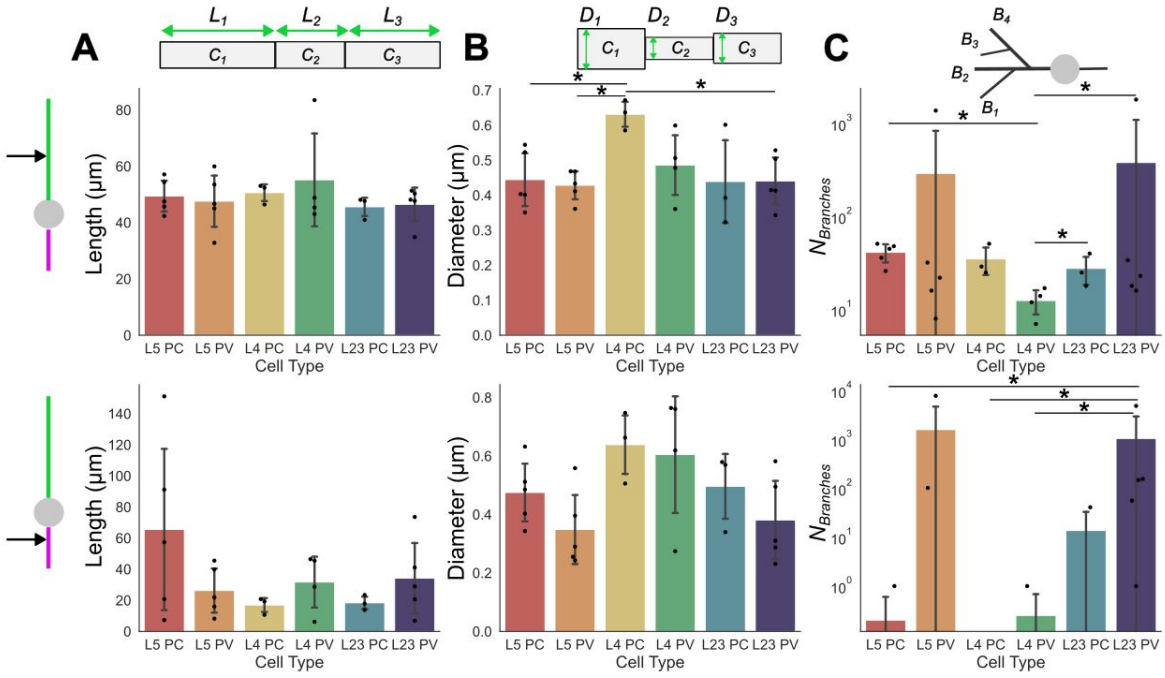

Figure 5.2: **Dendritic and axonal compartment characterizations.** Compartmental properties averaged across neuron cell-subtypes of dendrites (top row) and axons (bottom row). Individual points plotted on/above the bars are the compartmental quantity average for individual models; bars are the mean values across models. **A)** average compartment lengths (L_i), **B)** average compartment diameter (D_i). **C)** average number of branches. Error bars are standard deviations. Significance determined using Mann Whitney U tests; single star represents $p < 0.05$.

5.2.2 Subtype- and layer-specific membrane potential polarization from uniform electric fields

We first examined the mean membrane potential polarization of these models across layers and subtypes, independently of their morphological variability. To do this, we apply a uniform electric field to the neuron models across all its compartments (Figure (5.3A)) (see Methods section). The field sign and strength will influence whether depolarization or hyperpolarization is observed in the neurons' somatic compartments, and influence the neuronal response. We quantified this response through i) the mean membrane potential polarization (i.e., $\langle V \rangle$); and 2) membrane potential polarization variability (i.e., $\langle CV_V \rangle$) across independent trials (see Figure (5.3B) and Methods section). The mean membrane potential polarization quantifies the net effect of field strength on neuronal excitability, while the variability reflects its impact on spiking activity evoked by the applied field. In each trial, neurons were exposed to independent noise realizations of low amplitude, insufficient to cause spontaneous firing.

While not statistically significant (see Methods), differences in mean polarization and polarization variability could be observed between subtypes and across layers. However, pooling the neurons by layer (neglecting subtypes), no significant difference between the mean somatic polarization could be observed. The lowest coefficient of variation of these membrane potentials, $\langle CV_V \rangle$, is observed for the L2/3 models, with the highest being the L4 models (Figure (5.3C)) indicating increased firing in that layer. By comparison, ignoring layers, and pooling the neuron models based on their subtypes only, there are

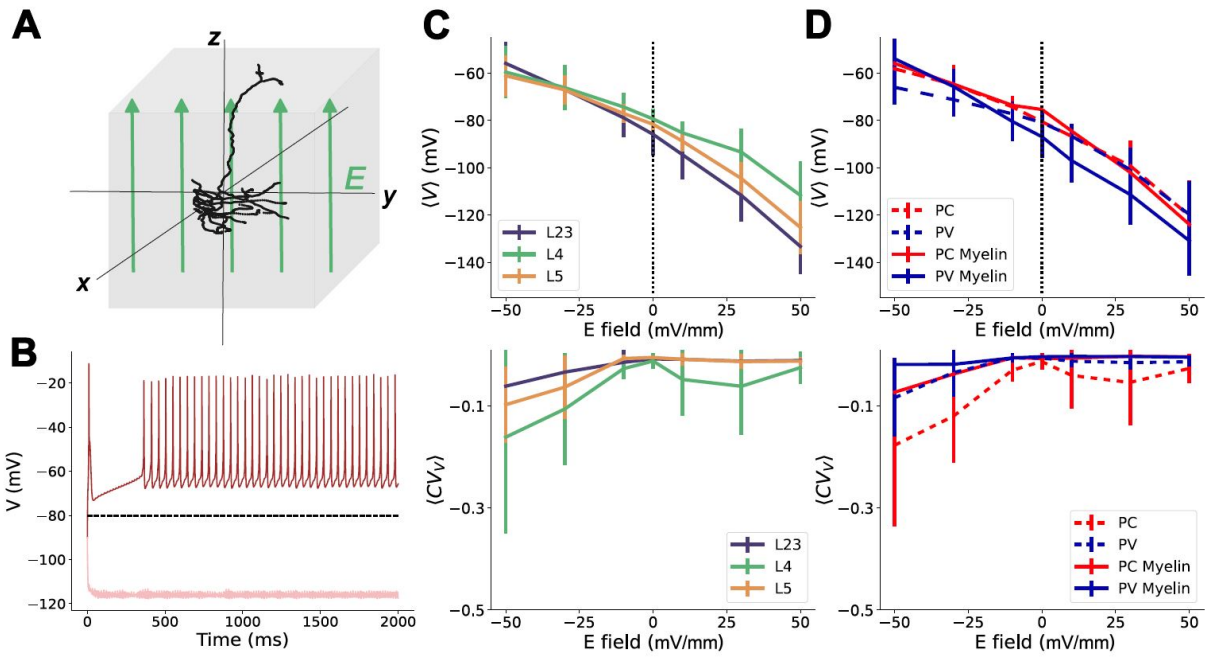

Figure 5.3: **Uniform electric fields impact on somatic membrane potential polarization. A)** Schematic of a uniform electric field, E, being applied to a neuron model; **B)** Example single trial responses of the somatic compartment of a PV layer 5 neuron model to a uniform field for $E = -50$ mV/mm (dark red), and $E = +50$ mV/mm (light red). The black dashed line is the average response to noise ($E = 0$ mV/mm) over ten trials. **C)** Top: Average polarization of the somatic membrane potential ($\langle V \rangle$) across trials pooled by layer. Error bars are the standard deviation measured across trials. Bottom: average coefficient of variation ($\langle CV_V \rangle$) of the membrane potential at different E-field strengths, pooled by layer. Error bars are the standard deviations across trials. **D)** Top: Average membrane potential across trials pooled by neuron sub-type. Bottom: average $\langle CV_V \rangle$ of neurons at different E-field strengths pooled by neuron sub-type. Solid lines are myelinated; dashed lines are unmyelinated. Error bars are the standard deviation.

visible differences between the depolarization responses of PC and PV cells (Figure (5.3D)). Of note, the differences observed between subtypes manifest differently in the cases where the PV neuron models are myelinated or not. For unmyelinated PV neurons, the same field strength leads to less depolarization than is observed in the PC models at the same field strength. However, in the myelinated PV models, the response to the same field strength eventually catches up with the PC models in terms of depolarization. Interestingly, the myelinated PV models also hyperpolarize more aggressively than either the PC or unmyelinated PV models (Figure (5.3D)), suggesting a difference in excitability induced by the applied field. The lack of statistically significant differences observed in any of these poolings suggests limitations to the extent of specificity attainable via NIBS techniques for circuit control. The average CV_V for the pooled subtypes suggests that PC cells are more excitable and experience increased firing. Based on the stronger deviation in this curve compared to the PV models, as well as the similarly shaped curves in the same plot pooled by layers, the majority of the variation within the present selection of models comes from the L4 PC models.

In addition to interrogating the effect of model subtype and/or layer on their contributions to response variability in NIBS, we also verified the impact of neuron orientation within a uniform field (see Supplemental Figure (5.6)). Considering three orientations ($0°, 90°$ and $180°$) of an exemplar neuron, in agreement with existing results in transcranial direct current approaches [265, 194, 269], the neuron's depolarization is influenced by its position particularly in the dendritic and axonal compartments. However, the net response to the applied field remains largely conserved at the soma, and does not differ sig-

nificantly from the somatic membrane potential polarization observed in the other models (Supplemental Figure (5.6B)). That is, for neurons populating layers 2/3, 4 and 5, uniform electric fields are unable to achieve sufficient specificity of neuron subtypes based on their specific orientation in space.

5.2.3 Examining the relationship between morphological variability and response specificity

In light of the results shown in Fig. 5.3, it becomes of interest to ask: what drives subtype- and layer-specificity? Specifically, we sought to determine whether any of the characterized morphological attributes substantially influence the response of the neurons to uniform electric fields. Returning to the physical metrics used earlier to describe the neuron subtypes and layers (Figure (5.1B) and (5.2A-C)), the relationship of these properties to response can be investigated by quantifying how morphological characteristics correlate with observed changes in cellular polarization. To examine the trends of individual model responses with respect to applied field strength, we here quantified *susceptibility*, a linear measure of the slope of the response which represents the cell-specific subthreshold somatic polarization per unit electric field applied and is analogous to the polarization length used in prior studies [264, 321] The susceptibility quantifies the predisposition to control by the applied field and can be linked to various morphological traits to assess specificity.

As with the characterization of physical traits, susceptibility can also be broken down into considering both whole-cell and compartmental-scale physical characteristics. Looking

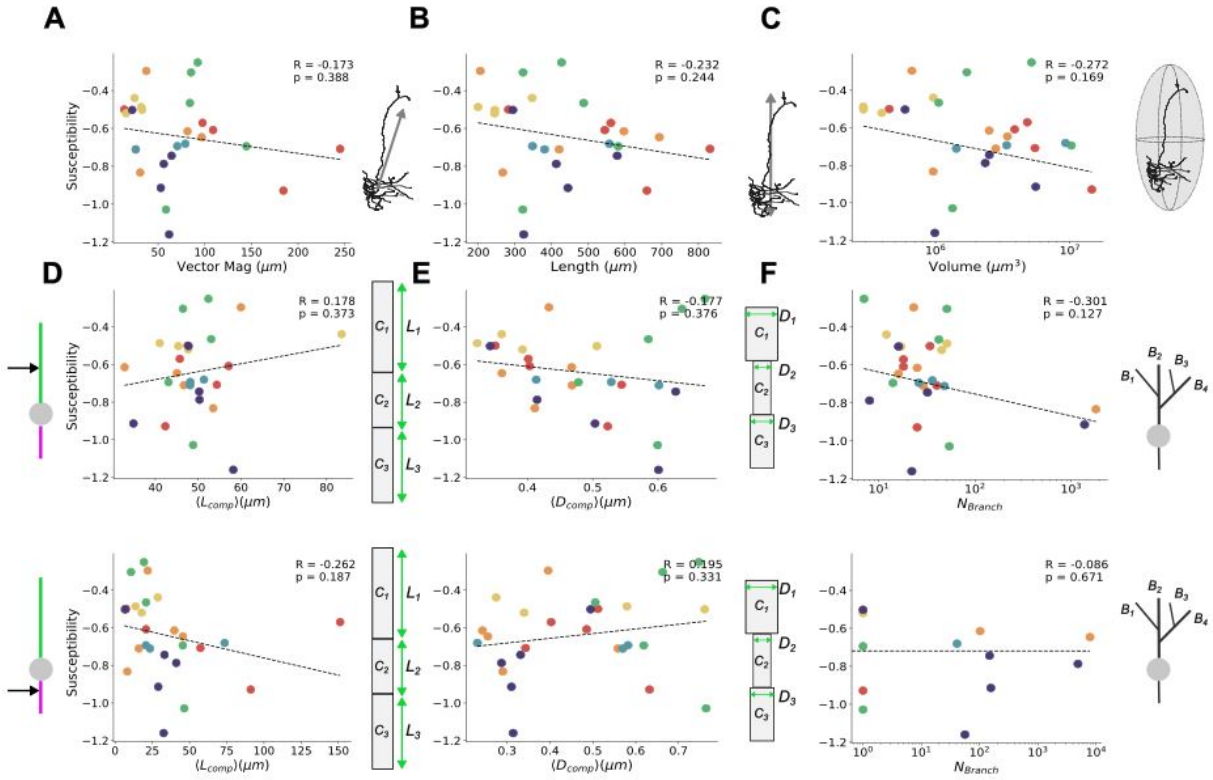

Figure 5.4: **Relating field effects to morphological characterization metrics.** Susceptibility of average somatic membrane potential polarization (see Figure (5.3C-D)) per neuron as a function of their **A)** vector magnitude, **B)** neuron length, and **C)** volume occupied. At the level of dendritic (upper) and axonal (lower) compartment properties (see Figure (5.2)), the susceptibility of the average somatic membrane potential polarization is shown as a function of **D)** average compartment length, **E)** average compartment diameters, and **F)** number of branches. All susceptibilities are calculated from response in the upright (0°) orientation. Schematics to the right of each plot correspond to the quantity on their x-axis. The Pearson correlation coefficients, R, their significance, p, and the line of best fit are found using SciPy's linear regression package [340].In line with the scheme used in Figures (5.1) and (5.2), the colours of the points correspond to the layer and cell type of each neuron (red = PC L5, orange = PV L5, yellow = PC L4, green = PV L4, blue = PC L23, and violet = PV L23).

at the susceptibility agnostically (irrespective of the neuron subtype or layer) with respect to whole cell metrics (i.e., vector magnitude, length, volume occupied, and the number of branches), all yielded non-significant correlations, while the occupied volume showing the highest correlation (Figure (5.4)). At the compartmental level, investigation of the susceptibility of compartment-level metrics also yielded no significant correlations, with dendritic and axonal branching showing the highest correlation among their respective compartmental attributes. These results suggest that controlling individual cell types with uniform electric fields is limited in its specificity, due to the high variability in cellular morphologies both between cell types and across layers. There was also no notable clustering among the cell types and layers for any of the morphological properties with respect to their susceptibility.

To more rigorously interrogate this result, we re-assessed the relationship between the whole-cell physical metrics (e.g. vector magnitude, volume and length) and susceptibility for partial correlation when holding the relevant covariable morphology traits constant (see Methods). From this more detailed assessment, too, there was no significant partial correlation between these measures and the susceptibility (see Supplemental Figure (5.7) and Table (5.3)). Moreover, we then performed dimensionality reduction on all the morphology traits and susceptibilities shown in Figure (5.4) to create a uniform manifold approximation (UMAP) (see Supplemental Figure (5.8)). From the UMAP, we found no noticeable clustering of any given cell-type and/or layer, suggestive of considerable net morphological similarity across the models.

Based on a range of whole-cell and compartment-based physical metrics, our null results

suggest that cellular morphology, on its own, has no significant influence on the specificity of uniform electric fields. However, an important confound remains: the neuron models considered exhibit important compartment-to-compartment variability in biophysical properties (e.g., ion channel conductances)[316, 317]. Such variability may play an important role in blurring differences in the response of cells across layers and subtypes. To control for this additional source of variability, ionic conductance values of a subset of neuron models were fixed and made equal across all cellular compartments. That is, the ionic conductance values of the L2/3 PC neuron models were extracted from each model and averaged for each ion channel type. The resulting averaged values were then manually applied across each compartment of these models (see Methods). These newly constructed neuron models do not possess any variability in ion channel conductance properties; however, they do retain variability in other compartment-to-compartment level biophysical properties such as resistance, capacitance, and the decay rate of the calcium dynamics. Exposing these biophysically-controlled neuron models to the same uniform E-field protocol as before, our simulations show that morphology does not contribute significantly to specificity: Changes in mean somatic polarization (see Figure (5.5A)) could not be differentiated between the different models. Calculating susceptibility, we also examined the effect of morphological traits. For comparison purposes, we added those to the existing scatter plots computed before (see Figure (5.5B-D)) where biophysical variability was not controlled for. Yet again, we did not find any morphological trait passing the statistical significance threshold, and thus strengthen our null result that no singular morphological trait drives neuron response as independent of biophysical properties.

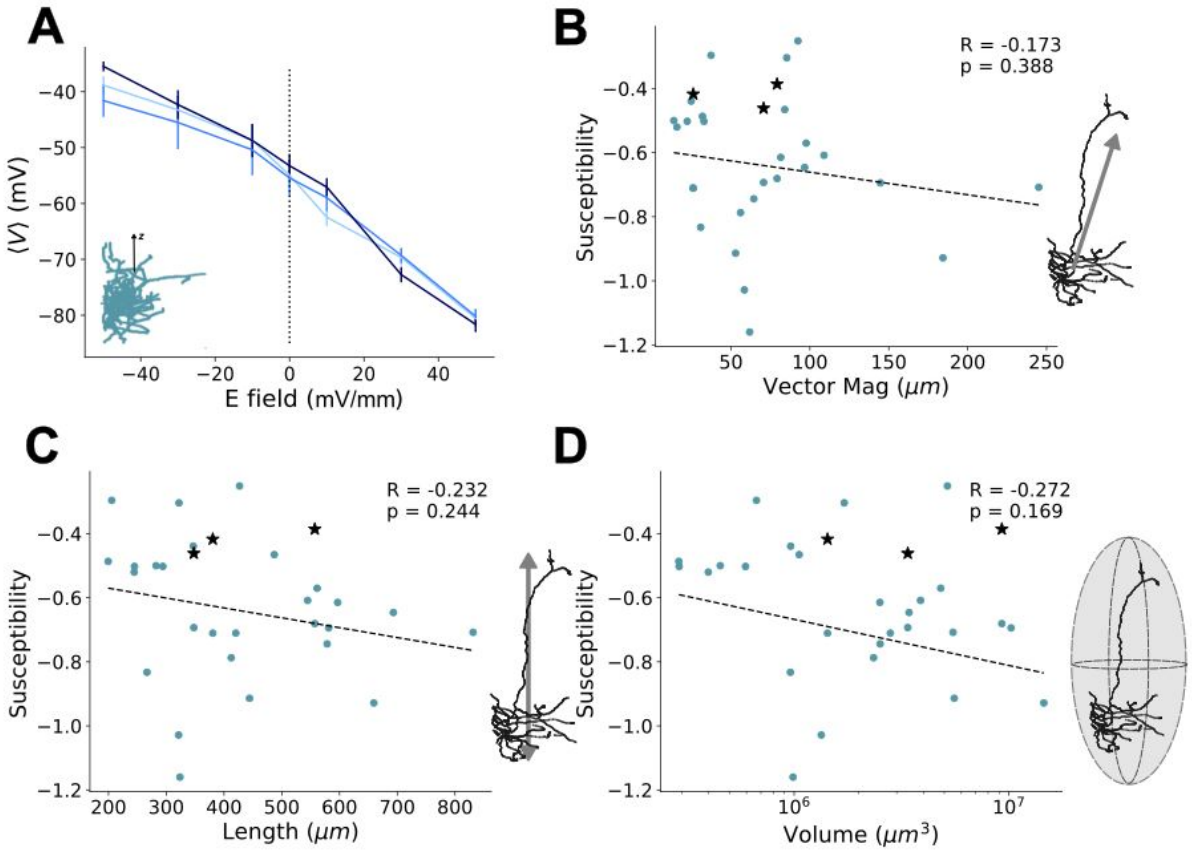

Figure 5.5: **Lack of morphological specificity holds even with fixed ionic properties. A)** For a subsample of neuron models (i.e., PC L2/3 models), ionic conductance were set to the same fixed value across all dendritic and axonal compartments (see Methods). Change in polarization to a uniform electric field was measured from the somatic compartment. Different shades of blue denote individual models. Replotting the susceptibility-morphological property scatter plots from Figure (5.4A-C) for **B)** vector magnitude, **C)** length and **D)** volume. The susceptibility of the controlled models from panel **A)** are added to the scatter plots as black stars.

5.3 Discussion

Previous NIBS studies have demonstrated that single neurons are affected and entrained by low field strengths [172, 3, 177, 15, 19]. The extent of specificity for which NIBS holds over single neurons is less clear. Some experimental studies failed to observe any difference in the entrainment of excitatory and inhibitory neurons [171, 172], yet identifying the source - if any - of NIBS specificity between neurons remains experimentally intractable. Our computational investigation found minimal differences in the acute specificity of neuron subtypes, echoing previous experimental observations [171, 172]. No significant correlation between response variability and physical morphology could be identified. These results further align with experimental work revealing that the highly complex, variable morphologies observed in neural tissue had no effect on the conservation of physiological waveforms and circuit functions of neurons [243]. Similarly, recent computational work in L5 pyramidal cells has shown morphological variance to be insufficient to reproduce electrical variability observed empirically [17].

Among the morphological sources of variability we considered was myelination, which is known to influence neuron response to NIBS [297, 284, 257]. The minor differences in the PV, but not PC, models in the myelinated and unmyelinated versions (see Figure (5.3D)) suggest that response variability due to myelination is non-uniform and, consistent with a recent work [3], requires >15% coverage to manifest. This may help reconcile our observations with previous computational work not considering myelination, which

found layer-specific differences in the E-field strength required to depolarize neurons in L2/3 and L5/6 [264]. However, recent studies involving myelination have shown a minimal difference required to evoke firing from L2/3, L4, and L5 neurons [3, 4]. As the effect of myelination scales with its abundance, less myelinated brain regions, or shorter axons of inhibitory neurons may respond more similarly compared to their unmyelinated equivalents (see Figure (5.3D)), and hence be less depolarized than excitatory neurons. Indeed, such effects may explain differences in our results and other myelinated models that predicted specific activation of cells across subtypes and layers. Where those studies use morphologies from multiple regions of the brain [170], reported differences may hence be attributable to more salient morphological variability present between different brain regions compared to those found within the same region, as we have done in our case. We hypothesize that such region-specific distinctions may also be involved in the discrepancies between those studies and the lack of significant difference found between subtype responses in experimental protocols [172].

In addition to layer- and subtype-based neuron groupings, we sought to explore the influence of physical morphology on evoked polarization (see Figure (5.4)). Previous compartment-level studies of simplified neuron models identified multiple physical traits influencing the field strength required to evoke firing [359] (while this study considered hippocampal neurons overall, we consider the results of the simplified models comparable). Based on those findings, one could infer that an "optimally susceptible" neuron (that is, one with the lowest required field strength to fire) would have long, thick dendrites with many branches that disperse minimally from the primary axis the applied field lays on.

Moreover, such a neuron would have long, narrow axons with minimal branching that disperses widely from the field axis. For the (realistic) models considered here, no class of or individual neuron(s) possess the collective grouping of traits that would require an electric field strength lower than that required by the other neurons to evoke depolarization. In line with this, our simulations did not identify any singular physical trait as the driving source response specificity to the same stimuli between neurons (see Figure (5.4)), even when accounting for partial correlations (see Supplemental Figure (5.7) and Table (5.3)) and the possible influence of variability in compartmental ionic conductances (see Figure (5.5)). These results collectively suggest that the difference between individual neuron models and their response likely results from a convolution of morphological and biophysical properties, rather than morphological traits alone.

Further supporting the seeming convolution of physical traits is the lack of clear clustering observed in the UMAP (Supplemental Figure (5.8)) created from the data in Figure (5.4), which suggests a significant heterogeneity of and overlap in morphological features and response across the neurons. This aligns with recent work on human neocortical pyramidal cells that, using dimensionality reduction, found considerable intrinsic electrophysiological similarity between layers [226]. Having such overlap in physical traits despite individual morphologies appearing markedly different additionally fits with the ability of cells of widespread morphological variability to create robust firing patterns [206, 242, 243, 241]. That is, it supports the idea that neurons may possess widespread degeneracy [8], whereby they can respond in qualitatively similar ways despite being comprised of different features. Importantly, as is further discussed below in the Limitations section, our null

results are constrained in their scope and do not encompass all possible factors that may contribute to neuron-specific responses.

In light of our null results, we feel compelled to mention that we do **not** claim that morphology does not affect neuron response to electric fields, but rather, we conclude that 1) there is no singular trait doing so in isolation; and 2) that the high morphological variability observed across neurons may limit the specificity with which they may be non-invasively targeted. Indeed, our null results suggest that (realistic) morphology is not, in isolation, a defining feature responsible for the observed variability in neuron response to uniform electric field stimulation (see Figure (5.4)). This is in agreement with recent work on detailed biophysical models of L5 PC neurons found morphological variability to be insufficient to reproduce electrical variability [17]. Moreover, earlier results in somatogastric neurons [243], suggest that the electrophysiological properties of neurons can be conserved without complex, morphological diversity. These results support, then, that the approximations made in many models of NIBS protocols that use mean-field type approaches, whether for the whole model population or for subtypes within the population [146]: The assumptions made in designing such computational models to not include specific morphology in their frameworks may be sufficient for capturing electrical properties.

We believe reporting null results represents a crucial step in evaluating the scope of applicability of NIBS and replicability of existing studies. In recent years, the number of studies pertaining to the use of NIBS has exploded, however, with that momentum, there has been limited replication or consistency in the stimulation protocols used [148]. Despite their infrequency in publication, null results are often helpful to researchers in furthering

research in meaningful directions [124]. This is particularly important for the blooming NIBS field, given the extremely vast stimulation parameter space: null results may hence serve to streamline optimizing the framework and scope of NIBS paradigms.

5.3.1 Limitations

The morphology models used in this work come from a relatively small collection of neurons found in the primary visual cortex of mice. While the small sample size is due to the experimentally limited number of such detailed models available [317], this does contribute to lower statistical power in the results, as is common in the majority of neuroscience studies [41]. Importantly, the models all being based on mouse primary visual cortex morphologies limit the extrapolation of the results of these simulations to any expectations for human cells, as it has been shown that a number of neuron properties do not scale from non-human to human neurons [224, 26, 64]. In line with this, recent results showed that human L5 PC neurons have unexpected biophysical properties for their size [26], despite the composition and allometry of the human cortex scaling relative to other species [91, 133, 27]. Further, as these models are simulated in isolation, they disregard any potential influence from conductive tissue, distance-to-skull or other cell interactions that may bolster response through biophysical mechanisms, such as ephaptic coupling [268, 15, 177, 201]. White noise is added to account for some of these effects, however, the net efficacy may still be impacted. Additional model-specific limitations can be found in the Allen Institute technical papers and documentation [316, 317].

The neuron models were predominantly simulated in one orientation in free space. However, the overall effects of orientation were considered by rotating the neuron models 0°, 90° and 180° about the y-axis and recording from the somatic, axonal and dendritic compartments in all three orientations (see Methods and Figure (5.6)). The observed effect of this change is relatively small at the somatic compartment, although the overall polarization of the model changes. NIBS studies of biophysical models found this minimal effect results from the axon branching and myelination, which drastically reduces the effects of orientation on activation threshold [3]. The layers considered may also reduce the effect of orientation, as L1 and L6 have previously shown more variability in preferential orientation [4, 194]. The average membrane potential in response to orientation changes is more attenuated at the soma than the dendrites and axons, which are two to three times more susceptible to polarization at their terminals than somas [265].

The models considered in the present work are additionally simulated in isolation, and hence disregard the potential influence of conductive tissue, distance-to-skull, or other cell interactions. One of the immediate possibilities with this framework is that, for real neurons, the minimum field strength required to facilitate depolarization may be greater than in these models where the field is applied uniformly. Alternatively, the synaptic coupling with other neurons may bolster their response and allow for activation at lower field strengths than reported here. To account for this latter possibility, we have added white noise of constant amplitude to mimick recurrent input from other neurons (see Methods, Neuron Models). We acknowledge that this approach neglects the potential effects of network/recurrent correlations, which can bolster response to NIBS far beyond what a single

neuron can achieve [267, 15]. This is true even in small networks, where ephaptic coupling can influence the strength of field required to entrain cells [177, 201]. Therefore, the exact propagation of current through *in vivo* tissue might differ from what is modelled here. This may be of particular importance when considering limits where the neurons are at a greater distance from the current source, or the possibility that connectivity patterns may contribute to the specificity with which neurons can be non-invasively recruited. These important questions are left for future work.

Among factors not considered in the present study are membrane time constants, which vary by multiple orders of magnitude within and between cell types, layers, and brain regions [226], and reflects cellular excitability and integration of temporally-varying stimuli in the neuron [103, 181]. This leads to varied responsiveness between neurons to rhythmic input, and contributes to the resultant dynamics of synaptic plasticity in transcranial alternating current stimulation frameworks [249]. In addition to synaptic plasticity, by simulating the neurons in isolation, we also neglect potential influences by synaptic inputs, and recurrent connections. This is of particular note, as recurrent connections increase the correlated activity among neurons [351, 135] and their absence may have marked effect on neuron response to transcanial electrical stimulation. Moreover, recurrent connectivity influences synaptic low-pass filtering that can introduce slower dynamics in the activity of individual neurons different than those of adaptive currents [30]. Collectively, these factors may influence the response variability of individual neurons, and particularly the selectivity of such neurons in cortical circuit settings.

5.4 Methods

5.4.1 Neuron models

The models used here were created by the Allen Institute for Brain Science based on the morphologies and biophysical properties of real neurons found in the primary visual cortex of mice [316, 317]. That is, these computational mathematical models of single neurons were created based on slice electrophysiology and morphology reconstruction data (see below). A primary objective of the Allen Institute in developing these models was to incorporate active dendritic conductances due to their importance in the input-output relationship of cortical neurons [316]. This was accomplished by including active, Hodgkin-Huxley nonlinear conductances in the dendrites. For the *excitatory* neuron models there are four separate compartment types incorporated: axonal, somatic, basal dendritic, and apical dendritic. In contrast, the *inhibitory* neuron models only use three types of compartments: axonal, somatic, and dendritic. For both model types active and passive properties are considered.

The morphologies of each neuron are rendered in 3D using the NEURON coding environment from imported SWC files. These models feature a singular, spherical somatic compartment, serving as the initial point from which child branches emerge, extending outward into their respective branches[316, 317]. As branches are added further from the somatic compartment, their diameters were made to match the expected decrease in diameter observed with increasing branch order. Only models with an overall decrease in

dendritic diameter with increased branching order were accepted [316].

Once the morphology of the model is in place, the passive and active properties of each model were fit on electrophysiological data. In the optimization of the 26 free parameters in these models (18 active conductance densities, 4 intracellular Ca^{2+} dynamics parameters and 4 passive parameters), fitting is assessed based on 11 electrophysiological features including time to first spike, time to last spike, as well as action potential width and height (see [316] are references therein). For every o those features, an absolute $Z-$score was calculated and the highest score parameter set was retained.

The passive parameters (e.g. specific membrane capacitance, membrane resistance, intracellular resistivity, etc.) are assumed to be uniformly distributed across all compartments and are, for a given model, set to a singular value. The value itself can be found using NEURON's multiple run fitter. As a result, compartment passive parameters were varied to find the best match to experimental voltage traces, under the assumption the active properties were absent [317, 318].

In contrast to the passive parameters, the active channel properties are uniformly distributed in space across compartments [316] in the different compartment types (e.g. somatic, axonal, dendritic) such that every type receives an independent set of channels (see Table 5.1). As with the passive parameters, the numerical values for these active properties were fitted so that the response of the model to step input current matches electrophysiological data. Specifically, the free active parameters include 18 active conductance densities (i.e., $g_{bar,j}$) which corresponds to the maximum conductance density of type j (e.g. Na+)

in a given compartment [317]. Except for these free active parameters, all other parameters for the active mechanisms are employed based on those from Hay et al (2011) [134].

These free active parameters are complemented by additional parameters that account for intracellular Ca2+ dynamics and Ca2+ entry due to transmembrane currents [316]. This model includes a time constant for Ca2+ removal, as well as the binding ratio of the Ca2+ buffer [317], and is given by

$$\frac{dCa_i}{dt} = -10000\frac{i_{Ca}\gamma}{2Fd} - \frac{Ca_i - m_{Ca_i}}{\tau_d}, \tag{5.1}$$

where Ca_i is the Ca^{2+} concentration at time t in compartment i, F is the Faraday constant, d is the depth of the submembrane shell, τ_d is the removal rate of Ca^{2+}, γ is the % of free unbuffered Ca^{2+} , m_{Cai} is a constant baseline concentration, and i_{Cai} is the ionic current. With the exception of the calcium dynamics, the active properties of the various ion channels all evolve according to Hodgkin-Huxley equations. The specific equations and parameters for a given model can be found in the ".mod" files downloadable from the Cell Types Database of the Allen Brain Atlas (`https://celltypes.brain-map.org/data`).

For the purposes of the simulations done in this work, two types of models were considered: those based on pyramidal cell (PC) morphologies and those based on parvalbumin cell (PV) morphologies. A summary of the number of models used from each type and layer is shown in Table 5.2. All simulations were conducted in a mixed Python - NEURON environment, with the models having been created in a NEURON environment [141, 339, 316]. Subsequent data analysis was performed using the NumPy, Matplotlib, Seaborn,

Active properties	Axon	Soma	Dendrites
Ih		✓	✓
Im			✓
Na	✓	✓	✓
Kd	✓		
Kv2-like	✓		
Kv3-like	✓	✓	✓
SK-type potassium	✓	✓	
Low-voltage Ca2+	✓	✓	
High-voltage Ca2+	✓	✓	
Ca2+ decay dynamics	✓	✓	
Ca2+ gamma dynamics	✓	✓	

Table 5.1: **Active properties morphology models** Reproduced table from Allen Institute technical paper [316] listing all active parameters present in the Biophysical - All Active models. Check marks denote the presence of that property in those compartment types.

Cell type	Cortical layer	No. morphs
PC	2/3	3
	4	5
	5	5
PV	2/3	5
	4	4
	5	5

Table 5.2: **Morphological model types** Summary table of the number of morphological models (No. morphs) for each cell type and cortical layer used in the simulations performed here. Pyramidal cells are PC and parvalbumin cells are PV.

SciPy, and Pandas Python libraries [240, 150, 345, 340, 217].

In the NEURON environment, the membrane potentials of the models are calculated using the cable equation:

$$\frac{\partial V}{\partial t} + I_{net} = \frac{\partial^2 V}{\partial x^2}, \tag{5.2}$$

where I_{net} and V are the net current (ionic and injected) and membrane potential, respectively. This is then approximated to its spatially discretized form such that the neuron is reduced to a set of connected compartments, and Eq (5.2) becomes a family of equations,

$$c_j \frac{dv_j}{dt} + i_{ion,j} = \sum_k \frac{v_k - v_j}{r_{jk}} + i_{inj,j}, \tag{5.3}$$

where c_j is the membrane capacitance of compartment j, r_{jk} is the resistance between compartment j and k, $i_{inj,j}$ are the injected currents, and $i_{ion,j}$ includes all currents through ionic channel conductances. The right-hand side of the equation is the sum of the axial currents that enter the compartment from its adjacent neighbours. The ionic currents, i_{ion}, of the neuron models then evolve according to $i_{ion} = g(v - e_{ion})$, where v is the internal voltage, e_{ion} is the Nernst potential, and g relates the active conductances densities, g_{bar}, to the relevant Hodgkin-Huxley parameters (see individual model ".mod" mechanism files for equations [316], and chapters 3 and 4 of the NEURON handbook [59] for detailed expansion on this derivation of the cable equation).

Within this framework, any spatial variation in the membrane current is approximated as its value at the center of a given compartment. Within NEURON's framework, compartments of the same size are grouped together as a section which contains all of these compartments as segments of the section [141, 59]. This is done for computational effi-

ciency, as Eq (5.3) may then be re-formulated as,

$$C_m \frac{dv_j}{dt} + i_j = \frac{d}{4R_a} \frac{v_{j+1} - 2v_j + v_{j-1}}{\Delta x^2}, \tag{5.4}$$

where Δx and d are the compartment length and diameter, respectively. If these are the same between compartments, as is the case for a section, then $R_a \Delta x / \pi (d/2)^2$ is the axial resistance, and $C_m \pi d \Delta x$ is the compartment capacitance.

The electric field is applied to all compartments in a cell using NEURON's extracellular function [141]. We neglect the distance component of the field, that is the field is scaled to be connected in series with the conductance of the last extracellular layer of the model and added in millivolts. For these simulations, we use a uniform electric field with magnitude, E, in the positive z-direction, such that each compartment receives a field given by:

$$E_j = E \cos\phi + \xi_j, \tag{5.5}$$

where j is the compartment number, ϕ_j is the angle between the middle of compartment j and the z-axis, and ξ_j is Gaussian white noise added to that compartment to account for fluctuations and inputs not explicitly modelled, such as synaptic activity or ephaptic interactions, which may modulate neuronal excitability and facilitate activation at lower field strengths. To account for the orientation of the individual compartments, we calculate the angle ϕ_j based on the *a priori* known Cartesian coordinates of each compartment [316, 141]. In these calculations, in line with the design of the models detailed previously, the

somatic compartment is assumed to be located at the origin.

Taking these steps guarantees that field magnitude in a compartment scales with its orientation (e.g., only compartments in perfect alignment with the field receive its full magnitude). The scaling of the field per-compartment based on compartment orientation is particularly important when we consider the effects of model-orientation on the observed response. When the model is rotated, this is done again using the known Cartesian coordinates of each compartment and a rotation matrix to reorient all compartments to their new positions. The angles, ϕ_j, of the new positions are then calculated and again used to adjust the compartment-wise experienced field strength.

In addition to the applied field, our model also includes background noise ξ, resulting in voltage fluctuations even when $E = 0\ mV/mm$. This noise was assumed to be Gaussian white noise (i.e., $\mu_\xi = 0$; $\sigma_\xi = 4$) and was added alongside the field to each compartment. Realizations of this noise are independent across neuron models, compartments and trials. Ten trials each of subthreshold field strengths $E = \{-50, -30, -10, 0, 10, 30, 50\}\ mV/mm$ were applied, in line with ranges that have been used for similar models [359, 264]. The cell response was read out from the somatic compartment as a membrane potential and the average response across trials was taken to quantify the specificity of the cell.

5.4.2 Characterizing neural morphology

In the present framework, the Cartesian coordinates for all compartments in the models are known. This allows for both whole-cell and compartmental characterizations of the

morphologies to be made. For macroscopic measures, that is characterizations that encompass the whole cell, we take three quantities 1) the vector magnitude, 2) the length in the z-direction, and 3) the elliptical volume. We define the vector magnitude as the mean square root of the sum of the squares for the Cartesian coordinates of all compartments in a given model and calculate it to $R_j = \langle\sqrt{x^2 + y^2 + z^2}\rangle_N$, where N is the number of compartments in model j. For the z-direction length (referred to hereafter as length), the value L is calculated as simply the difference between the maximum and minimum z-direction coordinates (this represents the effective length of the neuron as established in [321]). Finally, the elliptical volume is calculated by halving the length (z) and equivalent maximum distances in the x- and y- directions. The ellipsoidal volume is then calculated as:

$$V = \frac{4\pi}{3}\left(\frac{x_{max}}{2}\right)\left(\frac{y_{max}}{2}\right)\left(\frac{z_{max}}{2}\right) = \frac{\pi}{6}(x_{max}y_{max}z_{max}) \tag{5.6}$$

Additionally, at the level of whole cells, we sought to investigate the effects of orientation. To do this, the models were rotated about the y-axis using a rotational matrix within the field at $\theta = 0°, 90°$, and $180°$. At each orientation, the models were simulated with the same $E = \{-50, -30, -10, 0, 10, 30, 50\}$ mV/mm fields. For these simulations, recordings of the stimulation responses were taken for all compartment types to create a more complete polarization profile. Notably, in these simulations the response is recorded at the center of a given section to approximate the value of all segments within the section.

For the more mesoscopic measures, that is those at the level of the compartments that

comprise the models, we consider again three quantities: 1) the average compartmental length, 2) the average compartmental diameter, and 3) the number of branches. For each of these metrics, we further separate into the dendritic and axonal measures. These metrics are defined in the model reconstruction files themselves [317, 141], and were subsequently extracted and averaged across morphologies for the same neuron subtype and/or layer.

5.4.3 Simulations and analysis

For the simulations conducted here, the cells are artificially positioned such that the somatic section, a singular section for all models, is at the origin and all other compartment coordinates are normalized with respect to this compartment. This is done using the *a priori* known Cartesian coordinates for every segment in the models. Additionally, the orientations were taken to be in standard depiction format, that is with the dendritic arbour in the positive z-direction. To improve the biophysical accuracy of the models, myelin was added to the axonal compartments of the neuron models by randomly selecting a fraction of the axonal segments and setting their ionic conductances (and by extension their ionic currents) to be zero. The myelinated segments in a given simulation were chosen from a Bernoulli trial for each axonal segment with a probability of myelination $p = 0.7$ in the PV neuron models and $p = 0.15$ for PC models (see Figure (5.1C)). These values of myelination probability were chosen in line with the percentage of the axon length expected to be myelinated from experimental work on these neuron types [57].

The physical characteristics of the models were separated based on their layers and

subtypes. As the groupings of neurons are small, and therefore cannot be assumed to have normally distributed properties, and each neuron's properties are assumed to be independent of the other neurons, the differences between groupings were assessed for significance using a Mann Whitney U Test from SciPy's statistics library [340]. For the same reasons, comparisons between the responses of neuron groupings were also assessed for significance using Mann Whitney U Tests.

To validate that the observed results are not convolved by the ionic properties, a subset of the neurons were resimulated with their ionic properties manually reset to average values. That is, the conductances, g_{ion}^{comp}, of the ionic channels for each of the PC L2/3 models were averaged for each compartment type (somatic, dendritic, apical and axonal). The resultant values, $\langle g_{ion}^{comp} \rangle$, were manually set for each of the corresponding compartments in those models. These models were then re-simulated in the same uniform electric field protocol in the upright (positive $z-$axis) orientation, with their membrane potentials measured again at the somatic compartment.

5.4.4 Susceptibility

The curves of membrane potential resulting from the application of various applied field strengths as recorded at the somatic compartment in the upright (or 0°) orientation serve as a representation of the susceptibility of a neuron to the applied field. Here, we measure susceptibility, a measure analogous to the polarization length [264, 321], using the slope of the membrane potential polarization curve with respect to applied field strength:

$$S = \frac{\langle V \rangle_{-50} - \langle V \rangle_{+50}}{\Delta E} \tag{5.7}$$

where ΔE is the difference between the E-field strengths for the cases (here equal to -100 mV/mm) and $\langle V \rangle_i$ are the average membrane potentials at field strengths $i = \{-50, +50\}$ mV/mm. As $\Delta E < 0$ here, the resulting values of S are also negative.

These susceptibility values offer a metric to quantify the influence of the physical morphology characteristics on the response of the neurons to stimulation by looking at their correlations. Correlations of these susceptibilities are calculated with respect to the different morphological traits using SciPy's linear regression function, which calculates the Pearson correlation coefficient, R, and its corresponding p-value using a Wald Test with t-distribution of the test statistic [340]. These correlations then allow us to discern which morphological trait (if any) may contribute to the specificity of the NIBS protocol.In addition to the linear regression analysis, partial correlations were calculated for morphology traits with their susceptibility using the Pingouin Statistics package in Python [337]. The morphology traits held constant in each of these analyses were decided based on having a significant correlation with the other available ones (see Supplemental Figure (5.7A)).

5.5 Appendix

5.5.1 Supplemental Figures and Tables

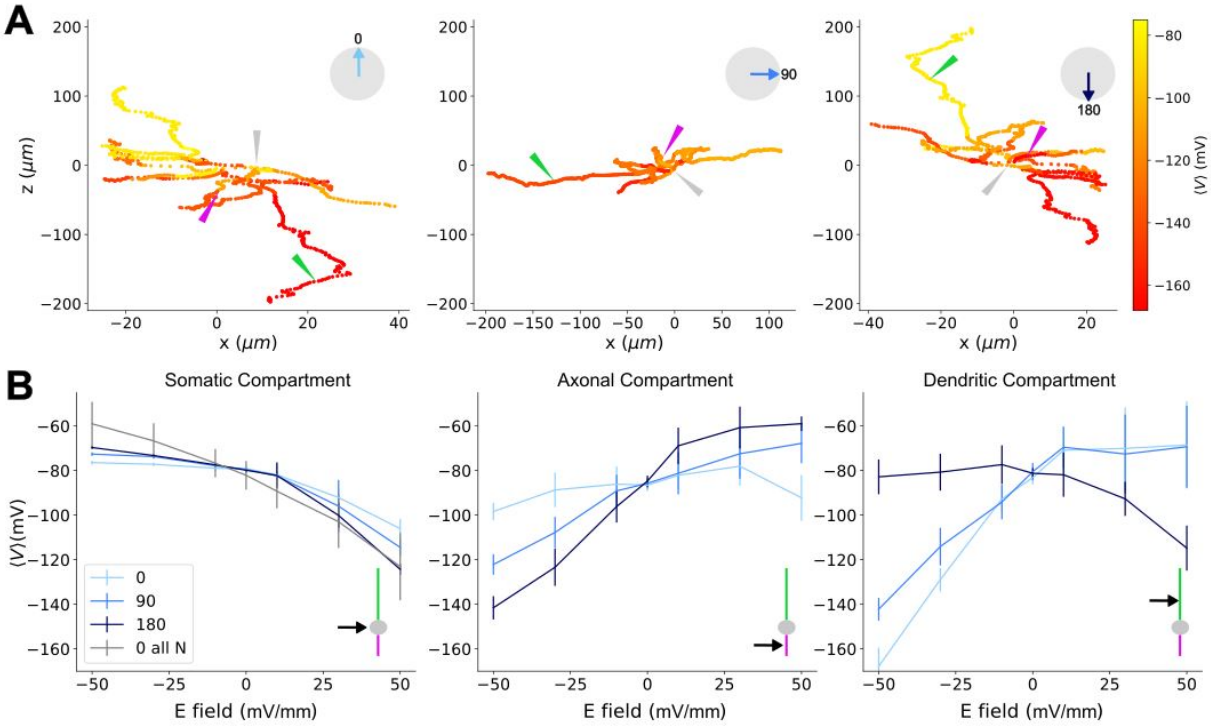

Figure 5.6: **Orientation effects on the polarization profile of neurons. A)** Average membrane potential per compartment for $E = -50\text{mV/mm}$ applied to an example L5 PV neuron model as it is rotated 0^o, 90^o and 180^o (left to right) with respect to the y-axis. Orientation is indicated in upper right of each plot by the arrows on the circles. The lightness of blue on the arrow corresponds to the curves on plots in (B). **B)** The relationship between the example neuron model orientation and average membrane potential with respect to the applied E-field, error bars are standard deviation. The simplified neuron schematic in the bottom right of each plot indicates which compartment type is being plotted (left to right: somatic, axonal, dendritic). The exact section of the neuron being recorded from is indicated by the colour-matched triangles in the rightmost panel of (A). In the left panel of (B) the average membrane potential at 0^o orientation from the somatic compartment of all models is indicated by the grey line with the error bars as their standard deviation. The inter-model mean was compared with the single model mean using a MannWhitneyU Test and no significant difference was found ($p > 0.05$).

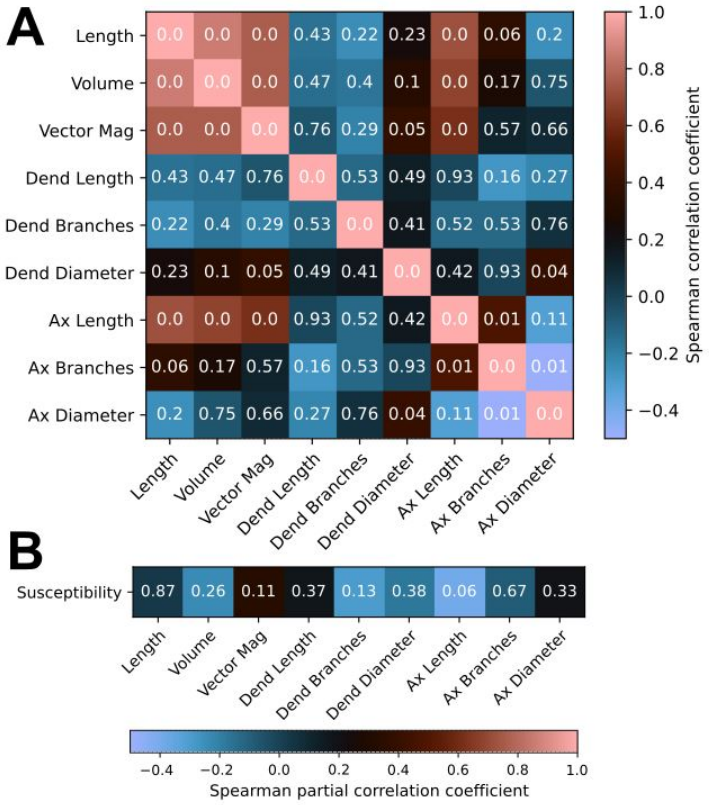

Figure 5.7: **Partial correlation analysis shows no significant correlation between susceptibility and morphology traits. A)** Heat map of the spearman correlation coefficient between each of the morphology traits considered in this work. Significance (p-values) for these correlations are written on each block rounded to two decimal places. Cases with $p < 0.01$ (shown as $p = 0.0$ in heatmap) are considered correlated and controlled for in the partial correlation analysis. **B)** Heatmap of the spearman partial correlation coefficients between the susceptibility and each morphology trait when controlling for significantly correlated traits as determined from **(A)**. The p-values are shown on each block. The exact values for the correlation coefficients and p-values are reported in Supplemental Table 5.3.

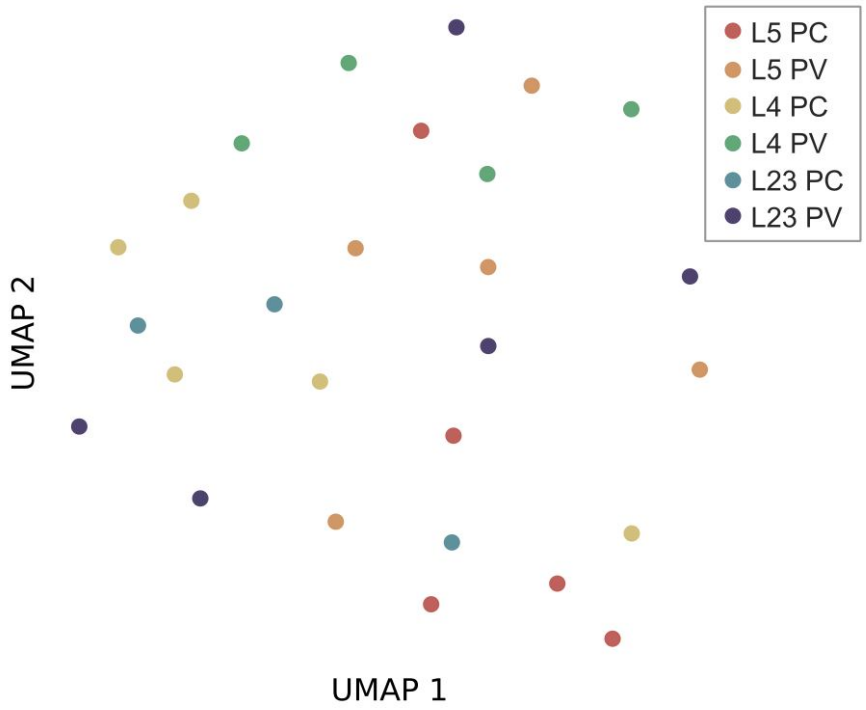

Figure 5.8: **Dimensionality reduction shows no clustering between neuron types or layers.** Performing dimensionality reduction on the nine morphology traits considered in Figure 5.4 and susceptibilities of the neurons to create a uniform manifold approximation (UMAP) shows no clear clustering of the neurons in reduced space.

Morphology trait	**r**	**p**
Length	0.03413	0.87419
Volume	-0.24106	0.25648
Vector Mag	0.33154	0.11349
Dend Length	0.17849	0.37305
Dend Branches	-0.30075	0.12741
Dend Diameter	-0.17740	0.37602
Ax Length	-0.39228	0.05795
Ax Branches	-0.08573	0.67069
Ax Diameter	0.19463	0.33064

Table 5.3: The numerical values of the spearman partial correlation coefficients, r, and their significance values, p, for the morphology traits and susceptibilities as plotted in Supplemental Fig 5.7B.

6

Summary and Conclusion

In this thesis, we considered heterogeneity in neural systems and the influence of its static properties as it pertains to circuit-level dynamics and single-neuron activity. We proposed a candidate mechanism for the adaptation of neural excitability that canvases both the homeostatic response of individual neurons to their input and the circuit-level heterogeneity that results. From this, we model neural excitability as a heterogeneous and homeostatically regulated property of the network and interrogate the influence of past

activity on increasing and decreasing the heterogeneity in the network. Thereafter, using recent datasets, we investigate the influence of human cortical excitatory and inhibitory excitability on the firing rate, correlations, and weight sensitivity in a network model. Finally, having explored the electrophysiological side of heterogeneity, we turned our attention toward morphological heterogeneity and explored its relationship to the variability observed in neural response.

6.1 Comments on Chapter 3

Chapter 3 represents the core of this thesis. In it, we begin our exploration of neural heterogeneity in the context of excitability. Specifically, we build a model to explore this heterogeneity as a dynamic property of the network. Based on previous work, which showed homogeneous excitability to promote instability and pathological dynamics [275, 153, 152], we endowed a network of excitatory neurons with a candidate mechanism for intrinsic plasticity. The main purpose of this article was to use this mechanism to explore the malleability of excitability heterogeneity, and elucidate the factors that regulate it. As our candidate mechanism is a rate-based, homeostatic version of intrinsic plasticity, we leveraged parameters that affected neuron activity to determine the factor(s) regulating heterogeneity in the network.

Applying a persistent stimulus to every neuron in the network, we found that the heterogeneity was reduced when the mean input of all of the neurons was close to zero. For the excitatory neurons in the network, this was accomplished by applying a fixed

negative input. This is particularly important as the resultant state was hyperexcitable in addition to its increased homogeneity, which supported the view that network quiescence may serve as a pathway to pathological dynamics, such as seizure generation [320, 275]. Conversely, when a fixed positive input was applied, the level of heterogeneity in the network increased. Together, these results indicated that the candidate mechanism was capable of manipulating the level of heterogeneity in the network in an activity-dependent manner.

External stimulation, while efficient for testing the limits of malleability, provided little insight into the network-level factors that may influence heterogeneity. To that end, we consider the idea of neuronal milieus - that is, the local environment in which each neuron exists. For our network, there were three factors that determined a neuron's milieu: the degree of connectivity, the presynaptic weights and the presynaptic firing rate. Exploring these factors, it was found that increased mean and variance of either the degree of connectivity or the presynaptic firing rate resulted in an increased level of cell-to-cell heterogeneity. That is, the variability between the milieu of the neurons supports the heterogeneity of the overall population. This suggests, then, that factors which contribute to differentiating neuron milieus in vivo, such as input decorrelation [272, 285, 7], may help support heterogeneity in the network. How this manifests in networks with inhibitory as well as excitatory neurons is beyond the scope of the present work, but remains an additional open question of interest for future works.

Indeed, the role of interneurons in supporting or reducing heterogeneity, poses several interesting questions. From a modelling perspective, this includes whether inhibitory neu-

rons should be modelled to obey the same intrinsic plasticity rules. Speculatively, as the neurons have such distinct excitability profiles (see Chapter (4)), it may indeed be the case that there are separate rules for their adaptation mechanisms. Investigation into such a mechanism may also provide insight into the contribution(s) of homeostatic adaptation of excitability to the robustness of networks to fluctuations in activity. Moreover, as we have established the milieu as the in-network driver of heterogeneity, it would be pertinent in future work to investigate how inhibitory neurons enhance or limit the milieu-variability available. An example of this, in terms of network dynamics, is the presence of inhibitory cells allows for a much richer landscape of dynamics, such as oscillatory behaviour and non-equilibrium states to be explored.

6.2 Comments on Chapter 4

Chapter 4 represents a continuation of the exploration of excitability heterogeneity in Chapter 3 from a different angle. While the heterogeneity explored in Chapter 3 was malleable, as we were interested in exploring the extent to which heterogeneity could be manipulated in the network, in Chapter 4 we instead sought to explore the effects of real cortical between- and within-cell-type heterogeneity. The main purpose of this chapter was to investigate what effects excitability heterogeneity of cortical neurons had on the dynamics of a network. We explored this with a data-inspired adaptation of a Wilson-Cowan network of excitatory and inhibitory neurons whose excitabilities are drawn from distributions from real human neurons.

Leveraging the human cortical neuron electrophysiology dataset made publicly available by the Allen Institute for Brain Science [58, 182], we first characterized the excitabilities of the neurons. From this, we found that excitatory and inhibitory neurons displayed quantifiable between- and within-cell-type excitability heterogeneity. These excitabilities were conserved within the E and I cells across cortical layers and brain regions. Thus, we limited our groupings of the excitabilities to their cell types. The excitability heterogeneity in cell types represented a deviation from the assumptions in previous models [220, 275, 153, 152] that the distribution of excitabilities in E and I cells is approximately equal. Further characterization showed the excitatory population to be more hypoexcitable than the inhibitory population, with only a small amount of overlap between populations. Thus, we sought to explore what consequences this between- and within-cell-type heterogeneity had on the network dynamics.

Informing a Wilson-Cowan network model with the dataset excitabilities, we first explored the between-cell-type excitability. From our simulations, we found that the between-cell-type excitability was important in achieving the asynchronous irregular dynamics similar to those observed in experimental work [92, 49, 272, 191]. Though here we investigate this in terms of the broad categories of excitatory and inhibitory neurons, it has interesting implications for the importance of between-cell-type excitability in more specific subtypes (e.g. PV, SOM, etc.). This is particularly true as, in mouse data, the subtypes of inhibitory neurons have distinct excitability profiles [237]. In future work, a more detailed grouping of the between-cell-type excitability heterogeneity may provide insight into the underpinings of more complex range of network dynamics, as well as contributions from

the circuit motifs of different cell types rather than random connectivity [93, 58].

Beyond the between-cell-type excitability, we were also interested in the influence of the within-cell-type excitability heterogeneity. Specifically, the presence of within-cell-type excitability heterogeneity reduced the firing rate of the network compared to a homogeneously excitable network. The synchrony of the network in response to different noise correlations was additionally influenced by the heterogeneity, with networks with low noise correlation being moderately more decorrelated by heterogeneity. Interestingly, this effect was reversed in networks receiving high levels of noise correlation. This was somewhat surprising as previous results have suggested that heterogeneous networks are better decorrelators than their homogeneous counterparts [248]. Indeed, a growing body of work has postulated the inhibitory neurons to act as decorrelationary of excitatory input [272, 285, 7]. Importantly, the homogeneous case we consider here is that of the effective excitabilities in the two cell types considered here. This could then indicate that the between-cell-type excitability itself plays a role in the decorrelation. Further understanding of what, if any, decorrelation is improved by heterogeneous excitability is of great interest both for its implications in information encoding, and how it may contribute to the balance of excitatory and inhibitory cells [7, 112].

Moreover, beyond the effects on the firing rate and synchrony, we also probed whether human excitability heterogeneity influences the network's sensitivity to changes in the presynaptic weights. Altering each type of weight (i.e. $w^{EE}, w^{EI}, w^{IE}, w^{II}$) in the network and measuring the effects on the firing rate, we found that the within-cell-type heterogeneity led to both populations of neurons being sensitive to changes in the excitatory but

not inhibitory weights. Our result thus suggests that the heterogeneity observed in cortical neurons may contribute to robustness in the population to certain synaptic weight changes. Similarly, the synchrony of the network was insensitive to inhibitory presynaptic weight changes. This surprising insensitivity seemingly arises due to the hyperexcitability and lower within-cell-type excitability heterogeneity of the inhibitory cell population, resulting in a very all-or-none level of firing. This may then suggest, as subtypes of interneurons have been shown in other work to have unique excitabilities [237], that in a more detailed network, some inhibitory neurons with higher heterogeneity in their excitabilities may be more sensitive to presynaptic weight changes than others.

Having this improved understanding of the baseline level of heterogeneity in human neurons and an understanding of how they influence network dynamics, it would be of future interest to continue this work through a lens similar to that used in Chapter 3. That is, exploration of how adaptation might affect both the dynamics of this data-influenced network could provide important insight into the robustness of this distribution of excitabilities. Furthermore, in cases where all or some of the neurons are driven into aberrant excitability, insight into the onset of various pathological states may arise.

6.3 Comments on Chapter 5

Chapter 5 is an expansion of the scope of heterogeneity investigated in this thesis. In Chapters 3 and 4, we considered heterogeneity through the lens of neural excitability. However, beyond the electrophysiological aspects, morphology also contributes to cell-to-

cell heterogeneity. In Chapter 5, we investigate the relationship between the morphological characteristics of biophysically detailed models of mouse excitatory and inhibitory neurons from the Allen Institute for Brain Science to their response to uniform electric field stimulation.

The morphologies of neurons, which are highly variable between- and within- neuron subtypes [56, 42, 226], were first considered in their individual traits. The characterization of the neurons subsequently revealed within- and between-cell-type variability in both whole cell (e.g. length, volume), and compartment level (e.g. dendritic branching, axonal diameter) morphological features. Sorting the features by cell subtype and layer, as has often been of interest to classify neurons, we then sought to relate these features to the variability in response.

Simulating each neuron being exposed to uniform electric field stimulation, we analyzed the resulting membrane potential response of the neuron models at varied field strengths with respect to the physical features (e.g. length, branching, etc.) of the neuron models. The main purpose of this article was to determine if one or more features of the morphology could be related to the response strength of a neuron. Previous studies, using less detailed biophysical models, have suggested that neuron morphology might explain some of the high variability observed in neuron response to these techniques [263, 264]. Indeed, this question, although experimentally intractable, has been of great interest in neuromodulation and non-invasive stimulation frameworks as a target for selective recruitment of neurons. Ultimately, we found the variability in the individual morphological features of each neuron limited the selectivity with which the neurons could be recruited.

Each model, when stimulated with increasing strengths of electric field had a different membrane potential response. Taking the average of the membrane potential for each electric field strength, we quantified the slope as the susceptibility of the neuron. Correlation and partial correlation analysis of the morphological features of each neuron with its susceptibility showed that there was no significant correlation between a neuron's response and any of its morphological traits. These null results align with with what has been observed in other recent works [243, 226, 17, 8], which show that not all types of heterogeneity are important to response variability. This is postulated, in part, to be a version of degeneracy. That is, there exist multiple combinations of morphological features that may yield the same activity. These results have many implications for heterogeneity itself. Specifically, they suggest that some versions of heterogeneity are highly influential on the network dynamics, such as the excitability we investigated in Chapters 3 and 4, and others, like the morphology we consider here, are less so.

Importantly, owing to the small number of available detailed biophysical neuron models in the dataset, our results are limited due to their sample size. A more widespread sample of neurons, or extending into other neuron types, such as SOM or VIP interneurons, could have features that are more easily correlated with their susceptibility to uniform electric fields. In addition, we restrict ourselves to the use of uniform electric fields, rather than time variant currents, such as transcranial alternating current stimulation. Exploring the effect of time variability to the stimulus applied may result in a stronger correlation to some of the morphological features, or may further the robustness of our results with uniform fields. Further exploration of the extent to which different features of heterogeneity are

or are not influential on neural response and dynamics would provide a great deal of meaningful insight for future modelling work.

References

[1] Larry F Abbott and Thomas B Kepler. "Model neurons: from hodgkin-huxley to hopfield". In: *Statistical Mechanics of Neural Networks: Proceedings of the XIth Sitges Conference Sitges, Barcelona, Spain, 3–7 June 1990*. Springer. 2005, pp. 5–18.

[2] LF Abbott and Gwendal LeMasson. "Analysis of neuron models with dynamically regulated conductances". In: *Neural Computation* 5.6 (1993), pp. 823–842.

[3] Aman S Aberra, Angel V Peterchev, and Warren M Grill. "Biophysically realistic neuron models for simulation of cortical stimulation". In: *Journal of neural engineering* 15.6 (2018), p. 066023.

[4] Aman S Aberra et al. "Simulation of transcranial magnetic stimulation in head model with morphologically-realistic cortical neurons". In: *Brain stimulation* 13.1 (2020), pp. 175–189.

[5] Kalana G Abeywardena et al. "The impact of excitability heterogeneity and synaptic coupling on resilience and stability of a macro-scale brain network". In: *PLOS Complex Systems* 2.7 (2025), e0000057.

[6] Edgar Douglas Adrian. "The basis of sensation". In: *WW Norton Co* (1928).

[7] Yashar Ahmadian and Kenneth D Miller. "What is the dynamical regime of cerebral cortex?" In: *Neuron* 109.21 (2021), pp. 3373–3391.

[8] Larissa Albantakis et al. "The Brain's Best Kept Secret Is Its Degenerate Structure". In: *Journal of Neuroscience* 44.40 (2024).

[9] Reka Albert, Hawoong Jeong, and Albert-Laszlo Barabasi. "Error and attack tolerance of complex networks". In: *Nature* 406 (2000), p. 378.

[10] Ryan PD Alexander and Derek Bowie. "Intrinsic plasticity of cerebellar stellate cells is mediated by NMDA receptor regulation of voltage-gated Na+ channels". In: *The Journal of Physiology* 599.2 (2021), pp. 647–665.

[11] Johnatan Aljadeff, Merav Stern, and Tatyana Sharpee. "Transition to chaos in random networks with cell-type-specific connectivity". In: *Physical review letters* 114.8 (2015), p. 088101.

[12] Stefano Allesina and Si Tang. "Stability criteria for complex ecosystems". In: *Nature* 483.7388 (2012), pp. 205–208.

[13] Leandro M Alonso and Eve Marder. "Visualization of currents in neural models with similar behavior and different conductance densities". In: *Elife* 8 (2019), e42722.

[14] Leandro M Alonso, Mara CP Rue, and Eve Marder. "Gating of homeostatic regulation of intrinsic excitability produces cryptic long-term storage of prior perturbations". In: *Proceedings of the National Academy of Sciences* 120.26 (2023), e2222016120.

[15] Costas A Anastassiou et al. "The effect of spatially inhomogeneous extracellular electric fields on neurons". In: *Journal of Neuroscience* 30.5 (2010), pp. 1925–1936.

[16] Daria Antonenko et al. "Inter-individual and age-dependent variability in simulated electric fields induced by conventional transcranial electrical stimulation". In: *Neuroimage* 224 (2021), p. 117413.

[17] Alexis Arnaudon et al. "Controlling morpho-electrophysiological variability of neurons with detailed biophysical models". In: *Iscience* 26.11 (2023).

[18] Elizabeth C Arnold et al. "Epilepsy-induced reduction in HCN channel expression contributes to an increased excitability in dorsal, but not ventral, hippocampal CA1 neurons". In: *Eneuro* 6.2 (2019).

[19] Florian Aspart, Michiel WH Remme, and Klaus Obermayer. "Differential polarization of cortical pyramidal neuron dendrites through weak extracellular fields". In: *PLoS Computational Biology* 14.5 (2018), e1006124.

[20] Massimo Avoli et al. "Specific imbalance of excitatory/inhibitory signaling establishes seizure onset pattern in temporal lobe epilepsy". In: *Journal of neurophysiology* 115.6 (2016), pp. 3229–3237.

[21] Sinziana Avramescu and Igor Timofeev. "Synaptic strength modulation after cortical trauma: a role in epileptogenesis". In: *Journal of Neuroscience* 28.27 (2008), pp. 6760–6772.

[22] Roman Baravalle and Fernando Montani. "Heterogeneity across neural populations: Its significance for the dynamics and functions of neural circuits". In: *Physical Review E* 103.4 (2021), p. 042308.

[23] Joseph W Baron. "Eigenvalue spectra and stability of directed complex networks". In: *Physical Review E* 106.6 (2022), p. 064302.

[24] Andisheh Bastani and Shapour Jaberzadeh. "Differential modulation of corticospinal excitability by different current densities of anodal transcranial direct current stimulation". In: *PloS one* 8.8 (2013), e72254.

[25] Stanhope Bayne-Jones. "Dr. Karl Landsteiner—Nobel Prize Laureate in Medicine, 1930". In: *Science* 73.1901 (1931), pp. 599–604.

[26] Lou Beaulieu-Laroche et al. "Allometric rules for mammalian cortical layer 5 neuron biophysics". In: *Nature* 600.7888 (2021), pp. 274–278.

[27] Lou Beaulieu-Laroche et al. "Enhanced dendritic compartmentalization in human cortical neurons". In: *Cell* 175.3 (2018), pp. 643–651.

[28] Heinz Beck and Yoel Yaari. "Plasticity of intrinsic neuronal properties in CNS disorders". In: *Nature Reviews Neuroscience* 9.5 (2008), pp. 357–369.

[29] Ettore Beghi. "The epidemiology of epilepsy". In: *Neuroepidemiology* 54.2 (2020), pp. 185–191.

[30] Manuel Beiran and Srdjan Ostojic. "Contrasting the effects of adaptation and synaptic filtering on the timescales of dynamics in recurrent networks". In: *PLoS computational biology* 15.3 (2019), e1006893.

[31] Jan Benda. "Neural adaptation". In: *Current Biology* 31.3 (2021), R110–R116.

[32] Jan Benda and R Matthias Hennig. "Spike-frequency adaptation generates intensity invariance in a primary auditory interneuron". In: *Journal of computational neuroscience* 24.2 (2008), pp. 113–136.

[33] Jan Benda and Andreas VM Herz. "A universal model for spike-frequency adaptation". In: *Neural computation* 15.11 (2003), pp. 2523–2564.

[34] Jan Benda, André Longtin, and Len Maler. "Spike-frequency adaptation separates transient communication signals from background oscillations". In: *Journal of Neuroscience* 25.9 (2005), pp. 2312–2321.

[35] Jan Benda, Leonard Maler, and André Longtin. "Linear versus nonlinear signal transmission in neuron models with adaptation currents or dynamic thresholds". In: *Journal of Neurophysiology* 104.5 (2010), pp. 2806–2820.

[36] Aanchal Bhatia, Sahil Moza, and Upinder Singh Bhalla. "Precise excitation-inhibition balance controls gain and timing in the hippocampus". In: *Elife* 8 (2019), e43415.

[37] Amitabh Bhattacharya et al. "An overview of noninvasive brain stimulation: basic principles and clinical applications". In: *Canadian Journal of Neurological Sciences* 49.4 (2022), pp. 479–492.

[38] Anil Bhattacharyya. "On a measure of divergence between two multinomial populations". In: *Sankhyā: the indian journal of statistics* (1946), pp. 401–406.

[39] Marom Bikson et al. "Mechanisms of acute and after effects of transcranial direct current stimulation". In: *Practical guide to transcranial direct current stimulation: principles, procedures and applications* (2019), pp. 81–113.

[40] Arne V Blackman et al. "Target-cell-specific short-term plasticity in local circuits". In: *Frontiers in synaptic neuroscience* 5 (2013), p. 11.

[41] V Bonapersona et al. "Increasing the statistical power of animal experiments with historical control data". In: *Nature neuroscience* 24.4 (2021), pp. 470–477.

[42] Sam A Booker and Imre Vida. "Morphological diversity and connectivity of hippocampal interneurons". In: *Cell and tissue research* 373.3 (2018), pp. 619–641.

[43] Pascale Boulenguez et al. "Down-regulation of the potassium-chloride cotransporter KCC2 contributes to spasticity after spinal cord injury". In: *Nature medicine* 16.3 (2010), pp. 302–307.

[44] Emelie Braun et al. "Comprehensive cell atlas of the first-trimester developing human brain". In: *Science* 382.6667 (2023), eadf1226.

[45] Paul C Bressloff and Stephen Coombes. "Dynamics of strongly coupled spiking neurons". In: *Neural computation* 12.1 (2000), pp. 91–129.

[46] Katiele VP Brito and Fernanda S Matias. "Neuronal heterogeneity modulates phase synchronization between unidirectionally coupled populations with excitation-inhibition balance". In: *Physical Review E* 103.3 (2021), p. 032415.

[47] Paul Broca. "Sur le principe des localisations cérébrales". In: *Bulletin de la Société d'Anthropologie* 2 (1861), pp. 190–204.

[48] Peter R Brotchie et al. "Head position signals used by parietal neurons to encode locations of visual stimuli". In: *Nature* 375.6528 (1995), pp. 232–235.

[49] Nicolas Brunel. "Dynamics of sparsely connected networks of excitatory and inhibitory spiking neurons". In: *Journal of computational neuroscience* 8.3 (2000), pp. 183–208.

[50] Nicolas Brunel and Mark CW Van Rossum. "Lapicque's 1907 paper: from frogs to integrate-and-fire". In: *Biological cybernetics* 97.5 (2007), pp. 337–339.

[51] Andre R Brunoni, Michael A Nitsche, and Colleen K Loo. *Transcranial Direct Current Stimulation in Neuropsychiatric Disorders Clinical Principles and Management*. Springer, 2021. ISBN: 9783030761356.

[52] Marc Aurel Busche et al. "Clusters of hyperactive neurons near amyloid plaques in a mouse model of Alzheimer's disease". In: *Science* 321.5896 (2008), pp. 1686–1689.

[53] John Charles Butcher. *Numerical methods for ordinary differential equations*. John Wiley & Sons, 2016.

[54] Russell Butler et al. "Decorrelated input dissociates narrow band γ power and BOLD in human visual cortex". In: *Journal of Neuroscience* 37.22 (2017), pp. 5408–5418.

[55] György Buzsáki and Kenji Mizuseki. "The log-dynamic brain: how skewed distributions affect network operations". In: *Nature Reviews Neuroscience* 15.4 (2014), pp. 264–278.

[56] Santiago y Cajal. "Histologie du système nerveux de l'homme et des vertébré." In: *A. Maloine* (1909).

[57] Cody L Call and Dwight E Bergles. "Cortical neurons exhibit diverse myelination patterns that scale between mouse brain regions and regenerate after demyelination". In: *Nature communications* 12.1 (2021), pp. 1–15.

[58] Luke Campagnola et al. "Local connectivity and synaptic dynamics in mouse and human neocortex". In: *Science* 375.6585 (2022), eabj5861.

[59] Nicholas T Carnevale and Michael L Hines. *The NEURON book*. Cambridge University Press, 2006.

[60] Camille Carpentier et al. "Reinterpreting the relationship between number of species and number of links connects community structure and stability". In: *Nature Ecology & Evolution* 5.8 (2021), pp. 1102–1109.

[61] Mark S Cembrowski and Vilas Menon. "Continuous variation within cell types of the nervous system". In: *Trends in Neurosciences* 41.6 (2018), pp. 337–348.

[62] Mark S Cembrowski and Nelson Spruston. "Heterogeneity within classical cell types is the rule: lessons from hippocampal pyramidal neurons". In: *Nature Reviews Neuroscience* 20.4 (2019), pp. 193–204.

[63] Mark S Cembrowski et al. "Spatial gene-expression gradients underlie prominent heterogeneity of CA1 pyramidal neurons". In: *Neuron* 89.2 (2016), pp. 351–368.

[64] Homeira Moradi Chameh et al. "Distinctive biophysical features of human cell-types: insights from studies of neurosurgically resected brain tissue". In: *Frontiers in Synaptic Neuroscience* 15 (2023), p. 1250834.

[65] C Savio Chan et al. "'Rejuvenation'protects neurons in mouse models of Parkinson's disease". In: *Nature* 447.7148 (2007), pp. 1081–1086.

[66] Frances S Chance, Larry F Abbott, and Alex D Reyes. "Gain modulation from background synaptic input". In: *Neuron* 35.4 (2002), pp. 773–782.

[67] Thomas Chartrand et al. "Morphoelectric and transcriptomic divergence of the layer 1 interneuron repertoire in human versus mouse neocortex". In: *Science* 382.6667 (2023), eadf0805.

[68] Mircea I Chelaru and Valentin Dragoi. "Efficient coding in heterogeneous neuronal populations". In: *Proceedings of the National Academy of Sciences* 105.42 (2008), pp. 16344–16349.

[69] Lu Chen et al. "Homeostatic plasticity and excitation-inhibition balance: The good, the bad, and the ugly". In: *Current opinion in neurobiology* 75 (2022), p. 102553.

[70] Christina YC Chou et al. "Principles of visual cortex excitatory microcircuit organization". In: *The Innovation* 6.1 (2025).

[71] Steven M Chrysafides, Stephen J Bordes, and Sandeep Sharma. "Physiology, resting potential". In: *StatPearls [Internet]*. StatPearls Publishing, 2023.

[72] Patricia S Churchland and Terrence J Sejnowski. *The computational brain*. MIT press, 1992.

[73] GDPG Cirillo et al. "Neurobiological after-effects of non-invasive brain stimulation". In: *Brain stimulation* 10.1 (2017), pp. 1–18.

[74] Jan Clemens, Nofar Ozeri-Engelhard, and Mala Murthy. "Fast intensity adaptation enhances the encoding of sound in Drosophila". In: *Nature communications* 9.1 (2018), p. 134.

[75] Harald Cramér. *Mathematical methods of statistics*. Vol. 26. Princeton university press, 1999.

[76] Nathan E Crone et al. "Functional mapping of human sensorimotor cortex with electrocorticographic spectral analysis. II. Event-related synchronization in the gamma band." In: *Brain: a journal of neurology* 121.12 (1998), pp. 2301–2315.

[77] Gaël Daoudal and Dominique Debanne. "Long-term plasticity of intrinsic excitability: learning rules and mechanisms". In: *Learning & memory* 10.6 (2003), pp. 456–465.

[78] Graeme W Davis. "Homeostatic control of neural activity: from phenomenology to molecular design". In: *Annu. Rev. Neurosci.* 29.1 (2006), pp. 307–323.

[79] Harold T Davis. *Introduction to nonlinear diffrential and integral equations*. Dover Publications, 1962.

[80] Eran Dayan et al. "Noninvasive brain stimulation: from physiology to network dynamics and back". In: *Nature neuroscience* 16.7 (2013), pp. 838–844.

[81] Peter Dayan and Laurence F Abbott. *Theoretical neuroscience: computational and mathematical modeling of neural systems*. MIT press, 2005.

[82] Dominique Debanne, Yanis Inglebert, and Michaël Russier. "Plasticity of intrinsic neuronal excitability". In: *Current opinion in neurobiology* 54 (2019), pp. 73–82.

[83] Niraj S Desai, Lana C Rutherford, and Gina G Turrigiano. "Plasticity in the intrinsic excitability of cortical pyramidal neurons". In: *Nature neuroscience* 2.6 (1999), pp. 515–520.

[84] Alain Destexhe and Terrence J Sejnowski. "The Wilson-Cowan model, 36 years later". In: *Biological cybernetics* 101 (2009), p. 1.

[85] Matteo Di Volo and Alain Destexhe. "Optimal responsiveness and information flow in networks of heterogeneous neurons". In: *Scientific reports* 11.1 (2021), p. 17611.

[86] Odin Dumas. "A Computational Investigation of Myelination and Epilepsy". MA thesis. University of Ottawa, 2024.

[87] Grégory Dumont, Georg Northoff, and André Longtin. "A stochastic model of input effectiveness during irregular gamma rhythms". In: *Journal of computational neuroscience* 40.1 (2016), pp. 85–101.

[88] James Eberwine and Junhyong Kim. "Cellular deconstruction: finding meaning in individual cell variation". In: *Trends in cell biology* 25.10 (2015), pp. 569–578.

[89] Gerald M Edelman and Joseph A Gally. "Degeneracy and complexity in biological systems". In: *Proceedings of the national academy of sciences* 98.24 (2001), pp. 13763–13768.

[90] Eran Eldar, Jonathan D Cohen, and Yael Niv. "The effects of neural gain on attention and learning". In: *Nature neuroscience* 16.8 (2013), pp. 1146–1153.

[91] Guy N Elston, Ruth Benavides-Piccione, and Javier DeFelipe. "The pyramidal cell in cognition: a comparative study in human and monkey". In: *The Journal of Neuroscience* 21.17 (2001), RC163.

[92] Bard Ermentrout. "Neural networks as spatio-temporal pattern-forming systems". In: *Reports on progress in physics* 61.4 (1998), p. 353.

[93] Claudia Espinoza et al. "Parvalbumin+ interneurons obey unique connectivity rules and establish a powerful lateral-inhibition microcircuit in dentate gyrus". In: *Nature communications* 9.1 (2018), p. 4605.

[94] Adrienne Fairhall. "Adaptation and natural stimulus statistics". In: (2014).

[95] Daniel E Feldman. "Synaptic mechanisms for plasticity in neocortex". In: *Annual review of neuroscience* 32.1 (2009), pp. 33–55.

[96] Daniel E Feldman. "The spike-timing dependence of plasticity". In: *Neuron* 75.4 (2012), pp. 556–571.

[97] Katie A Ferguson and Jessica A Cardin. "Mechanisms underlying gain modulation in the cortex". In: *Nature Reviews Neuroscience* 21.2 (2020), pp. 80–92.

[98] Michael Feyerabend et al. "Single neuron diversity supports area functional specialization along the visual cortical pathways". In: *bioRxiv* (2024), pp. 2024–12.

[99] Peter SB Finnie and Karim Nader. "The role of metaplasticity mechanisms in regulating memory destabilization and reconsolidation". In: *Neuroscience & Biobehavioral Reviews* 36.7 (2012), pp. 1667–1707.

[100] Richard FitzHugh. "Impulses and physiological states in theoretical models of nerve membrane". In: *Biophysical journal* 1.6 (1961), pp. 445–466.

[101] Manoela V Fogaça and Ronald S Duman. "Cortical GABAergic dysfunction in stress and depression: new insights for therapeutic interventions". In: *Frontiers in cellular neuroscience* 13 (2019), p. 448587.

[102] Thomas C Foster. "Calcium homeostasis and modulation of synaptic plasticity in the aged brain". In: *Aging cell* 6.3 (2007), pp. 319–325.

[103] Nicolas Fourcaud-Trocmé et al. "How spike generation mechanisms determine the neuronal response to fluctuating inputs". In: *Journal of neuroscience* 23.37 (2003), pp. 11628–11640.

[104] Zachary Fournier, Leandro M Alonso, and Eve Marder. "Circuit function is more robust to changes in synaptic than intrinsic conductances". In: *bioRxiv* (2024).

[105] Zachary Fournier, Leandro M Alonso, and Eve Marder. "Rhythmic circuit function is more robust to changes in synaptic than intrinsic conductances". In: *eLife* 13 (2025), RP102938.

[106] Robert C Froemke. "Plasticity of cortical excitatory-inhibitory balance". In: *Annual review of neuroscience* 38.1 (2015), pp. 195–219.

[107] Flavio Frohlich and Justin Riddle. "Conducting double-blind placebo-controlled clinical trials of transcranial alternating current stimulation (tACS)". In: *Translational Psychiatry* 11.1 (2021), p. 284.

[108] BH Gähwiler. "Organotypic monolayer cultures of nervous tissue". In: *Journal of neuroscience methods* 4.4 (1981), pp. 329–342.

[109] Crispin W. Gardiner. *Stochastic Methods: A Handbook for the Natural and Social Sciences*. 4th ed. Vol. 13. Springer Series in Synergetics. Berlin, Heidelberg: Springer-Verlag Berlin Heidelberg, 2009, pp. xviii + 447. ISBN: 978-3-540-70712-7. DOI: 10.1007/978-3-540-70713-4. URL: https://link.springer.com/book/10.1007/978-3-540-70713-4.

[110] Mark R Gardner and W Ross Ashby. "Connectance of large dynamic (cybernetic) systems: critical values for stability". In: *Nature* 228.5273 (1970), pp. 784–784.

[111] Célia Gasselin, Yanis Inglebert, and Dominique Debanne. "Homeostatic regulation of h-conductance controls intrinsic excitability and stabilizes the threshold for synaptic modification in CA1 neurons". In: *The Journal of physiology* 593.22 (2015), pp. 4855–4869.

[112] Richard Gast, Sara A Solla, and Ann Kennedy. "Neural heterogeneity controls computations in spiking neural networks". In: *Proceedings of the National Academy of Sciences* 121.3 (2024), e2311885121.

[113] Sarah Genon, Simon B Eickhoff, and Shahrzad Kharabian. "Linking interindividual variability in brain structure to behaviour". In: *Nature Reviews Neuroscience* 23.5 (2022), pp. 307–318.

[114] Wulfram Gerstner and Werner M Kistler. *Spiking neuron models: Single neurons, populations, plasticity*. Cambridge university press, 2002.

[115] Wulfram Gerstner et al. *Neuronal dynamics: From single neurons to networks and models of cognition*. Cambridge University Press, 2014.

[116] Gourab Ghoshal and Albert-László Barabási. "Ranking stability and super-stable nodes in complex networks". In: *Nature communications* 2.1 (2011), p. 394.

[117] Julijana Gjorgjieva et al. "Intrinsic neuronal properties switch the mode of information transmission in networks". In: *PLoS computational biology* 10.12 (2014), e1003962.

[118] Mitchell Glickstein. "The discovery of the visual cortex". In: *Scientific American* 259.3 (1988), pp. 118–127.

[119] Jean-Marc Goaillard and Eve Marder. "Ion channel degeneracy, variability, and covariation in neuron and circuit resilience". In: *Annual review of neuroscience* 44.1 (2021), pp. 335–357.

[120] D Golomb, D Hansel, and G Mato. "Mechanisms of synchrony of neural activity in large networks". In: *Handbook of biological physics*. Vol. 4. Elsevier, 2001, pp. 887–968.

[121] David Golomb and John Rinzel. "Dynamics of globally coupled inhibitory neurons with heterogeneity". In: *Physical review E* 48.6 (1993), p. 4810.

[122] Nathan W Gouwens et al. "Classification of electrophysiological and morphological neuron types in the mouse visual cortex". In: *Nature neuroscience* 22.7 (2019), pp. 1182–1195.

[123] Nathan W Gouwens et al. "Integrated morphoelectric and transcriptomic classification of cortical GABAergic cells". In: *Cell* 183.4 (2020), pp. 935–953.

[124] Tom A. de Graaf and Alexander T. Sack. "When and How to Interpret Null Results in NIBS: A Taxonomy Based on Prior Expectations and Experimental Design". In: *Frontiers in Neuroscience* 12 (Dec. 2018). DOI: 10.3389/fnins.2018.00915. URL: https://doi.org/10.3389/fnins.2018.00915.

[125] Zijin Gu et al. "Heritability and interindividual variability of regional structure-function coupling". In: *Nature Communications* 12.1 (2021), p. 4894.

[126] Andrea Guerra et al. "Variability in non-invasive brain stimulation studies: reasons and results". In: *Neuroscience letters* 719 (2020), p. 133330.

[127] Nikolas Haller et al. "Gamma transcranial alternating current stimulation improves mood and cognition in patients with major depression". In: *Journal of psychiatric research* 130 (2020), pp. 31–34.

[128] Mark Hallett. "Transcranial magnetic stimulation: a primer". In: *Neuron* 55.2 (2007), pp. 187–199.

[129] Xiaofeng Han et al. "Whole human-brain mapping of single cortical neurons for profiling morphological diversity and stereotypy". In: *Science Advances* 9.41 (2023), eadf3771.

[130] Eric Hanse. "Associating synaptic and intrinsic plasticity". In: *The Journal of Physiology* 586.Pt 3 (2008), p. 691.

[131] Alkomiet Hasan et al. "Repetitive noninvasive brain stimulation to modulate cognitive functions in schizophrenia: a systematic review of primary and secondary outcomes". In: *Schizophrenia bulletin* 42.suppl_1 (2016), S95–S109.

[132] Toshiaki Hashimoto et al. "Reduced brainstem size in children with autism". In: *Brain and Development* 14.2 (1992), pp. 94–97.

[133] Alexis M Hattox and Sacha B Nelson. "Layer V neurons in mouse cortex projecting to different targets have distinct physiological properties". In: *Journal of neurophysiology* 98.6 (2007), pp. 3330–3340.

[134] Etay Hay et al. "Models of neocortical layer 5b pyramidal cells capturing a wide range of dendritic and perisomatic active properties". In: *PLoS computational biology* 7.7 (2011), e1002107.

[135] Moritz Helias, Tom Tetzlaff, and Markus Diesmann. "The correlation structure of local neuronal networks intrinsically results from recurrent dynamics". In: *PLoS computational biology* 10.1 (2014), e1003428.

[136] Ernst Hellinger. "Neue begründung der theorie quadratischer formen von unendlichvielen veränderlichen." In: *Journal für die reine und angewandte Mathematik* 1909.136 (1909), pp. 210–271.

[137] Henry H Heng et al. "Heterogeneity mediated system complexity: The ultimate challenge for studying common and complex diseases". In: *The value of systems and complexity sciences for healthcare*. Springer, 2016, pp. 107–120.

[138] Amanda Henton and Thanos Tzounopoulos. "What's the buzz? The neuroscience and the treatment of tinnitus". In: *Physiological reviews* 101.4 (2021), pp. 1609–1632.

[139] Christoph S Herrmann et al. "Transcranial alternating current stimulation: a review of the underlying mechanisms and modulation of cognitive processes". In: *Frontiers in human neuroscience* 7 (2013), p. 279.

[140] Michael Hines. "Efficient computation of branched nerve equations". In: *International journal of bio-medical computing* 15.1 (1984), pp. 69–76.

[141] Michael L Hines and Nicholas T Carnevale. "The NEURON simulation environment". In: *Neural computation* 9.6 (1997), pp. 1179–1209.

[142] Rebecca D Hodge et al. "Conserved cell types with divergent features in human versus mouse cortex". In: *Nature* 573.7772 (2019), pp. 61–68.

[143] Alan L Hodgkin. "The local electric changes associated with repetitive action in a non-medullated axon". In: *The Journal of physiology* 107.2 (1948), p. 165.

[144] Alan L Hodgkin and Andrew F Huxley. "A quantitative description of membrane current and its application to conduction and excitation in nerve". In: *The Journal of physiology* 117.4 (1952), p. 500.

[145] John J Hopfield. "Neural networks and physical systems with emergent collective computational abilities." In: *Proceedings of the national academy of sciences* 79.8 (1982), pp. 2554–2558.

[146] Wei A Huang et al. "Transcranial alternating current stimulation entrains alpha oscillations by preferential phase synchronization of fast-spiking cortical neurons to stimulation waveform". In: *Nature communications* 12.1 (2021), pp. 1–20.

[147] Z Josh Huang and Anirban Paul. "The diversity of GABAergic neurons and neural communication elements". In: *Nature Reviews Neuroscience* 20.9 (2019), pp. 563–572.

[148] Jeanette Hui, Sara Tremblay, and Zafiris J Daskalakis. "The current and future potential of transcranial magnetic stimulation with electroencephalography in psychiatry". In: *Clinical Pharmacology & Therapeutics* 106.4 (2019), pp. 734–746.

[149] Jacob M Hull et al. "Heterogeneity of voltage gated sodium current density between neurons decorrelates spiking and suppresses network synchronization in Scn1b null mouse models". In: *Scientific Reports* 13.1 (2023), p. 8887.

[150] John D Hunter. "Matplotlib: A 2D graphics environment". In: *Computing in science & engineering* 9.03 (2007), pp. 90–95.

[151] Axel Hutt, Andreas Mierau, and Jérémie Lefebvre. "Dynamic control of synchronous activity in networks of spiking neurons". In: *PloS one* 11.9 (2016), e0161488.

[152] Axel Hutt et al. "Diversity-induced trivialization and resilience of neural dynamics". In: *Chaos: An Interdisciplinary Journal of Nonlinear Science* 34.1 (2024).

[153] Axel Hutt et al. "Intrinsic neural diversity quenches the dynamic volatility of neural networks". In: *Proceedings of the National Academy of Sciences* 120.28 (2023), e2218841120.

[154] Jesper R Ipsen and Andre DH Peterson. "Consequences of Dale's law on the stability-complexity relationship of random neural networks". In: *Physical Review E* 101.5 (2020), p. 052412.

[155] Eugene M Izhikevich. *Dynamical systems in neuroscience*. MIT press, 2007.

[156] Ole Jensen and John E Lisman. "Position reconstruction from an ensemble of hippocampal place cells: contribution of theta phase coding". In: *Journal of neurophysiology* 83.5 (2000), pp. 2602–2609.

[157] James Jerger and James Hall. "Effects of age and sex on auditory brainstem response". In: *Archives of otolaryngology* 106.7 (1980), pp. 387–391.

[158] Frank Jessen et al. "Volume reduction of the entorhinal cortex in subjective memory impairment". In: *Neurobiology of aging* 27.12 (2006), pp. 1751–1756.

[159] Xiaolong Jiang et al. "Principles of connectivity among morphologically defined cell types in adult neocortex". In: *Science* 350.6264 (2015), aac9462.

[160] Viktor K Jirsa et al. "On the nature of seizure dynamics". In: *Brain* 137.8 (2014), pp. 2210–2230.

[161] Nelson Johansen et al. "Interindividual variation in human cortical cell type abundance and expression". In: *Science* 382.6667 (2023), eadf2359.

[162] Masako Kaibara and Warren T Blume. "The postictal electroencephalogram". In: *Electroencephalography and clinical neurophysiology* 70.2 (1988), pp. 99–104.

[163] Eric R Kandel et al. *Principles of neural science*. Vol. 4. McGraw-hill New York, 2000.

[164] David B Kastner and Stephen A Baccus. "Insights from the retina into the diverse and general computations of adaptation, detection, and prediction". In: *Current opinion in neurobiology* 25 (2014), pp. 63–69.

[165] David B Kastner, Stephen A Baccus, and Tatyana O Sharpee. "Critical and maximally informative encoding between neural populations in the retina". In: *Proceedings of the National Academy of Sciences of the United States of America* 112.8 (2015), pp. 2533–2538.

[166] Hyunju Kim et al. "Constructing and sampling directed graphs with given degree sequences". In: *New Journal of Physics* 14.2 (2012), p. 023012.

[167] Adrienne I Kinman et al. "Atypical hippocampal excitatory neurons express and govern object memory". In: *Nature Communications* 16.1 (2025), p. 1195.

[168] Hiroaki Kitano. "Biological robustness". In: *Nature Reviews Genetics* 5.11 (2004), pp. 826–837.

[169] DCW Klooster et al. "Technical aspects of neurostimulation: focus on equipment, electric field modeling, and stimulation protocols". In: *Neuroscience & Biobehavioral Reviews* 65 (2016), pp. 113–141.

[170] Maxim Komarov et al. "Selective recruitment of cortical neurons by electrical stimulation". In: *PLoS computational biology* 15.8 (2019), e1007277.

[171] Matthew R Krause et al. "Brain stimulation competes with ongoing oscillations for control of spike timing in the primate brain". In: *PLoS biology* 20.5 (2022), e3001650.

[172] Matthew R Krause et al. "Transcranial alternating current stimulation entrains single-neuron activity in the primate brain". In: *Proceedings of the National Academy of Sciences* 116.12 (2019), pp. 5747–5755.

[173] Arnold R Kriegstein and Marc A Dichter. "Morphological classification of rat cortical neurons in cell culture". In: *Journal of Neuroscience* 3.8 (1983), pp. 1634–1647.

[174] Pawel Kudela et al. "Modeling neural adaptation in auditory cortex". In: *Frontiers in neural circuits* 12 (2018), p. 72.

[175] Solomon Kullback and Richard A Leibler. "On information and sufficiency". In: *The annals of mathematical statistics* 22.1 (1951), pp. 79–86.

[176] Pravir Kumar et al. "Ion channels in neurological disorders". In: *Advances in protein chemistry and structural biology* 103 (2016), pp. 97–136.

[177] Josef Ladenbauer and Klaus Obermayer. "Weak electric fields promote resonance in neuronal spiking activity: Analytical results from two-compartment cell and network models". In: *PLOS Computational Biology* 15.4 (2019), e1006974.

[178] Pietro Landi et al. "Complexity and stability of ecological networks: a review of the theory". In: *Population ecology* 60.4 (2018), pp. 319–345.

[179] Rylan S Larsen and P Jesper Sjöström. "Synapse-type-specific plasticity in local circuits". In: *Current opinion in neurobiology* 35 (2015), pp. 127–135.

[180] Ryan C Leach et al. "Differential age effects of transcranial direct current stimulation on associative memory". In: *The Journals of Gerontology: Series B* 74.7 (2019), pp. 1163–1173.

[181] Erwan Ledoux and Nicolas Brunel. "Dynamics of networks of excitatory and inhibitory neurons in response to time-dependent inputs". In: *Frontiers in computational neuroscience* 5 (2011), p. 25.

[182] Brian R Lee et al. "Signature morphoelectric properties of diverse GABAergic interneurons in the human neocortex". In: *Science* 382.6667 (2023), eadf6484.

[183] Jeremie Lefebvre. "Dynamics of a sensory network of ON and OFF cells with global delayed feedback". PhD thesis. University of Ottawa, 2010.

[184] Jérémie Lefebvre, Axel Hutt, and Flavio Frohlich. "Stochastic resonance mediates the state-dependent effect of periodic stimulation on cortical alpha oscillations". In: *Elife* 6 (2017), e32054.

[185] Jeremie Lefebvre, Andre Longtin, and Victor G LeBlanc. "Neural adaptation facilitates oscillatory responses to static inputs in a recurrent network of ON and OFF cells". In: *Journal of computational neuroscience* 31.1 (2011), pp. 73–86.

[186] Jérémie Lefebvre et al. "Myelin-induced gain control in nonlinear neural networks". In: *Communications Physics* 8.145 (2025). Open access. DOI: 10.1038/s42005-025-02055-8. URL: https://www.nature.com/articles/s42005-025-02055-8.

[187] Jérémie Lefebvre et al. "Stimulus statistics shape oscillations in nonlinear recurrent neural networks". In: *Journal of Neuroscience* 35.7 (2015), pp. 2895–2903.

[188] Gwendal LeMasson, Eve Marder, and LF Abbott. "Activity-dependent regulation of conductances in model neurons". In: *Science* 259.5103 (1993), pp. 1915–1917.

[189] Annick Lesne. "Robustness: confronting lessons from physics and biology". In: *Biological Reviews* 83.4 (2008), pp. 509–532.

[190] Moshe Levy. "Social phase transitions". In: *Journal of Economic Behavior & Organization* 57.1 (2005), pp. 71–87.

[191] Jingwen Li and Woodrow L Shew. "Tuning network dynamics from criticality to an asynchronous state". In: *PLOS Computational Biology* 16.9 (2020), e1008268.

[192] Shuang Li, Veronica Choi, and Thanos Tzounopoulos. "Pathogenic plasticity of Kv7. 2/3 channel activity is essential for the induction of tinnitus". In: *Proceedings of the National Academy of Sciences* 110.24 (2013), pp. 9980–9985.

[193] John Lisman. "Excitation, inhibition, local oscillations, or large-scale loops: what causes the symptoms of schizophrenia?" In: *Current opinion in neurobiology* 22.3 (2012), pp. 537–544.

[194] Anli Liu et al. "Immediate neurophysiological effects of transcranial electrical stimulation". In: *Nature communications* 9.1 (2018), pp. 1–12.

[195] Andre Longtin. "Nonlinear oscillations, noise and chaos in neural delayed feedback". PhD thesis. McGill University, 1989.

[196] Andre Longtin. "Stochastic dynamical systems". In: *Scholarpedia* 5.4 (2010), p. 1619.

[197] Bonnie E Lonze and David D Ginty. "Function and regulation of CREB family transcription factors in the nervous system". In: *Neuron* 35.4 (2002), pp. 605–623.

[198] Virginia López-Alonso et al. "Inter-individual variability in response to non-invasive brain stimulation paradigms". In: *Brain stimulation* 7.3 (2014), pp. 372–380.

[199] Zhengyu Ma et al. "Cortical circuit dynamics are homeostatically tuned to criticality in vivo". In: *Neuron* 104.4 (2019), pp. 655–664.

[200] Robert MacArthur. "Fluctuations of animal populations and a measure of community stability". In: *ecology* 36.3 (1955), pp. 533–536.

[201] Mufti Mahmud and Stefano Vassanelli. "Differential modulation of excitatory and inhibitory neurons during periodic stimulation". In: *Frontiers in neuroscience* 10 (2016), p. 62.

[202] Gaby Maimon, Andrew D Straw, and Michael H Dickinson. "Active flight increases the gain of visual motion processing in Drosophila". In: *Nature neuroscience* 13.3 (2010), pp. 393–399.

[203] David Manheim. "The fragile world hypothesis: Complexity, fragility, and systemic existential risk". In: *Futures* 122 (2020), p. 102570.

[204] Eve Marder. "Variability, compensation, and modulation in neurons and circuits". In: *Proceedings of the National Academy of Sciences* 108.supplement_3 (2011), pp. 15542–15548.

[205] Eve Marder and Jean-Marc Goaillard. "Variability, compensation and homeostasis in neuron and network function". In: *Nature Reviews Neuroscience* 7.7 (2006), pp. 563–574.

[206] Eve Marder, Marie L Goeritz, and Adriane G Otopalik. "Robust circuit rhythms in small circuits arise from variable circuit components and mechanisms". In: *Current opinion in neurobiology* 31 (2015), pp. 156–163.

[207] Henry Markram et al. "Reconstruction and simulation of neocortical microcircuitry". In: *Cell* 163.2 (2015), pp. 456–492.

[208] Shimon Marom and Eve Marder. "A biophysical perspective on the resilience of neuronal excitability across timescales". In: *Nature Reviews Neuroscience* 24.10 (2023), pp. 640–652.

[209] Theresa M Marschall et al. "Deafferentation as a cause of hallucinations". In: *Current opinion in psychiatry* 33.3 (2020), pp. 206–211.

[210] Julio Martinez-Trujillo. "Why do primates have view cells instead of place cells?" In: *Trends in Cognitive Sciences* (2025).

[211] Michael Mascagni. "The backward euler method for numerical solution of the Hodgkin–Huxley equations of nerve conduction". In: *SIAM journal on numerical analysis* 27.4 (1990), pp. 941–962.

[212] Robert M May. "Stability in multispecies community models". In: *Mathematical Biosciences* 12.1-2 (1971), pp. 59–79.

[213] Robert M May. "Will a large complex system be stable?" In: *Nature* 238.5364 (1972), pp. 413–414.

[214] David W McCandless. *Epilepsy: animal and human correlations*. Springer Science & Business Media, 2011.

[215] Kevin Shear McCann. "The diversity–stability debate". In: *Nature* 405.6783 (2000), pp. 228–233.

[216] Warren S McCulloch and Walter Pitts. "A logical calculus of the ideas immanent in nervous activity". In: *The bulletin of mathematical biophysics* 5.4 (1943), pp. 115–133.

[217] Wes McKinney et al. "pandas: a foundational Python library for data analysis and statistics". In: *Python for high performance and scientific computing* 14.9 (2011), pp. 1–9.

[218] Chandrakala Meena et al. "Emergent stability in complex network dynamics". In: *Nature Physics* 19.7 (2023), pp. 1033–1042.

[219] JF Mejias and A Longtin. "Optimal heterogeneity for coding in spiking neural networks". In: *Physical Review Letters* 108.22 (2012), p. 228102.

[220] Jorge F Mejias and André Longtin. "Differential effects of excitatory and inhibitory heterogeneity on the gain and asynchronous state of sparse cortical networks". In: *Frontiers in computational neuroscience* 8 (2014), p. 107.

[221] A Mierau, W Klimesch, and J Lefebvre. "State-dependent alpha peak frequency shifts: Experimental evidence, potential mechanisms and functional implications". In: *Neuroscience* 360 (2017), pp. 146–154.

[222] John P Miller and Gwen A Jacobs. "Relationships between neuronal structure and function". In: *Journal of experimental biology* 112.1 (1984), pp. 129–145.

[223] Patrick J Mineault et al. "Enhanced spatial resolution during locomotion and heightened attention in mouse primary visual cortex". In: *Journal of Neuroscience* 36.24 (2016), pp. 6382–6392.

[224] Hemanth Mohan et al. "Dendritic and axonal architecture of individual pyramidal neurons across layers of adult human neocortex". In: *Cerebral Cortex* 25.12 (2015), pp. 4839–4853.

[225] Vera Moliadze, Andrea Antal, and Walter Paulus. "Electrode-distance dependent after-effects of transcranial direct and random noise stimulation with extracephalic reference electrodes". In: *Clinical Neurophysiology* 121.12 (2010), pp. 2165–2171.

[226] Homeira Moradi Chameh et al. "Diversity amongst human cortical pyramidal neurons revealed via their sag currents and frequency preferences". In: *Nature communications* 12.1 (2021), p. 2497.

[227] Homeira Moradi Chameh et al. "Hyperpolarization activated cation channel mediated intrinsic plasticity changes underlie the malleability of with-in cell-type electrophysiological heterogeneity". In: *biorxiv* (2025).

[228] Catherine Morris and Harold Lecar. "Voltage oscillations in the barnacle giant muscle fiber". In: *Biophysical journal* 35.1 (1981), pp. 193–213.

[229] Riccardo Mozzachiodi and John H Byrne. "More than synaptic plasticity: role of nonsynaptic plasticity in learning and memory". In: *Trends in neurosciences* 33.1 (2010), pp. 17–26.

[230] Hisato Nakazono et al. "Phase and frequency-dependent effects of transcranial alternating current stimulation on motor cortical excitability". In: *PLoS One* 11.9 (2016), e0162521.

[231] David L Nelson and Michael M Cox. *Principles of biochemistry*. Sara Tenney, 2008.

[232] Philip Nelson. *Biological physics*. WH Freeman New York, 2004.

[233] Sacha B Nelson and Vera Valakh. "Excitatory/inhibitory balance and circuit homeostasis in autism spectrum disorders". In: *Neuron* 87.4 (2015), pp. 684–698.

[234] Edward W Ng and Murray Geller. "A table of integrals of the error functions". In: *Journal of Research of the National Bureau of Standards B* 73.1 (1969), pp. 1–20.

[235] Mikhail S Nikulin et al. "Hellinger distance". In: *Encyclopedia of mathematics* 78 (2001).

[236] Michael A Nitsche et al. "Transcranial direct current stimulation: state of the art 2008". In: *Brain stimulation* 1.3 (2008), pp. 206–223.

[237] Cian O'Donnell et al. "Beyond excitation/inhibition imbalance in multidimensional models of neural circuit changes in brain disorders". In: *Elife* 6 (2017), e26724.

[238] Tomokazu Ohshiro, Dora E Angelaki, and Gregory C DeAngelis. "A normalization model of multisensory integration". In: *Nature neuroscience* 14.6 (2011), pp. 775–782.

[239] Timothy O'Leary et al. "Correlations in ion channel expression emerge from homeostatic tuning rules". In: *Proceedings of the National Academy of Sciences* 110.28 (2013), E2645–E2654.

[240] Travis E Oliphant. *A guide to NumPy*. Vol. 1. Trelgol Publishing USA, 2006.

[241] Adriane G Otopalik, Jason Pipkin, and Eve Marder. "Neuronal morphologies built for reliable physiology in a rhythmic motor circuit". In: *Elife* 8 (2019), e41728.

[242] Adriane G Otopalik et al. "Sloppy morphological tuning in identified neurons of the crustacean stomatogastric ganglion". In: *Elife* 6 (2017), e22352.

[243] Adriane G Otopalik et al. "When complex neuronal structures may not matter". In: *Elife* 6 (2017), e23508.

[244] Ray D Owen. "Heterogeneity of Antibodies to the Human Blood Groups in Normal and Immune Sera". In: *The Journal of Immunology* 73.1 (1954), pp. 29–39.

[245] Timothy O'Leary and Eve Marder. "Temperature-robust neural function from activity-dependent ion channel regulation". In: *Current Biology* 26.21 (2016), pp. 2935–2941.

[246] Timothy O'Leary et al. "Cell types, network homeostasis, and pathological compensation from a biologically plausible ion channel expression model". In: *Neuron* 82.4 (2014), pp. 809–821.

[247] Alejandro Torrado Pacheco et al. "Sleep promotes downward firing rate homeostasis". In: *Neuron* 109.3 (2021), pp. 530–544.

[248] Krishnan Padmanabhan and Nathaniel N Urban. "Intrinsic biophysical diversity decorrelates neuronal firing while increasing information content". In: *Nature neuroscience* 13.10 (2010), pp. 1276–1282.

[249] Aref Pariz et al. "Selective control of synaptic plasticity in heterogeneous networks through transcranial alternating current stimulation (tACS)". In: *PLOS Computational Biology* 19.4 (2023), e1010736.

[250] James Park et al. "Inputs drive cell phenotype variability". In: *Genome research* 24.6 (2014), pp. 930–941.

[251] Puja Patel and Solomon L Moshé. "The evolution of the concepts of seizures and epilepsy: What's in a name?" In: *Epilepsia Open* 5.1 (2020), pp. 22–35.

[252] Maria A Patestas and Leslie P Gartner. *A textbook of neuroanatomy.* Blackwell Publishing, 2006.

[253] Walter Paulus. "Transcranial electrical stimulation (tES–tDCS; tRNS, tACS) methods". In: *Neuropsychological rehabilitation* 21.5 (2011), pp. 602–617.

[254] Wilder Penfield and Theodore Rasmussen. *The cerebral cortex of man; a clinical study of localization of function.* Macmillan, 1950.

[255] Piero Perucca, François Dubeau, and Jean Gotman. "Widespread EEG changes precede focal seizures". In: *PloS one* 8.11 (2013), e80972.

[256] Adolf Pfefferbaum et al. "A quantitative magnetic resonance imaging study of changes in brain morphology from infancy to late adulthood". In: *Archives of neurology* 51.9 (1994), pp. 874–887.

[257] Friederike Pfeiffer and Alia Benali. "Could non-invasive brain-stimulation prevent neuronal degeneration upon ion channel re-distribution and ion accumulation after demyelination?" In: *Neural regeneration research* 15.11 (2020), p. 1977.

[258] Eleonora Piccoli et al. "Recent innovations in non-invasive brain stimulation (NIBS) for the treatment of unipolar and bipolar depression: a narrative review". In: *International Review of Psychiatry* (2022), pp. 1–12.

[259] H Pockberger. "Electrophysiological and morphological properties of rat motor cortex neurons in vivo". In: *Brain research* 539.2 (1991), pp. 181–190.

[260] Rafael Polanía, Michael A Nitsche, and Christian C Ruff. "Studying and modifying brain function with non-invasive brain stimulation". In: *Nature neuroscience* 21.2 (2018), pp. 174–187.

[261] Sadrack A Powanwe. "Brain rhythm fluctuations: envelope-phase modelling and phase synchronization". PhD thesis. University of Ottawa, 2021.

[262] Astrid A Prinz, Dirk Bucher, and Eve Marder. "Similar network activity from disparate circuit parameters". In: *Nature neuroscience* 7.12 (2004), pp. 1345–1352.

[263] Thomas Radman. *Neural targets of electric field stimulation.* City University of New York, 2009.

[264] Thomas Radman et al. "Role of cortical cell type and morphology in subthreshold and suprathreshold uniform electric field stimulation in vitro". In: *Brain stimulation* 2.4 (2009), pp. 215–228.

[265] Asif Rahman et al. "Cellular effects of acute direct current stimulation: somatic and synaptic terminal effects". In: *The Journal of physiology* 591.10 (2013), pp. 2563–2578.

[266] Rahul K Rathour and Rishikesh Narayanan. "Degeneracy in hippocampal physiology and plasticity". In: *Hippocampus* 29.10 (2019), pp. 980–1022.

[267] Davide Reato et al. "Effects of weak transcranial alternating current stimulation on brain activity—a review of known mechanisms from animal studies". In: *Frontiers in human neuroscience* 7 (2013), p. 687.

[268] Davide Reato et al. "Low-intensity electrical stimulation affects network dynamics by modulating population rate and spike timing". In: *Journal of Neuroscience* 30.45 (2010), pp. 15067–15079.

[269] Davide Reato et al. "Principles of transcranial direct current stimulation (tDCS): introduction to the biophysics of tDCS". In: *Practical Guide to Transcranial Direct Current Stimulation: Principles, Procedures and Applications* (2019), pp. 45–80.

[270] Thomas P Reber et al. "Single-neuron mechanisms of neural adaptation in the human temporal lobe". In: *Nature Communications* 14.1 (2023), p. 2496.

[271] Alfonso Renart et al. "Mean-driven and fluctuation-driven persistent activity in recurrent networks". In: *Neural computation* 19.1 (2007), pp. 1–46.

[272] Alfonso Renart et al. "The asynchronous state in cortical circuits". In: *science* 327.5965 (2010), pp. 587–590.

[273] Alex Reyes et al. "Target-cell-specific facilitation and depression in neocortical circuits". In: *Nature neuroscience* 1.4 (1998), pp. 279–285.

[274] John H Reynolds and David J Heeger. "The normalization model of attention". In: *Neuron* 61.2 (2009), pp. 168–185.

[275] Scott Rich et al. "Loss of neuronal heterogeneity in epileptogenic human tissue impairs network resilience to sudden changes in synchrony". In: *Cell Reports* 39.8 (2022).

[276] Scott Rich et al. "Neurostimulation stabilizes spiking neural networks by disrupting seizure-like oscillatory transitions". In: *Scientific Reports* 10 (2020), p. 15408.

[277] Justin Riddle and Flavio Frohlich. "Targeting neural oscillations with transcranial alternating current stimulation". In: *Brain Research* 147491 (2021).

[278] Justin Riddle, David R Rubinow, and Flavio Frohlich. "A case study of weekly tACS for the treatment of major depressive disorder". In: *Brain Stimulation: Basic, Translational, and Clinical Research in Neuromodulation* 13.3 (2020), pp. 576–577.

[279] Diana Rien, Roland Kern, and Rafael Kurtz. "Octopaminergic modulation of contrast gain adaptation in fly visual motion-sensitive neurons". In: *European Journal of Neuroscience* 36.8 (2012), pp. 3030–3039.

[280] Lars M Rimol et al. "Cortical volume, surface area, and thickness in schizophrenia and bipolar disorder". In: *Biological psychiatry* 71.6 (2012), pp. 552–560.

[281] John Rinzel and G Bard Ermentrout. "Analysis of neural excitability and oscillations". In: *Methods in neuronal modeling* 2 (1998), pp. 251–292.

[282] Lorenzo Rocchi et al. "Variability and predictors of response to continuous theta burst stimulation: a TMS-EEG study". In: *Frontiers in neuroscience* 12 (2018), p. 400.

[283] Karen M Rodrigue and Naftali Raz. "Shrinkage of the entorhinal cortex over five years predicts memory performance in healthy adults". In: *Journal of Neuroscience* 24.4 (2004), pp. 956–963.

[284] R Ronzano et al. "Microglia-neuron interaction at nodes of Ranvier depends on neuronal activity through potassium release and contributes to remyelination". In: *Nature communications* 12.1 (2021), pp. 1–18.

[285] Robert Rosenbaum et al. "The spatial structure of correlated neuronal variability". In: *Nature neuroscience* 20.1 (2017), pp. 107–114.

[286] Julian Rossbroich et al. "Linear-nonlinear cascades capture synaptic dynamics". In: *PLoS computational biology* 17.3 (2021), e1008013.

[287] Alex Roxin. "The role of degree distribution in shaping the dynamics in networks of sparsely connected spiking neurons". In: *Frontiers in computational neuroscience* 5 (2011), p. 8.

[288] Alex Roxin et al. "On the distribution of firing rates in networks of cortical neurons". In: *Journal of Neuroscience* 31.45 (2011), pp. 16217–16226.

[289] Harry Rubin. "The significance of biological heterogeneity". In: *Cancer and Metastasis Reviews* 9.1 (1990), pp. 1–20.

[290] Michael J Russell et al. "Individual differences in transcranial electrical stimulation current density". In: *Journal of biomedical research* 27.6 (2013), p. 495.

[291] E Salinas and T Sejnowski. "Correlated neuronal activity and the flow of neural information". In: *Nature Reviews Neuroscience* 2 (8 2001), pp. 539–550.

[292] Emilio Salinas and Nicholas M Bentley. "Gain modulation as a mechanism for switching reference frames, tasks, and targets". In: *Coherent Behavior in Neuronal Networks*. Springer, 2009, pp. 121–142.

[293] Emilio Salinas and Peter Thier. "Gain modulation: a major computational principle of the central nervous system". In: *Neuron* 27.1 (2000), pp. 15–21.

[294] Rahul Satija and Alex K Shalek. "Heterogeneity in immune responses: from populations to single cells". In: *Trends in immunology* 35.5 (2014), pp. 219–229.

[295] Federico Scala et al. "Phenotypic variation of transcriptomic cell types in mouse motor cortex". In: *Nature* 598.7879 (2021), pp. 144–150.

[296] Hallel I Schreier, Yoav Soen, and Naama Brenner. "Exploratory adaptation in large random networks". In: *Nature communications* 8.1 (2017), p. 14826.

[297] Abby Scurfield and David C Latimer. "A computational study of the impact of inhomogeneous internodal lengths on conduction velocity in myelinated neurons". In: *PloS one* 13.1 (2018), e0191106.

[298] Kimberly Siletti et al. "Transcriptomic diversity of cell types across the adult human brain". In: *Science* 382.6667 (2023), eadd7046.

[299] R Angus Silver. "Neuronal arithmetic". In: *Nature Reviews Neuroscience* 11.7 (2010), pp. 474–489.

[300] Frances K Skinner. "Conductance-based models". In: *Scholarpedia* 1.11 (2006), p. 1408.

[301] Joram Soch. *The Book of Statistical Proofs*. `https://doi.org/10.5281/zenodo.14646799`. Accessed: 2025-11-08. 2024.

[302] Henning Sprekeler. "Functional consequences of inhibitory plasticity: homeostasis, the excitation-inhibition balance and beyond". In: *Current opinion in neurobiology* 43 (2017), pp. 198–203.

[303] William Stacey et al. "What is the present-day EEG evidence for a preictal state?" In: *Epilepsy research* 97.3 (2011), pp. 243–251.

[304] Mircea Steriade, Igor Timofeev, and François Grenier. "Natural waking and sleep states: a view from inside neocortical neurons". In: *Journal of neurophysiology* 85.5 (2001), pp. 1969–1985.

[305] David C Sterratt and Bruce P Graham. "Principles of Neuronal Modelling OR Principles of Computational". In: ().

[306] Tristan Manfred Stöber et al. "Degeneracy in epilepsy: multiple routes to hyperexcitable brain circuits and their repair". In: *Communications Biology* 6.1 (2023), p. 479.

[307] Steven H Strogatz. *Nonlinear dynamics and chaos: with applications to physics, biology, chemistry, and engineering*. Chapman and Hall/CRC, 2024.

[308] Raheem Suleman. *A brief history of electroconvulsive therapy*. 2020.

[309] Andrew M Swensen and Bruce P Bean. "Robustness of burst firing in dissociated purkinje neurons with acute or long-term reductions in sodium conductance". In: *Journal of Neuroscience* 25.14 (2005), pp. 3509–3520.

[310] A. Talidou et al. "Homeostatic coordination and up-regulation of neural activity by activity-dependent myelination". In: *Nat Comput Sci* 2 (2022), 665–676. DOI: https://doi.org/10.1038/s43588-022-00315-z. URL: https://www.nature.com/articles/s43588-022-00315-z.

[311] Afroditi Talidou et al. "Homeostatic coordination and up-regulation of neural activity by activity-dependent myelination". In: *Nature Computational Science* 2.10 (2022), pp. 665–676.

[312] Si Tang, Samraat Pawar, and Stefano Allesina. "Correlation between interaction strengths drives stability in large ecological networks". In: *Ecology letters* 17.9 (2014), pp. 1094–1100.

[313] Terence Tao. *Topics in random matrix theory*. Vol. 132. American Mathematical Soc., 2012.

[314] Bosiljka Tasic et al. "Shared and distinct transcriptomic cell types across neocortical areas". In: *Nature* 563.7729 (2018), pp. 72–78.

[315] Kamyar Tavakoli. "Dynamical complexity of nonlinear dynamical systems with multiple delays". PhD thesis. University of Ottawa, 2023.

[316] *Technical white paper: biophysical modeling – all active*. Tech. rep. Allen Institute for Brain Science, 2016. URL: https://community.brain-map.org/t/documentation-cell-types-database/2845.

[317] *Technical white paper: biophysical modeling – perisomatic*. Tech. rep. Allen Institute for Brain Science, 2017. URL: https://community.brain-map.org/t/documentation-cell-types-database/2845.

[318] *Technical white paper: electrophysiology*. Tech. rep. Allen Institute for Brain Science, 2017. URL: https://community.brain-map.org/t/documentation-cell-types-database/2845.

[319] Daniella Terney et al. "Increasing human brain excitability by transcranial high-frequency random noise stimulation". In: *Journal of Neuroscience* 28.52 (2008), pp. 14147–14155.

[320] Igor Timofeev, Sylvain Chauvette, and Sara Soltani. "Neocortical focus: experimental view". In: *International review of neurobiology* 114 (2014), pp. 9–33.

[321] Harry Tran, Sina Shirinpour, and Alexander Opitz. "Effects of transcranial alternating current stimulation on spiking activity in computational models of single neocortical neurons". In: *NeuroImage* 250 (2022), p. 118953.

[322] Sara Tremblay et al. "Clinical utility and prospective of TMS–EEG". In: *Clinical Neurophysiology* 130.5 (2019), pp. 802–844.

[323] Stefan Treue and Julio C Martinez Trujillo. "Feature-based attention influences motion processing gain in macaque visual cortex". In: *Nature* 399.6736 (1999), pp. 575–579.

[324] Shreejoy J Tripathy et al. "Intermediate intrinsic diversity enhances neural population coding". In: *Proceedings of the National Academy of Sciences* 110.20 (2013), pp. 8248–8253.

[325] Daniel Trotter. "Ramifications of vesicle release properties on information processing at central synapses". MA thesis. University of Ottawa, 2021.

[326] Daniel Trotter, Taufik Valiante, and Jeremie Lefebvre. "Intrinsic plasticity underlies malleability of neural network heterogeneity". In: *bioRxiv* (2025), pp. 2025–06.

[327] Daniel Trotter et al. "Morphological variability may limit single-cell specificity to electric field stimulation". In: *Frontiers in Synaptic Neuroscience* 17 (2025).

[328] Dennis R Trune, Curt Mitchell, and David S Phillips. "The relative importance of head size, gender and age on the auditory brainstem response". In: *Hearing research* 32.2-3 (1988), pp. 165–174.

[329] Christoforos Tsantoulas and Stephen B McMahon. "Opening paths to novel analgesics: the role of potassium channels in chronic pain". In: *Trends in neurosciences* 37.3 (2014), pp. 146–158.

[330] Yusuf Zahid Tufail. *Development of a neurostimulation method using pulsed ultrasound*. Arizona State University, 2011.

[331] Gina Turrigiano, LF Abbott, and Eve Marder. "Activity-dependent changes in the intrinsic properties of cultured neurons". In: *Science* 264.5161 (1994), pp. 974–977.

[332] Gina G Turrigiano. "Homeostatic plasticity in neuronal networks: the more things change, the more they stay the same". In: *Trends in neurosciences* 22.5 (1999), pp. 221–227.

[333] Gina G Turrigiano and Sacha B Nelson. "Homeostatic plasticity in the developing nervous system". In: *Nature reviews neuroscience* 5.2 (2004), pp. 97–107.

[334] Ranjith Unnikrishnan and Martial Hebert. "Measures of similarity". In: *2005 Seventh IEEE Workshops on Applications of Computer Vision (WACV/MOTION'05)-Volume 1*. Vol. 1. IEEE. 2005, pp. 394–394.

[335] Nathaniel Urban and Shreejoy Tripathy. "Circuits drive cell diversity". In: *Nature* 488.7411 (2012), pp. 289–290.

[336] Victor V Uteshev, Alexander G Gusev, and Evgeny A Sametsky. "Network control mechanisms—cellular milieu". In: *Neuronal Networks in Brain Function, CNS Disorders, and Therapeutics*. Elsevier, 2014, pp. 135–144.

[337] Raphael Vallat. "Pingouin: statistics in Python." In: *J. Open Source Softw.* 3.31 (2018), p. 1026.

[338] Jason VanAlstine, Steven R Cox, and Dianne M Roden. "Cultural diversity in the United States and its impact on human development". In: *Journal of the Indiana Academy of the Social Sciences* 18.1 (2015), p. 10.

[339] Guido vanRossum. "Python reference manual". In: *Department of Computer Science [CS]* R 9525 (1995).

[340] Pauli Virtanen et al. "SciPy 1.0: fundamental algorithms for scientific computing in Python". In: *Nature methods* 17.3 (2020), pp. 261–272.

[341] Johannes Vosskuhl, Daniel Strüber, and Christoph S Herrmann. "Non-invasive brain stimulation: a paradigm shift in understanding brain oscillations". In: *Frontiers in human neuroscience* 12 (2018), p. 211.

[342] Brian J Wainger et al. "Intrinsic membrane hyperexcitability of amyotrophic lateral sclerosis patient-derived motor neurons". In: *Cell reports* 7.1 (2014), pp. 1–11.

[343] Gilles Wainrib and Jonathan Touboul. "Topological and dynamical complexity of random neural networks". In: *Physical review letters* 110.11 (2013), p. 118101.

[344] Florian Walter, Florian Röhrbein, and Alois Knoll. "Computation by time". In: *Neural Processing Letters* 44.1 (2016), pp. 103–124.

[345] Michael L Waskom. "Seaborn: statistical data visualization". In: *Journal of Open Source Software* 6.60 (2021), p. 3021.

[346] Alison I Weber and Adrienne L Fairhall. "The role of adaptation in neural coding". In: *Current opinion in neurobiology* 58 (2019), pp. 135–140.

[347] Alison I Weber, Kamesh Krishnamurthy, and Adrienne L Fairhall. "Coding principles in adaptation". In: *Annual review of vision science* 5.1 (2019), pp. 427–449.

[348] William H Welch. "Adaptation in pathological processes". In: *Science* 5.126 (1897), pp. 813–832.

[349] John A White et al. "Synchronization and oscillatory dynamics in heterogeneous, mutually inhibited neurons". In: *Journal of computational neuroscience* 5.1 (1998), pp. 5–16.

[350] Clarissa J Whitmire and Garrett B Stanley. "Rapid sensory adaptation redux: a circuit perspective". In: *Neuron* 92.2 (2016), pp. 298–315.

[351] Martin T Wiechert et al. "Mechanisms of pattern decorrelation by recurrent neuronal circuits". In: *Nature neuroscience* 13.8 (2010), pp. 1003–1010.

[352] Hugh R Wilson and Jack D Cowan. "A mathematical theory of the functional dynamics of cortical and thalamic nervous tissue". In: *Kybernetik* 13 (2 1973), pp. 55–80.

[353] Hugh R Wilson and Jack D Cowan. "Excitatory and inhibitory interactions in localized populations of model neurons". In: *Biophysical Journal* 12 (1 1972), pp. 1–24.

[354] Yue Kris Wu et al. "Homeostatic mechanisms regulate distinct aspects of cortical circuit dynamics". In: *Proceedings of the National Academy of Sciences* 117.39 (2020), pp. 24514–24525.

[355] Yuhuan Xie, Yian Ann Chen, and Michael D De Bellis. "The relationship of age, gender, and IQ with the brainstem and thalamus in healthy children and adolescents: a magnetic resonance imaging volumetric study". In: *Journal of Child Neurology* 27.3 (2012), pp. 325–331.

[356] Chuanzuo Yang et al. "Epileptic seizures in a heterogeneous excitatory network with short-term plasticity". In: *Cognitive Neurodynamics* 15 (2021), pp. 43–51.

[357] Jane Yang et al. "Minimal requirements for a neuron to coregulate many properties and the implications for ion channel correlations and robustness". In: *Elife* 11 (2022), e72875.

[358] Ee-Lynn Yap and Michael E Greenberg. "Activity-regulated transcription: bridging the gap between neural activity and behavior". In: *Neuron* 100.2 (2018), pp. 330–348.

[359] Guo-Sheng Yi et al. "Morphology controls how hippocampal CA1 pyramidal neuron responds to uniform electric fields: a biophysical modeling study". In: *Scientific reports* 7.1 (2017), pp. 1–13.

[360] Man Yi Yim, Ad Aertsen, and Stefan Rotter. "Impact of intrinsic biophysical diversity on the activity of spiking neurons". In: *Physical Review E—Statistical, Nonlinear, and Soft Matter Physics* 87.3 (2013), p. 032710.

[361] Fleur Zeldenrust, Boris Gutkin, and Sophie Denéve. "Efficient and robust coding in heterogeneous recurrent networks". In: *PLoS computational biology* 17.4 (2021), e1008673.

[362] Hongkui Zeng and Joshua R Sanes. "Neuronal cell-type classification: challenges, opportunities and the path forward". In: *Nature Reviews Neuroscience* 18.9 (2017), pp. 530–546.

[363] Wei Zhang and David J Linden. "The other side of the engram: experience-driven changes in neuronal intrinsic excitability". In: *Nature Reviews Neuroscience* 4.11 (2003), pp. 885–900.

[364] Robert S Zucker and Wade G Regehr. "Short-term synaptic plasticity". In: *Annual review of physiology* 64.1 (2002), pp. 355–405.